

Science with the Ultraviolet Explorer (UVEX)

S. R. KULKARNI,¹ FIONA A. HARRISON,¹ BRIAN W. GREFFENSTETTE,¹ HANNAH P. EARNSHAW,¹ IGOR ANDREONI,²
DANIELLE A. BERG,³ JOSHUA S. BLOOM,⁴ S. BRADLEY CENKO,⁵ RYAN CHORNOCK,⁴ JESSIE L. CHRISTIANSEN,⁶
MICHAEL W. COUGHLIN,⁷ ALEXANDER WUOLLET CRISWELL,⁸ BEHNAM DARVISH,¹ KAUSTAV K. DAS,¹ KISHALAY DE,⁹
LUC DESSART,¹⁰ DON DIXON,¹¹ BAS DORSMAN,¹² KAREEM EL-BADRY,¹³ CHRISTOPHER EVANS,¹⁴ K. E. SAAVIK FORD,¹⁵
CHRISTOFFER FREMLING,¹ BORIS T. GÄNSICKE,¹⁶ SUVI GEZARI,¹⁷ Y. GÖTBERG,¹⁸ GREGORY M. GREEN,¹⁹
MATTHEW J. GRAHAM,¹ MARIANNE HEIDA,²⁰ ANNA Y. Q. HO,²¹ AMRUTA D. JAODAND,¹
CHRISTOPHER M. JOHNS-KRULL,²² MANSI M. KASLIWAL,¹ MARGARET LAZZARINI,¹ WENBIN LU,²³ RAFFAELLA MARGUTTI,⁴
D. CHRISTOPHER MARTIN,¹ DANIEL CHARLES MASTERS,⁶ BARRY MCKERNAN,¹⁵ SAMAYA M. NISSANKE,¹² B. PARAZIN,²⁴
DANIEL A. PERLEY,²⁵ E. STERL PHINNEY,²⁶ ANTHONY L. PIRO,²⁷ G. RAAIJMAKERS,¹² ANTONIO C. RODRIGUEZ,¹
PETER SENCHYNA,²⁸ LEO P. SINGER,²⁹ JESSICA J. SPAKE,³⁰ KEIVAN G. STASSUN,³¹ DANIEL STERN,³² HARRY I. TEPLITZ,⁶
DANIEL R. WEISZ,⁴ AND YUHAN YAO¹

¹*Division of Physics, Mathematics, and Astronomy, California Institute of Technology, Pasadena, CA 91125, USA*

²*Joint Space-Science Institute, University of Maryland, College Park, MD 20742, USA*

³*Department of Astronomy, The University of Texas at Austin, 2515 Speedway, Stop C1400, Austin, TX 78712, USA*

⁴*Department of Astronomy, University of California, Berkeley, CA 94720-3411, USA*

⁵*Astrophysics Science Division, NASA Goddard Space Flight Center, 8800 Greenbelt Road, Greenbelt, MD 20771, USA*

⁶*IPAC, California Institute of Technology, Pasadena, CA 91125, USA*

⁷*School of Physics and Astronomy, University of Minnesota, Minneapolis, MN 55455, USA*

⁸*University of Minnesota, Minneapolis, MN 55455, USA*

⁹*MIT-Kavli Institute for Astrophysics and Space Research, 77 Massachusetts Ave., Cambridge, MA 02139, USA*

¹⁰*Institut d'Astrophysique de Paris, CNRS-Sorbonne Université, 98 bis boulevard Arago, F-75014 Paris, France*

¹¹*Vanderbilt University, Nashville, TN 37235, USA*

¹²*GRAPPA, University of Amsterdam, Science Park 904, 1098 XH Amsterdam, Netherlands*

¹³*Center for Astrophysics | Harvard & Smithsonian, 60 Garden Street, Cambridge, MA 02138, USA*

¹⁴*UK Astronomy Technology Centre, Royal Observatory, Blackford Hill, Edinburgh, EH9 3HJ, UK*

¹⁵*Department of Science, CUNY Borough of Manhattan Community College, 199 Chambers Street, New York, NY 10007, USA*

¹⁶*Department of Physics, University of Warwick, Coventry, CV4 7AL, UK*

¹⁷*Space Telescope Science Institute, 3700 San Martin Drive, Baltimore, MD 21218, USA*

¹⁸*The Observatories of the Carnegie Institution for Science, 813 Santa Barbara Street, CA 91101, USA*

¹⁹*Max Planck Institute for Astronomy, D-69117 Heidelberg, Germany*

²⁰*ESO, Karl-Schwarzschild-Str 2, 85748 Garching b. München, Germany*

²¹*Miller Institute for Basic Research in Science, 468 Donner Lab, Berkeley, CA 94720, USA*

²²*Department of Physics & Astronomy, Rice University, 6100 Main St., Houston, TX, USA*

²³*Department of Astrophysical Sciences, Princeton University, Princeton, NJ 08544, USA*

²⁴*Northeastern University, Boston, MA 02115, USA*

²⁵*Astrophysics Research Institute, Liverpool John Moores University, IC2, Liverpool Science Park, Liverpool L3 5RF, UK*

²⁶*Theoretical Astrophysics, 350-17 Caltech, Pasadena, CA 91125, USA*

²⁷*The Observatories of the Carnegie Institution for Science, 813 Santa Barbara St., Pasadena, CA 91101, USA*

²⁸*The Observatories of the Carnegie Institution for Science, 813 Santa Barbara Street, Pasadena, CA 91101, USA*

²⁹*Astroparticle Physics Laboratory, NASA Goddard Space Flight Center, Code 661, Greenbelt, MD 20771, USA*

³⁰*Division of Geological and Planetary Sciences, California Institute of Technology, Pasadena, CA 91125, USA*

³¹*Department of Physics and Astronomy, Vanderbilt University, Nashville, TN 37235, USA*

³²*Jet Propulsion Laboratory, California Institute of Technology, 4800 Oak Grove Drive, Pasadena, CA 91109, USA*

ABSTRACT

The *Ultraviolet Explorer (UVEX)* will undertake a synoptic survey of the entire sky in near-UV (NUV) and far-UV (FUV) bands, probing the dynamic FUV and NUV universe, as well as perform a modern, all-sky imaging survey that reaches ≥ 50 times deeper than *GALEX*. Combined with a powerful broadband spectroscopic capability and timely response to target of opportunity discoveries, *UVEX* will address fundamental questions from the NASA Astrophysics Roadmap and the Astro2020 Decadal Survey, enabling unique and important studies across the breadth of astrophysics. Imaging and spectroscopic surveys with *UVEX* will probe key aspects of the evolution of galaxies by understanding how star formation and stellar evolution at low metallicities affect the growth and evolution of low-metallicity, low-mass galaxies in the local universe. Such galaxies contain half the mass in the local universe, and are analogs for the first galaxies, but observed at distances that make them accessible to detailed study. The *UVEX* time-domain surveys and prompt spectroscopic follow-up capability will probe the environments, energetics, and emission processes in the early aftermaths of gravitational wave-discovered compact object mergers, discover hot, fast UV transients, and diagnose the early stages of explosive phenomena. *UVEX* will become a key community resource by filling a gap in the new generation of wide-field, sensitive optical and infrared surveys provided by the Rubin, *Euclid*, and *Roman* observatories. We discuss the scientific potential of *UVEX*, including unique studies *UVEX* will enable for studying exoplanet atmospheres, hot stars, explosive phenomena, black holes, and galaxy evolution.

Keywords: surveys — ultraviolet: galaxies — ultraviolet: stars — ultraviolet: general — instrumentation: photometers — instrumentation: spectrographs

1. INTRODUCTION

Each band in the electromagnetic (EM) spectrum offers unique insights into our Universe. The ultraviolet (UV) is the band in which the hottest objects shine. This group includes not just the hottest stars but also radiation from accreting sources such as cataclysmic variables and active galactic nuclei (AGN) and emission from shocks. The hottest stars include not just massive stars but also sub-dwarfs, white dwarfs and common-envelope systems. The resulting UV radiation provides all the ionizing photons and dominates the energy input into the interstellar medium (ISM).

Relatedly, the UV band is ideally suited to the study of young explosive phenomena. The temperature of the ejecta falls monotonically with time (and could be reheated by subsequent radioactive heating or power provided by an engine). At the same time, the radius of the emitting region increases with time and the luminosity increases. X-ray emission is short lived. The emission first peaks in the UV before it peaks in the optical. Thus, UV observations not only provide physical diagnostics on progenitor timescales but act as a “sentinel” to trigger prompt follow-up observations by ground-based optical facilities.

At optical wavelengths the atmosphere is largely transparent. This transparency made it possible for optical investigation of the heavens. However, atmospheric attenuation increases rapidly as one proceeds to shorter (and longer) wavelengths. Molecules in the atmosphere strongly absorb short wavelength light, par-

ticularly ozone which has strong bands at 2000-3200 Å and molecular oxygen at shorter wavelengths. The absorption of solar radiation results in local atmospheric heating of the stratosphere (ozone) and thermosphere (oxygen). Wavelengths below 3200 Å are referred to as the vacuum UV and, as inferred from the designation, celestial UV radiation cannot be observed by ground-based telescopes. UV astronomy had to await the space age.

Absorption of UV photons is due to strong (“allowed”) ground state (“resonance”) transitions of atoms, ions, and molecules. Inversely, spectroscopic UV studies offer the most direct way to study the ISM (atoms, ions, and molecules). The Universe is exceedingly opaque for wavelengths below 912 Å (photon energy 13.6 eV), becoming optically thin in the X-ray band ($\gtrsim 100$ eV). The definitions of UV bands historically has depended, in great part, upon instrumental considerations (e.g., coatings and detectors). In this paper we term the band defined by the wavelength range 2000–3200 Å as the near-UV (NUV) and the band defined by 1300–2000 Å as the far-UV (FUV). The blue cutoff of the FUV band is dictated by the Ly α background that bathes not just the Earth but also the entire Solar System. The radiation arises from scattering of solar Ly α photons by hydrogen atoms in the exosphere of Earth and by the very local interstellar cloud that the Solar System is plunging into (see Kulkarni 2021 and references therein). Imaging missions in low-Earth orbit (LEO; e.g., *GALEX*) are plagued by bright oxygen lines (see discussion in §1.2).

For LEO missions the blue edge of the FUV band is longward of 1350 Å.

Sometimes the band defined by the Lyman edge (912 Å) and Lyman- α (1216 Å) is referred to as the Lyman band. This is a highly desirable band because it includes lines from hydrogen – the most abundant element in the Universe. Furthermore, the Hot Ionized Medium (HIM; temperature $\sim 10^6$ K) is probed by lines of O VI and O VII which lie in this band. However, it is a technically challenging band to study in the nearby Universe because of the lack of high efficiency coatings, as well as the challenge of producing high-efficiency detectors. The principal orbital missions to observe in this range were *Copernicus* (Rogerson et al. 1973) and the *Far Ultraviolet Spectroscopic Explorer* (*FUSE*; Sahnou et al. 2000).

Above we summarized the diagnostic power provided by UV observations. We next summarize the methodological advantages of the UV band.

1.1. Bonanza of Resonance Lines

In the now standard reference for the ISM, Draine (2011), the author notes, with some apparent sorrow, the simple fact that there are very few resonance lines in the optical band (see § 9.10 of that reference). It is simply a consequence of the elemental abundance and atomic physics that most of the “strong” (resonance) lines lie in the UV, particularly the FUV. For instance, three dominant metals have strong resonance lines (2s \rightarrow 2p) in the FUV, which conveniently probe a range of temperatures (Sutherland & Dopita 1993): C IV ($\lambda\lambda$ 1548.2, 1550.8 Å; 1×10^5 K), N V ($\lambda\lambda$ 1242.8, 1238.8 Å; 2×10^5 K) and O VI ($\lambda\lambda$ 1037.6, 1031.9 Å; 3×10^5 K). Next, the elemental abundances are best obtained from ground-state transitions (i.e., resonance lines). Only a few resonance lines (Na I, Al I, K I, Ca I, Ca II, Ti I, Ti II) lie in the optical band.

Unfortunately, owing to their low ionization potential, most of these lines are minority species in the diffuse ISM. The far-IR fine structure lines (FSLs) are, on energetic grounds, well suited to the study of the cooler phases of the Galactic ISM, e.g., the 157.7 μ m line of C II. However, large and cooled space telescopes are needed to study diffuse ISM via FSLs. *Copernicus*, one of the earliest space FUV missions, made fundamental advances in this field by studying the FSLs via high resolution FUV spectroscopy. UV spectroscopy is also well suited to the study of molecules, e.g, the electronic transitions of H₂. For gas above 10^6 K, the line tracers (e.g., lines of highly ionized oxygen) lie in the Lyman band and the less accessible EUV band. Figure 1 pro-

vides a graphical summary of the uniqueness of FUV spectroscopy.

1.2. Low(est) Background

The deepest astronomical observations are limited by backgrounds. Ground-based observatories, far away from urban centers and on a clear New Moon night, are limited by the glow produced in the atmosphere. The *Hubble Space Telescope* (*HST*) is well above most of the atmosphere. The primary background to *HST* is due to reflection of solar light by dust in the ecliptic plane, i.e., zodiacal light. There is some line emission from atomic oxygen in the thermosphere; see the Space Telescope Imaging Spectrograph (STIS) instrument handbook¹ for further details. The background is graphically summarized in Figure 2.

Since the Sun is not bright in the UV, the zodiacal light background decreases dramatically in the UV, particularly in the FUV. As a result, of all the UV-optical-IR bands, the FUV band is the darkest and as such is exceptionally well suited for detecting low surface brightness objects (O’Connell 1987). Indeed, this was demonstrated by the *GALEX* detection of star-forming regions in the outer regions of galaxies (e.g., Barnes et al. 2011). Note that, in contrast, the NUV sky background continues to be dominated by zodiacal light.

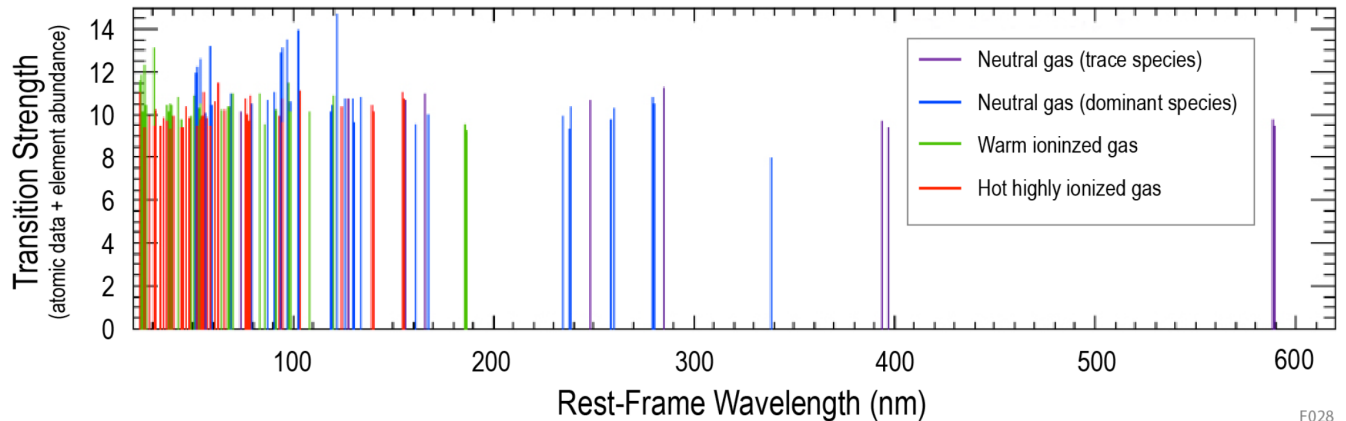
HST is in LEO. In contrast, the first major UV facility, the *International UV Explorer* (*IUE*), was located in a geo-synchronous orbit (GEO). In GEO there is no airglow emission and geo-coronal Ly α emission is significantly reduced. As a result, the FUV background is not only low but also very stable for missions in GEO.

2. PAST & FUTURE UV MISSIONS

The early history of the development of UV astronomy is beautifully captured in an informal biography of the UV astronomer Blair Savage.² The foundation of modern UV astronomy (including *HST*, in part) can be traced to *Stratoscope-I*, *Stratoscope-II* and the *Orbital Astronomical Observatory* (*OA*O) series. *OA*O-2 (1968–1973), by undertaking low-resolution FUV and NUV spectroscopy of a wide range of astronomical objects, dramatically showcased the great diagnostic power of UV spectroscopy. *OA*O-B carried a large 38-inch (97-cm) UV telescope optimized for spectroscopy of fainter objects. At that point in time this was the largest telescope NASA had built. Unfortunately, the fairing separation was not successful. *OA*O-3 (1972–1981; later re-

¹ <https://hst-docs.stsci.edu/hom>

² <https://ecuip.lib.uchicago.edu/multiwavelength-astronomy/ultraviolet/history/index.html>



F028

Figure 1. The strength (the product of the oscillator strength and the relative cosmic abundance) of resonance lines of elements (atoms, ions) as a function of rest wavelength. From Tripp (2019).

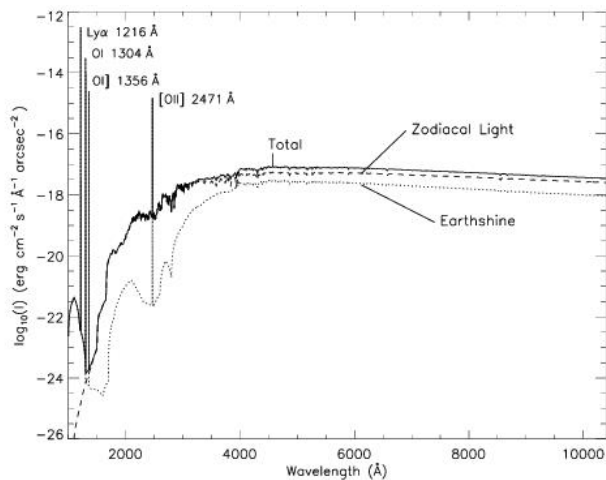


Figure 2. *HST* sky background intensity as a function of wavelength (Figure 6.1 of the STIS Instrument Handbook). The zodiacal contribution depends on the helio-ecliptic latitude and longitude. What is displayed is a “high” value. The geo-coronal airglow line intensities are plotted at “average” intensities and carry the unit of $\text{erg cm}^{-2} \text{s}^{-1} \text{arcsec}^{-2}$.

named *Copernicus*) undertook high spectral resolution absorption FUV spectroscopy of the diffuse ISM and laid the foundation for modern studies of the diffuse ISM. It may be of interest for the reader to learn that Nancy Grace Roman oversaw the *OAO* series.

We next summarize past UV missions which undertook sky surveys and follow it with the upcoming UV missions with launch dates in this decade. In order to qualify for the monicker of “sky survey”, we require a coverage of no less than $10,000 \text{ deg}^2$.

2.1. Sky Surveys: Past Missions

Brosch (1999) provides a comprehensive survey of past UV missions with a focus on sky surveys. The first UV sky survey was undertaken by the *TD-1A* mis-

sion over the period 1972–1974. Arguably *TD-1A* was the European Space Agency’s first astronomical mission.³ The three-axis stabilized spacecraft was placed in a low-Earth Sun-synchronous orbit. The two main experiments were S2/68, a spectrophotometric sky survey telescope (Boksenberg et al. 1973) and S59, the “Utrecht Orbiting UV Stellar Spectrometer”; de Jager et al. 1974). S2/68, managed by researchers at University College London, United Kingdom and the University of Liege, Belgium, consisted of an $f/3.5$ off-axis 27.5-cm paraboloid with a three-channel grating spectrometer covering the range 1350–2550 Å and a one-channel photometer centered on 2750 Å and a full width at half maximum (FWHM) of 310 Å (Boksenberg et al. 1973). This experiment resulted in the first sky survey of the NUV and FUV sky. The resulting catalog of 31,215 stars⁴ consisted of absolute fluxes in four passbands (2740 Å, 2365 Å, 1965 Å and 1565 Å). Great attention was paid to calibration and the resulting catalog served as absolute calibration system for NUV and FUV astronomy (Humphries et al. 1976). The S59 experiment obtained, over the duration of the mission, low-resolution spectra of the 200 brightest stars in three NUV bands (de Jager et al. 1975; van der Hucht et al. 1976).

³ In the sixties, a group of European countries formed two organizations: the European Space Research Organisation (ESRO) and the European Launcher Development Organisation (ELDO). Europe, post war, lacked capability in space and therefore used an American launcher, specifically, the Thor-Delta. Of the trio *TD-1A, B, C* missions envisaged by ESRO, only *TD-1A* was launched. ESRO and ELDO merged in 1972 to form the modern European Space Agency (ESA).

⁴ All un-reddened stars earlier than B and brighter than $V \approx 10$, the limiting magnitude of the classical Henry Draper optical spectral catalog; see <https://heasarc.gsfc.nasa.gov/W3Browse/all/td1.html>

Subsequent missions were primarily follow-up missions (e.g. *ANS*) or small field-of-view (FOV) missions. *IUE* launched into GEO in 1978 with a great complement of spectrographs and an orbit that provided high observing efficiency and a low FUV background, making the mission a stunning success.

However, it took three decades for the next all-sky UV missions, both launched in 2003. The *Galaxy Evolution Explorer* (*GALEX*) carried a 50-cm telescope equipped with micro-channel detectors and surveyed the sky simultaneously in the NUV (1750–2750 Å) and the FUV (1350–1750 Å) bands. The all-sky survey had a sensitivity of m_{AB} of 20.5, comparable to that of the Palomar Observatory Sky Survey (m_{AB} of 21). The angular resolution of *GALEX* was 5'' (FWHM) and the astrometry was good to 1''. The Korean satellite STSAT-1 carried, amongst other instruments, the “Far Ultraviolet Imaging Spectrograph” (*FIMS*) with a long (between 4° and 7°, depending on the channel) and wide (about 5 arcmin) slit and operated in the wavelength range 900–1750 Å [Edelstein et al. \(2006\)](#). The mission was optimized for spectroscopy of the Hot Ionized Medium ([Jo et al. 2017](#)), the diffuse continuum ([Seon et al. 2011](#)) and molecular hydrogen fluorescence ([Jo et al. 2019](#)).

2.2. Missions Under Development

2.2.1. Chinese Space Station Telescope (CSST)

The *Chinese Space Station Telescope* (*CSST*) project is based on a 2-m telescope equipped with an imager with six filters (NUV 2550–3200 Å and *ugriz* optical bands) and a slitless spectrograph covering the entire 1.1 deg² FOV ([Zhan 2018](#)). The project is optimized for cosmology ([Gong et al. 2019](#)) and as such images only high latitude regions; $|b| > 20^\circ$ will be covered by the imaging and slitless survey. Deeper exposures of a dozen well known fields (e.g., COSMOS, GOODS-N) with a total area of 400 deg² will also be undertaken. The 10-year duration mission is expected to be launched in 2023.

2.2.2. Spektr-UF (World Space Observatory)

The *Spektr-UF* (aka *World Space Observatory-UV*, *WSO-UV*) is a Russia-led mission ([Shustov et al. 2018](#)). It is the third in series of the Spektr family: *Spektr-R* (key component of the RadioAstron program) and *Spektr-RG* (*Spektr-Röntgen Gamma* or *SRG*; currently in operation). It is based on a 1.7-m Ritchey-Chrétien telescope in GEO, similar to *IUE*. *Spektr-UF* is primarily for detailed studies of astronomical objects. The mission is scheduled for launch in 2025.

The mission carries three spectrographs (high resolution FUV, high resolution NUV, and low resolution NUV+FUV) and two cameras with high angular resolution (FUV camera and NUV+optical camera). The

high resolution ($R \approx 50,000$) FUV spectrometer will be an able replacement to similar capabilities of the Cosmic Origin Spectrograph (COS). The low-resolution ($R \sim 1000$) Long Slit Spectrograph (LSS) will provide spectroscopy in the 1150–3050 Å wavelength range, with a spatial resolution between 0.1'' and 0.5''. The effective area of LSS is $\sim 2 \times 10^3$ cm² in the NUV and $\sim 5 \times 10^2$ cm² in the FUV (see Figure 4 in [Shustov et al. 2018](#)). The throughput⁵ at the center of the LSS band is 26%, which is comparable to the *UVEX* spectrograph throughput of 25% at ~ 1550 Å.

2.2.3. ULTRASAT

*ULTRASAT*⁶ is a NUV imaging space mission developed under the scientific leadership of the Weizmann Institute of Science with the primary goal of studying the hot transient and variable universe ([Sagiv et al. 2014](#)). The expected launch date is in 2025. The satellite carries a wide-field Schmidt telescope with a clear aperture of 33 cm. *ULTRASAT* will observe in the NUV (2200–2800 Å) with a wide FOV of 200 deg². The camera is equipped with a mosaic of four backside-illuminated Complementary metal-oxide-semiconductor (CMOS) detectors and will reach a sensitivity of ~ 22.3 mag (AB; 5σ) in 3×300 s exposures ([Asif et al. 2021](#)). *ULTRASAT* will be placed in GEO and data will be transferred to the ground in real time. Rapid data processing will allow transient alerts to be generated and distributed within 15 minutes to enable follow-up observations.

⁵ *WSO-UV* User’s Handbook https://wso-jcuva.ucm.es/WSO_UsersBook_rev.es.pdf

⁶ <https://www.weizmann.ac.il/ultrasat/>

Table 1. UV Surveys

Mission	Orbit	Ω	5σ (NUV)	5σ (FUV)
		deg ²	AB	AB
<i>TD-1A</i>	LEO	All Sky	5.7	6.2
<i>GALEX</i>	LEO	< 25,000	20.8	19.9
<i>CSST</i>	LEO	17,500	25.5	-
<i>ULTRASAT</i>	GEO	All Sky	22.3	-
<i>UVEX</i>	HEO	All Sky	25.0	25.0

NOTE—For the *TD-1A* mission, the sensitivity was inferred using the Thompson et al. (1978) catalog, considering the passbands centered at 2740Å for the NUV and 1565Å for the FUV. The exposure time assumed for *ULTRASAT* is 900s. The *GALEX* exposure time is 100s for the All-Sky Imaging Survey (Morrissey et al. 2007). The *UVEX* depths listed are the requirement depths; the estimated all-sky depths are 25.8 in both bands.

2.2.4. *CASTOR*

The *Cosmological Advanced Survey Telescope for Optical and UV Research (CASTOR)* is a proposed mission to perform high-resolution imaging and spectroscopy in UV and blue-optical bands.⁷ The mission recently completed a science maturation study funded by the Canadian Space Agency and is led by a network of Canadian universities and international partners, including JPL, the Indian Space Research Organization, and the United Kingdom Space Agency. The principal mode for *CASTOR* is wide-field imaging: with its 1-m off-axis telescope, it will deliver high-resolution images (FWHM=0.15") over a 0.25 deg² FOV in three photometric passbands, NUV (1500–3000Å), *u'* (3000–4000Å) and *g* (4000–5500Å). Additional modes are currently under development: a full-field low-resolution ($R=300-420$) spectroscopy mode in the NUV and *u'* channel with a grism, and a multi-slit medium resolution ($R=1000-2000$) NUV spectroscopy mode in a parallel small field. Planned for Sun-synchronous, dawn-dusk LEO, *CASTOR* has a baseline lifetime of five years, of which roughly two years will be dedicated to a “primary survey” of 7700 deg², defined by the overlap of the Rubin, *Euclid*, and *Roman* footprints, reaching a depth of $m_{AB} = 27.2$. The mission ranked the highest priority in the Canadian Long Range Plan in 2021.

2.3. A modern NUV & FUV Sky Survey

⁷ <https://www.castormission.org/>

Sky surveys constitute the blood of astronomy. These surveys give us a view into the Universe, limited only by the band of observations. As noted earlier, each band carries information – both unique and supporting other bands. There continues to be steady progress in sky surveys across the electromagnetic band. At optical wavelengths, PanSTARSS-1 (PS-1) concluded a survey of the optical sky visible from Hawaii. PS-1 represented a factor of ten jump relative to that of the Palomar Observatory Sky Survey. *SRG*, the Russian-German X-ray mission, is currently obtaining cadenced all-sky survey observations in the X-ray band (Sunyaev et al. 2021). The *SRG* eROSITA survey will be thirty times more sensitive than *ROSAT*, the previous defining X-ray all-sky survey. At radio (decimetric) wavelengths, VLA, ASKAP and MeerKAT have begun sky surveys. LOFAR will shortly complete an exquisite survey of the Northern sky in the meter-wave bands. In a couple of years, the forthcoming decade-long Legacy of Space and Time Survey (LSST) of the Vera Rubin Observatory will go ten times fainter than PS-1. In space, the Roman Telescope and Euclid will undertake ultra-deep NIR surveys.

GALEX was the last UV wide-area survey. It was matched to the Palomar sky survey (undertaken during the eighties and nineties of the previous century). Clearly, a UV all-sky survey matched to PS-1 would be timely and strategic. In the next section we summarize a proposed FUV and NUV imaging and spectroscopic mission which will handsomely match PS-1 and have the ability to undertake deep observations of selected regions with sensitivity matched to that of LSST.

3. UVEX: ULTRAVIOLET EXPLORER

GALEX and *FIMS* were both launched in 2003. The technology of these missions was that available in the nineties. Over the past thirty years there have been great advances in UV technology: designer high-efficiency coatings and large-format semiconductor detectors with nearly unit quantum efficiency (representing an order of magnitude improvement over the photoelectric detectors of *GALEX*). Next, as discussed in the previous section and dramatically illustrated in Figure 1, spectroscopy, particularly in the FUV band offers unique diagnostics of hot gas, be it from stars or accretion disks. Thus, an essential part of a modern UV mission would not only include exquisite imaging but also carry a sensitive spectrograph for the study of hot objects and explosive events. A study of the literature shows that the low resolution spectroscopy provided by COS/G140L on the Cosmic Origin Spectrograph is very well suited to this purpose.

These motivations led us to propose the “*Ultraviolet Explorer*” (*UVEX*). This FUV and NUV imaging and spectroscopic mission, located in high-Earth orbit (HEO), will undertake a full-sky survey in NUV and FUV bands and conduct spectroscopic studies of large samples to study the hot Universe and diagnose the ISM. The planned low latency allows for rapid response to events in the sky such as searching for early UV emission from neutron star coalescences and dissecting supernovae which are only a few hours old. The high efficiency of the spectrograph makes it possible to study well defined samples of static objects (hot stars, galaxies, AGN and so on). Below we summarize the key expected performance metrics of the mission.

3.1. *UVEX Instrument*

The novel *UVEX* instrument is designed to provide high-cadence, wide FOV imaging in two UV bands, simultaneous with moderate-resolution, long-slit spectroscopy from the FUV to the NUV. The instrument is capable of operating over a wide field-of-regard to enable rapid response target-of-opportunity (ToO) observations of transient and multi-messenger sources (§7 and §10). A summary of key instrument properties is provided in Table 2.

The telescope employs a standard all-reflective three-mirror anastigmat design, with an effective aperture of 75 cm. Light from the $3.5^\circ \times 3.5^\circ$ imaging FOV is sent through a dichroic beamsplitter, allowing simultaneous imaging in both FUV (1390–1900 Å) and NUV (2030–2700 Å) bands over this entire sky area. For offset spectroscopy, light bypasses the dichroic and is transmitted through a 1° long slit, with variable (but fixed) widths ranging from $2''$ to $16''$. A grating disperses the light, with resulting spectral resolution ranging from $R \sim 1600$ at 1150 Å to $R \sim 3500$ at 2750 Å (for the portion of the slit with $2''$ width).

The FUV and NUV imaging channels are both fed to 3×3 CMOS focal plane arrays, while light for the long-slit spectrograph is dispersed onto a single CMOS detector. All the sensors and their modular readout electronics are identical, but have individualized coatings for out-of-band light suppression.

3.2. *Layout of the paper*

This paper is primarily focused on the rich science returns from *UVEX*. If approved, the launch date will be towards the end of 2027. By then, the Vera Rubin Observatory will be in routine operation. Ground-based high-cadenced optical and NIR time domain surveys will continue to flourish. The sensitivity of gravitational wave (GW) astronomical facilities is expected to

Table 2. *UVEX* Instrument Overview

Instrument Characteristics	Value
Effective Aperture	75 cm
Focal Length / $f\#$	200 cm / 2.7
Imaging FOV	$3.5^\circ \times 3.5^\circ$
Imaging PSF (HPD)	$\leq 2.25''$
FUV Channel Bandpass	1390–1900 Å
NUV Channel Bandpass	2030–2700 Å
FUV Channel Sensitivity	24.5 mag (AB)
NUV Channel Sensitivity	24.5 mag (AB)
Spectrometer Slit Dimensions	$1^\circ \times (2\text{--}16)''$
Spectrometer Band	1150–2650 Å
Spectrometer Resolution	1600–3500
Spectrometer Effective Area	825 cm ²

NOTE—The imaging point spread function (PSF) listed value is the half-power diameter (HPD). Imaging sensitivity estimates correspond to a 5σ point source detection in a single “dwell” of ~ 900 s in a field with average background levels. The effective area of the spectrometer is estimated at a wavelength of 1660 Å.

increase by leaps and bounds over this period. In short, astronomers can look forward to an exciting decade. *UVEX* will be well positioned to serve the astronomical community across the entire gamut of fields of investigation. Below, in successive sections, we summarize possible advances that *UVEX* can contribute to: Stellar Astronomy (§4), The Magellanic Clouds & the Milky Way (§5), Galaxy Formation (§6), Cosmic Explosions (§7), Active Galactic Nuclei (§8), Tidal Disruption Events (§9), Multi-messenger Astronomy: Gravitational Wave Astronomy & High-energy neutrino astronomy (§10), and Exoplanets (§11).

4. STELLAR ASTRONOMY

In the previous century, astronomers developed basic understanding of (single) star formation through stellar death and separately were able to explain how, as a result of stellar nuclear synthesis and stellar outflows (winds, explosions) the periodic table was populated with “metals” (elements other than hydrogen and helium). With the foundations thus established, in this century, astronomers are addressing the next level(s) of complexity due to (1) binarity and (2) metallicity. It turns out that 50–70% of stars in the Universe are in binary systems with this fraction reaching unity for the most massive stars. For some fraction of these systems, as each of the stars evolve, mass can be lost from one

star and gained by the other star. The result, in most cases, is a “common envelope event” in which one star plunges into the envelope of the other star and forms a tight binary consisting of the core of that star and the companion. The possibilities of outcome (“phase space”) determined by the masses of the two stars and the orbital parameters (separation, eccentricity, mutual inclination) is exceedingly large. Add to that the complexity of poorly understood processes (e.g., common envelope evolution, impact of metallicity). In Figure 3, we display some of the key evolutionary pathways. Observations are key to making progress in this field. Here, we focus on systems with at least one white dwarf – the most common type of evolved binaries.

Even for single stars, the evolution of a star depends on not just the mass but metallicity and rotation. Mass loss from stars, particularly that from massive stars, is a critical player affecting the global ecology of a galaxy. It is clear that mass loss is directly tied to metallicity. However, our understanding of this important physical process is, at the present time, poor. Observations are needed to make further progress.

In terms of metallicity, the Sun is an average star in the Milky Way and we live in an average neighborhood. The frontier now lies in understanding star formation at low metallicity. This is interesting in its own right and has the great benefit of being relevant to star formation in the young Universe. To this end, the Magellanic Clouds have metallicities of 10–20% and 40–50% relative to the Sun⁸ for the Small Magellanic Cloud (SMC) and Large Magellanic Cloud (LMC), respectively (e.g., [McConnachie 2012](#)). These offer convenient nearby laboratories for the study of star formation and stellar evolution that are representative—in at least one very important aspect—of the early Universe.

In the following sections, we describe specific scientific programs with *UVEX* that will enable these broad goals and objectives. First, we discuss the opportunity to probe the physics of accretion in both the star-formation context (§ 4.1) and in the context of outflows from accreting compact objects (§ 4.2) and classical novae (§ 4.3), and the most common type of evolved binaries: ones hosting at least one white dwarf (§4.4). We end with a discussion of angular momentum evolution of evolved stars (§ 4.5).

4.1. Star Formation and Accretion

Stars first become visible in the optical and UV during the later stages of their formation when the newly formed protostar is present, surrounded by an active accretion disk. It is in these disks that planets form and accrete their initial atmospheres. The stars themselves are very magnetically active, showing kilogauss level average surface magnetic fields ([Johns-Krull 2007](#)), presumably due to vigorous dynamo activity resulting from relatively rapidly rotating stars which are either fully convective or nearly so. As the disks dissipate, leaving a planetary system around the young stars, the UV through X-ray emissions produced by the magnetic activity drives the chemistry in the atmospheres of the young planets. While the disk is still present, these high energy emissions help determine the ionization structure and chemistry in the disk, which is important in the action of both the magneto-rotational instability (MRI; e.g., [Balbus & Hawley 1998](#)) and the formation of magneto-centrifugally driven disk winds (e.g. [Gressel et al. 2015](#)), the two main candidates producing the viscosity that leads to disk accretion onto the star. For accreting young stars, it is this accretion of disk material onto the stellar surface that is the dominant contributor to the UV and blue optical emission observed. The accretion of disk material represents the last stage in the mass assembly of newly formed stars, and generally occurs within the first 10 Myr after the star is formed (e.g., [Wyatt 2008](#)) while it is evolving along the pre-main sequence (PMS) evolutionary tracks.

The current paradigm for accretion onto young, PMS stars is magnetospheric accretion (for a recent review, see [Hartmann et al. 2016](#)). Magnetospheric accretion posits that the strong magnetic fields on the surface of young stars truncates the disk near the co-rotation radius, forcing the accreting disk material to flow along the field lines such that the material impacts the stellar surface at near free-fall velocities. Theoretical work (e.g., [Koenigl 1991](#), [Shu et al. 1994](#), [Long et al. 2005](#), [Zanni & Ferreira 2013](#), [Romanova et al. 2018](#)) suggests that the coupling between the young star’s magnetosphere and its circumstellar disk is sufficient to regulate the stellar angular velocity for the lifetime of the disk. In this so-called “disk-locking” picture, angular momentum is magnetically transferred from the star to the disk, and eventually ejected in a mass outflow, directly coupling the accretion of material onto the stellar surface with fast outflows originating from this magnetospheric boundary. This picture of magnetospheric accretion and disk locking has been developed over many years, underpinned primarily by observations from nearby star forming regions such as Taurus, rho Ophiuchus, the Upper Scorpius region and a handful of others. These regions

⁸ We list the generally accepted ranges. The exact value depends on the adopted Solar metallicity scale and abundance pattern, type of metallicity tracer (e.g., stars, nebular emission), radial variations in metallicity, etc.

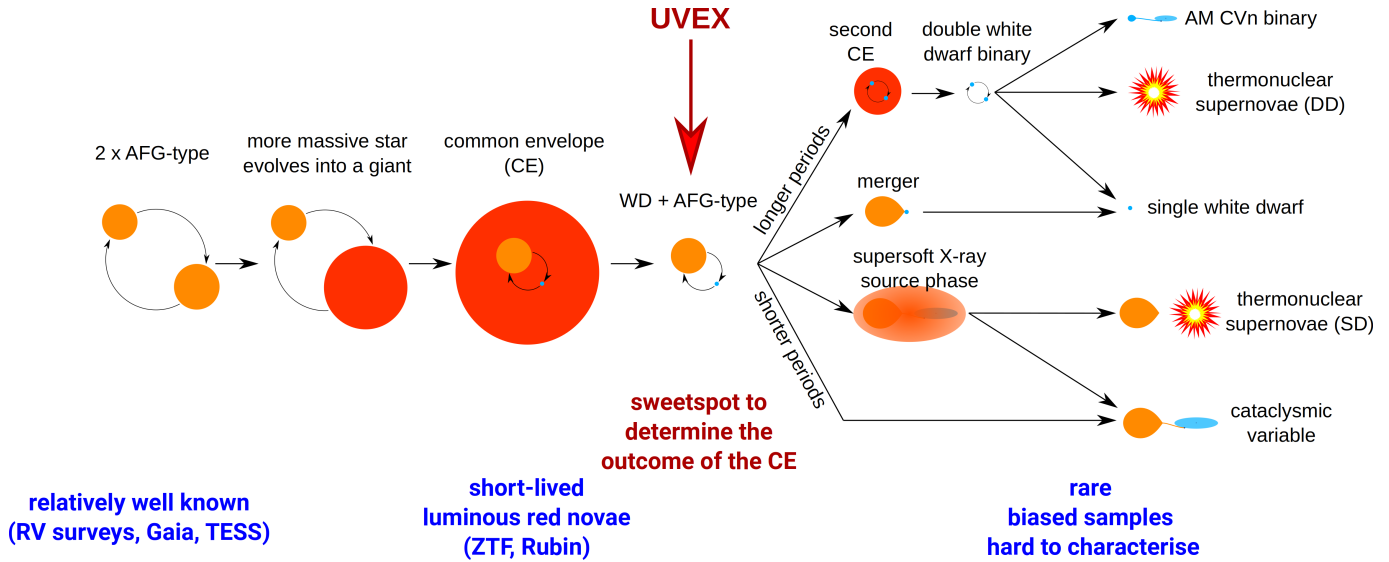


Figure 3. Schematic overview of the evolution of two AFG-type stars into a variety of compact binaries, which include low-frequency gravitational wave sources that *LISA* will detect in large numbers, and the progenitors of all types of thermonuclear supernovae, including SN Ia. The stellar masses and the orbital separation of the white dwarf + AFG-type star binaries emerging from the common envelope are determining the future evolution. *UVEX* will deliver FUV spectroscopy of ~ 250 post-common envelope WD+FGK binaries, i.e., systems within a critical phase that determines their future evolution.

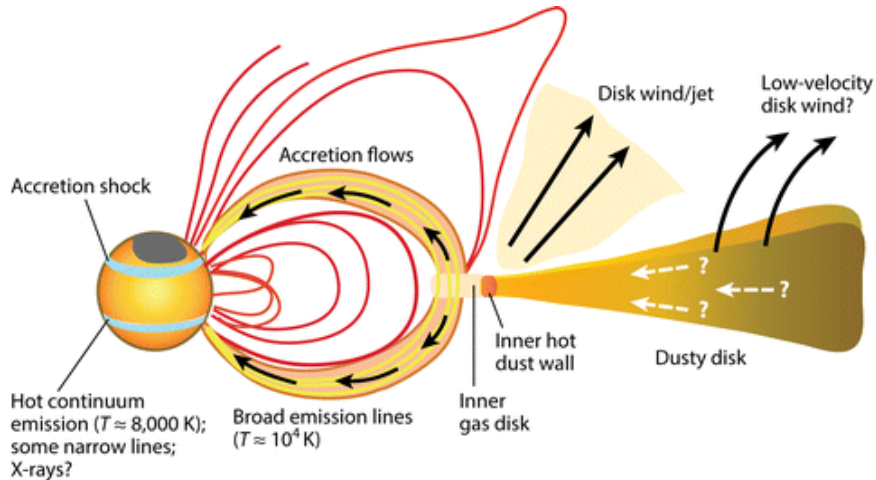


Figure 4. The close circumstellar environment of a young star (taken from Hartmann et al. 2016). Magnetospheric accretion occurs as disk material is captured by the stellar magnetic field, flowing toward the star and accreting near the stellar poles. At the base of the magnetospheric flow, the material falling at near free-fall velocities impacts the surface, creating a strong shock which produces substantial UV emission.

are generally considered low density, relatively low mass star forming regions, and they either completely lack, or have very few of, the highest mass, hottest stars (O-type stars) which produce copious amounts of ionizing radiation and strong stellar winds that have important feedback effects in the star formation process (Rosen & Krumholz 2020). Studies of the Orion Nebula Cluster (ONC) have also been significant in the development of these ideas. While higher in overall mass and containing the high-mass stars of the Trapezium in close proximity to many of the low-mass young stars in the ONC, this

region still is not representative of the highest mass star forming regions (Portegies Zwart et al. 2010).

Stars primarily form in clustered environments (Lada & Lada 2003), and the majority of stars in our Galaxy and probably most galaxies form in the most massive of these clusters (see review by Portegies Zwart et al. 2010). These environments have many O-type stars and their feedback processes are expected to have a substantial impact on the stars and planetary systems that are forming there. For example, the large flux of ionizing radiation is expected to increase the ionization in the

disk which will impact the sources of viscosity in the disk and the rate of disk accretion.

Taking both extinction and distance into consideration, perhaps the most favorable region of massive star formation for the study of feedback processes on low mass star formation and early stellar evolution is the Carina star forming complex. The Carina nebula complex (CNC) is located in the Carina spiral arm (e.g., Vallée 2014), and the CNC is one of the most active massive-star-forming regions in the Milky Way. Over 140 massive OB-stars (Alexander et al. 2016) and more than 1400 young stellar objects (Povich et al. 2011; Feigelson et al. 2011) have so far been identified in the CNC. The total number of stellar X-ray sources in Carina is $\sim 14,000$, suggesting that the CNC contains 10 times the young stellar content of the ONC (Townesley et al. 2011). The distance to the CNC, ~ 2.3 kpc, has been measured accurately using near-IR spectroscopy (e.g., Allen & Hillier 1993; Smith 2006). The number of O-stars in the CNC is comparable to that in other massive star forming regions in the Galaxy such as W43 and W51 (e.g., Blum et al. 1999; Okumura et al. 2000), but the CNC is two or three times nearer than those regions. Therefore, the CNC offers an excellent opportunity to study the physics of accretion onto newly formed low-mass stars in a region that is more representative of the regions in which most stars form. Study of the low-mass stellar population and its accretion activity will provide a unique way to uncover the role of massive star feedback on the formation and early evolution of young stars.

As shown in Figure 4, when the material accreting along the stellar magnetic fields reach the star, an accretion shock is expected to form. The material impacts the star at near free-fall velocities, which is on the order of ~ 300 km s $^{-1}$. As a result, a strong shock forms, initially heating the material up to a temperature of $\sim 10^6$ K. As the material cools and settles onto the star, its density increases and the post-shock material becomes optically thick when it reaches a temperature of $\sim 10^4$ K. As the material cools from 10^6 through 10^5 K, it is strongly emitting lines in the X-ray and UV region which can in turn heat the photosphere below and immediately around the accretion shock as shown in Figure 5. Many authors have studied the emission that result from this process (Valenti et al. 1993, Calvet & Gullbring 1998, Gullbring et al. 1998, Ingleby et al. 2013), and this work shows that the accretion-related emission dominates the stellar flux in the UV (Figure 5), making short wavelength observations the most sensitive to accretion onto young stars.

For the most strongly accreting stars, the accretion luminosity is strongly detected in the blue optical as well,

but as the accretion rate falls, NUV and FUV observations are required to make reliable accretion rate estimates for young stars. At the same time, knowledge of fundamental stellar parameters such as mass and radius are required to make these measurements, and this requires broad wavelength observations. The far red and near-IR permit the determination of stellar properties as the stellar flux dominates there (e.g., Figure 5) and the UV reveals the accretion luminosity, allowing the accretion rate to be measured.

UVEX operating with supporting ground-based facilities (e.g., Rubin, amongst other synoptic facilities) will provide the observations needed to measure accretion onto thousands of young stars in the CNC. An example of how these accretion rate determinations will be performed is shown in Figure 6 taken from Manara et al. (2012). This figure shows a two color diagram (using colors from *U* to *I*) of young stars in the ONC. Red optical and near-IR colors are used to estimate spectral types and reddening for each source. Similar data for the CNC will be available from LSST (e.g., Bonito et al. 2018) and other existing or planned ground-based surveys. The nearly vertical, thick solid line shows the locus where stars without accretion fall. The thinner white lines moving to the left and down from this locus shows where stars with differing amounts of accretion land. As shown in the Figure, many of the stars lie very close to the non-accreting locus. These stars are either not accreting at all, or accreting at levels too low to be measured using colors confined to the optical bands. Adding in FUV and NUV photometry from *UVEX* will effectively stretch this diagram out in both directions, but most importantly will stretch it in the horizontal direction, making it easier to accurately measure accretion rates and to distinguish the accretion emission from low accretion rate objects.

Fortunately the entire CNC will fit into a single pointing of *UVEX*. For comparison, the accreting young star AA Tau has a measured FUV and NUV magnitudes of 18.9 and 18.6, respectively (Findeisen & Hillenbrand 2010). If it were at the increased distance of the CNC, this star would have corresponding magnitudes of 24.9 and 24.7 in the FUV and NUV, respectively. A *UVEX* CNC survey could detect accreting young stars down to $\sim 0.3 M_{\odot}$, providing the first comprehensive study of accretion onto low-mass stars in a canonical high-mass star formation region.

GALEX did not survey this region and it did not have the sensitivity to reach the required depth. *HST* is capable of making similar observations with WFC3; however, ~ 4400 pointings would be required to cover a single *UVEX* pointing. As a result, *UVEX* is the best instru-

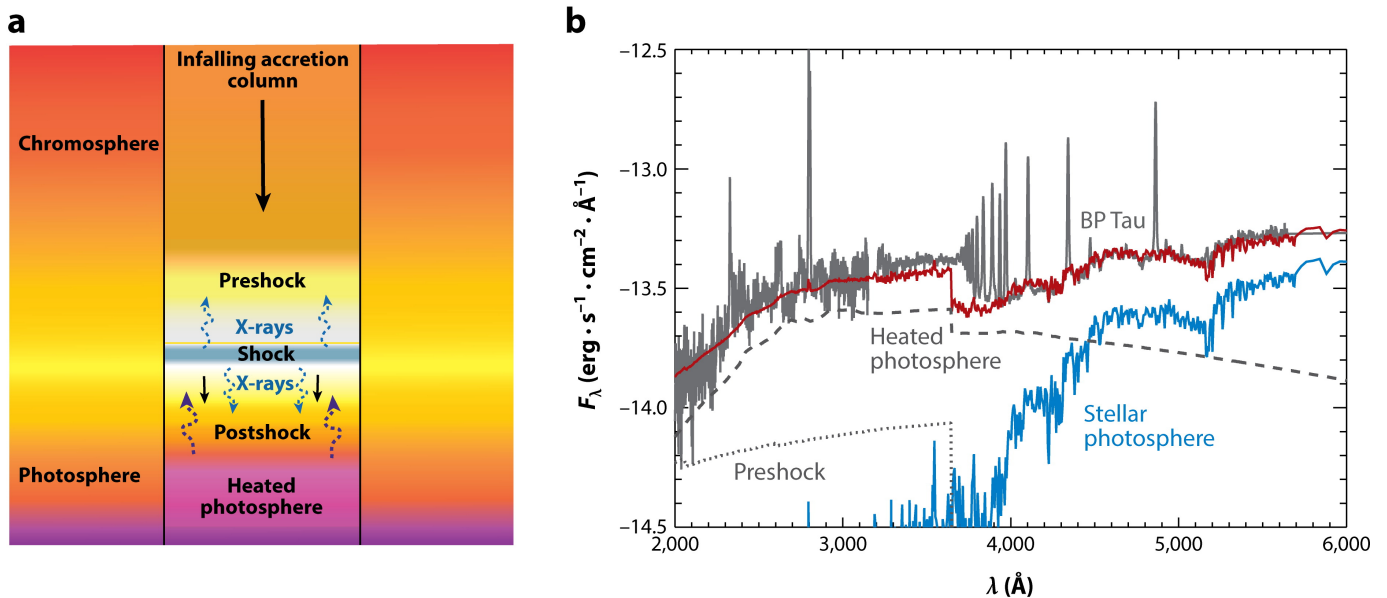


Figure 5. From Hartmann et al. (2016): (a) Schematic diagram of accretion shock structure showing the precursor or preshock region, the postshock or cooling region, and the heated photosphere below the shock. (b) Spectral energy distribution of the classical T Tauri star BP Tau (gray solid line), stellar photosphere (blue line), and accretion shock model (red line) showing contributions from the preshock (gray dotted line) and heated photosphere postshock (gray dashed line) regions.

ment to make the requisite observations to explore the role of high mass star feedback on the accretion physics of low-mass young stars.

4.2. Outflows from Accreting Compact Objects

Accretion occurs on a wide range of physical scales, from super-massive nuclear black holes to protostars. Here, we address accretion onto compact stellar objects. Galactic accreting white dwarfs (i.e., cataclysmic variables, CVs) and stellar mass black holes and neutron stars (i.e., X-ray binaries, XRBs) are excellent laboratories to study accretion processes and the accretion-ejection coupling mechanisms in great detail, across time scales suitable for human beings (Fender & Muñoz-Darias 2016). Moreover, accretion in these systems span a broad range in accretion rates, from 10^{-5} – 10^2 times the Eddington rate.

Most accreting stellar remnants spend the majority of their time in a quiescent state, punctuated by outbursts lasting a few days to months. Massive outflows are launched during those outbursts, which play an important role in the evolution of these systems. UV observations provide a unique window on these outflows. In this section, we focus on two distinct types of outbursts, each with their own phenomenology and open questions. In § 4.2.1, we discuss outbursts caused by the disk instability mechanism. These occur in a subset of CVs called dwarf novae (DNe) and in most XRBs that accrete material through Roche lobe overflow; the latter mainly occur in low-mass X-ray binaries (LMXBs). In

these systems, outflows in the shape of disk winds are launched in certain stages of the outbursts and actually carry away most of the material transferred from the donor star. In § 4.3, we discuss classical novae, outbursts driven by runaway thermonuclear burning of hydrogen accreted onto the surface of a white dwarf. While it has long been thought that the optical emission from classical novae was due directly to this hydrogen burning, it is now understood that the emission is actually from shocks caused by colliding outflows from the CV. Understanding these shocks may help us better understand shock-powered supernovae such as SN II_n. *UVEX* ToO observations of LMXBs, DNe, and nova outbursts will allow us to study accretion disc winds and outflows in unprecedented detail.

4.2.1. Dwarf novae and LMXB outbursts: accretion disc winds

DNe and LMXB outbursts are fundamentally driven by the same mechanism. Due to the compactness of neutron stars and black holes compared to white dwarfs, the accretion disk of LMXBs radiates primarily in the X-rays, while CVs radiate primarily in the UV. But both LMXB outbursts and DNe are explained by the disk instability model (DIM; for a review see Hameury 2020). In these systems, mass is transferred at a relatively constant rate from a non-degenerate donor star through Roche lobe overflow onto an accretion disk around the compact object. In quiescence, the mass transfer rate through the disk onto the compact object is low, the

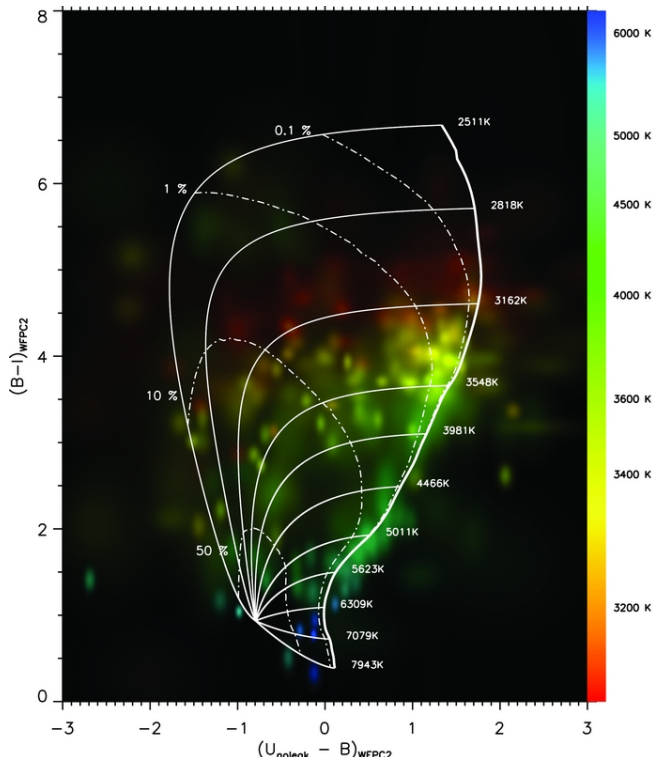


Figure 6. From Manara et al. (2012): Two color diagram of stars in the ONC. Each source has been corrected for extinction and represented as a normalized 2D Gaussian, corresponding to the photometric errors. Sources are color-coded according to their T_{eff} (scale at right). Thick line represents the calibrated isochrone for no accretion; thin lines represent the simulated displacements (for different T_{eff}) from the photospheric colors, obtained by adding an increasing amount of a model of the accretion luminosity analogous to that shown in Figure 5.

disk itself is cold and not ionized, and the system is faint. In this state, matter builds up in the disk and the temperature rises, until a critical point is reached and an outburst starts. In outburst, the mass transfer rate through the disk is greatly increased and the disk itself is extremely bright.

Although the DIM works well in explaining the basic properties of these outbursts, it is clear that more ingredients are necessary to match the observations, most importantly irradiation of the disk and outflows. Powerful disk winds are launched in the high state of these outbursts (Fender & Belloni 2004) and these winds carry away a significant amount of mass and angular momentum. Indeed, most of the transferred mass from the star never gets accreted onto the compact object. In this way, winds can fundamentally change the evolution of these systems.

The wind launching mechanisms for both XRBs and DNe are still very poorly understood. Line-driven winds

are one of the candidates (Proga & Kallman 2002), especially for disk winds in XRBs with high mass accretion rates. Thermal winds (Begelman et al. 1983) and magnetic winds (Ferreira & Pelletier 1995; Petrucci et al. 2008; Begelman et al. 2015) likely also play a role. More observations are needed to determine which mechanism dominates in different regimes. In addition, time-resolved optical spectroscopy has clearly shown that the disk winds are not present during the entire outburst (Muñoz-Darias et al. 2016). Combined X-ray, optical and radio observations indicate that there is a link between disk winds and jet ejection events in XRBs (Ponti et al. 2012); a similar phenomenon may be present in DNe (Coppejans & Knigge 2020). This connection is intriguing, but still very poorly understood.

Outflows from accretion disks of DNe are best studied in the UV, specifically UV spectroscopy. *HST* has provided some UV spectra of LMXB outbursts and DNe, but generally only one per outburst (e.g., Sion et al. 2004; Merritt et al. 2007). In fact, due to the fact that *HST* cannot perform very fast ToOs, the DNe outbursts were only caught by accident. *UVEX*, which will be able to re-point on a few hour timescale, will be able to catch these outbursts much better. By obtaining multiple UV spectra over the course of ~ 50 DN outbursts and ~ 5 LMXB outbursts over two years, coordinated with multi-wavelength follow-up, we will be able to study the launching mechanism of the winds and their relation to the jet.

4.3. Classical Novae: Interacting Outflows

Classical nova explosions arise from a thermonuclear runaway on the surface of a white dwarf accreting material from a binary companion (Bode & Evans 2008, Della Valle & Izzo 2020, Chomiuk et al. 2020). Although known for centuries, our understanding of these explosions has undergone a renaissance in the last decade – beginning with the discovery of γ -ray emission (with *Fermi*, Abdo et al. 2010) and correlated optical - γ -ray variability (Li et al. 2017, Aydi et al. 2020), bright radio synchrotron emission (Weston et al. 2016a, Weston et al. 2016b), and hard X-ray emission (Nelson et al. 2019, Sokolovsky et al. 2020). Together, these observations provide evidence of internal shocks between multiple outflows that can power a substantial fraction of the optical luminosity of novae.

Although the basic picture of shocks between multiple outflows (see Figure 7) explains several multi-wavelength aspects of nova observations, a consistent picture remains elusive. There is a large diversity in the observed γ -ray luminosity of novae (Franckowiak et al. 2018) and some do not exhibit any correlated optical be-

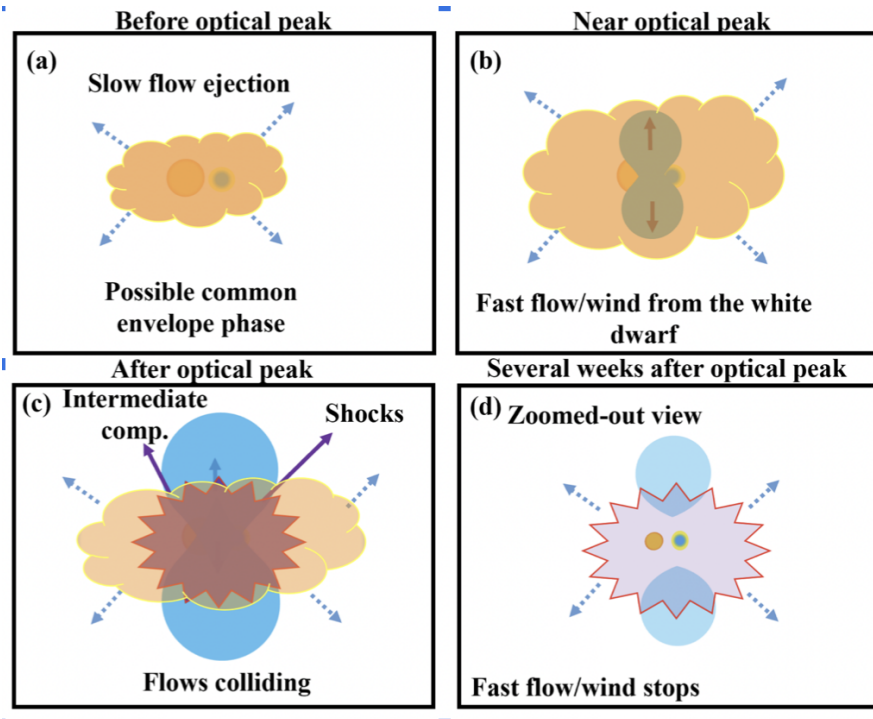


Figure 7. Schematic depiction of the evolution of a nova outburst, starting with the ejection of a slow equatorial outflow followed by a fast polar outflow. The existence of multiple outflows is established by both high resolution radio observations and optical spectroscopy (taken from Aydi et al. 2020).

havior (Li et al. 2020). Yet, spectroscopic observations consistently reveal evidence for multiple, distinct outflows in nova ejecta coincident with the optical peak of their light curves (Aydi et al. 2020). While this suggests that shocks should be ubiquitous in novae, the absence of correlated optical- γ -ray behavior in some novae points to substantially reduced efficiency of conversion of shock energy into EM radiation (Li et al. 2020).

The shock interaction region between fast polar and the slower equatorial outflows have also been suggested to harbor potent conditions for the formation of dust in $\approx 20\%$ of novae (Derdzinski et al. 2017), which is otherwise difficult to form in the hostile environment of novae. A powerful testable consequence of this scenario is the predicted i) viewing angle dependence of multi-wavelength evolution and the formation of dust in novae and ii) variations in the shock and dust formation properties as a function of the underlying white dwarf mass, which drives the amount of mass ejected and the photometric evolution of the nova (della Valle et al. 1992, Yaron et al. 2005).

UV spectroscopy is powerful in that the strongest lines of C, N, Ne, Mg that are produced in the ejecta are in that wavelength range (Shore 2012). These lines can be used to trace the ejecta density profiles, clumping, and filling factor to derive accurate ejection masses. Ne is particularly interesting for novae because some novae oc-

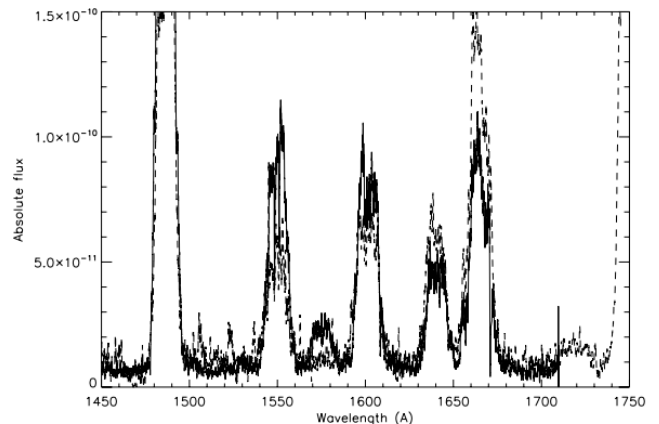


Figure 8. Comparison of the UV spectra of Nova Mon 2012 and Nova V1974 Cyg, taken from Shore et al. (2013).

cur on the most massive ONeMg white dwarfs that show very strong UV Ne emission. Due to limited ToO capabilities, *HST* and *IUE* have provided a limited number of UV spectra of only the brightest and most nearby novae. Figure 8 presents a handful of *HST*/*IUE* spectra of novae, showing a diversity of line profiles. The line profiles can further be used to estimate the ejecta geometry and density profiles (e.g., Shore et al. 2013). Combining the density and structure diagnostics to map out the variation in the multi-wavelength emission (radio, γ -rays)

together with the ejecta dynamics/geometry and white dwarf mass of the nova. will allow us to develop a holistic picture of mass ejection in nova outbursts. Based on current estimates of the nova rate in the Milky Way (De et al. 2021) and the Magellanic Clouds (Mróz et al. 2016), a total of ≈ 10 novae are expected to be accessible for UV spectroscopy during the *UVEX* 2-year baseline mission (accounting for Galactic extinction).

4.4. White Dwarf Companions

Historically, identifying binaries and obtaining the time series imaging and spectroscopy necessary to fully characterize these systems has been observationally taxing, relegating binary studies to an onerous niche field. However, modern all-sky imaging surveys (e.g., *Gaia*, *Kepler*, *TESS*) that provide high precision photometry and astrometry as a function of time, have revolutionized our understanding of ‘vanilla’ low-mass binaries (e.g., two comparably low-mass main sequence stars), as well as facilitated the discovery of a small number of more exotic systems (e.g., main sequence-white dwarf binaries). Similarly, ground-based optical spectroscopy has helped to characterize a small set of these systems in the Milky Way, but numbers remain small. Concerted efforts for large-scale optical spectroscopic identification of such binaries is only getting underway (SDSS-V, DESI, WEAVE, 4MOST).

Despite progress with optical binaries in the Milky Way, there remains very little exploration of binary systems with a hot component (e.g., systems with OB stars, stripped stars, white dwarfs). In many cases the hot companion is virtually impossible to discern with optical observations. Single hot companions may not affect the optical spectra or perhaps only leave indirect trace signatures (e.g., odd optical emission line combinations) in the otherwise normal spectrum of the optically dominant star.

In other cases, even when a binary system is identified (e.g., from optical light curves or spectra), key aspects of the system (e.g., mass loss, wind speeds) or basic characteristics of the hot component (e.g., mass, temperature) are only accessible in the UV, wavelengths at which few observations exist. Thus, though we now believe some of the most influential astrophysical phenomena originate from hot star binary systems, our census and physical understanding of these systems is lacking.

In addition, binaries born as two AFG-type stars will go through a phase where the more massive star has already evolved into a white dwarf, whereas its companion is still on the main sequence. At optical wavelengths, the white dwarf is totally swamped by the companion, but it dominates the UV emission of the system.

4.4.1. White dwarf companions to FGK-type stars in the Milky Way: imaging

The *UVEX* all-sky survey will identify $\sim 10,000$ FGK-type stars that exhibit a UV excess indicating the presence of a white dwarf companion that is undetectable at optical wavelengths. Some pilot studies have been carried out with *GALEX* (Parsons et al. 2016), but many of the nearby FGK-type stars were too bright for *GALEX*. The *UVEX* detectors do not have bright limit. Moreover, *UVEX* will increase the FUV footprint with respect to *GALEX* by 50%. This will allow an unbiased statistical study of the population of these binaries within the Milky Way. This will both enable a full all-sky search for white dwarf + FGK binaries, as well as allow the identification of the closest systems, hence those suitable to the most detailed follow-up studies.

4.4.2. White dwarf companions to FGK-type stars in the Milky Way: spectroscopy

The key parameters for the future outcome of white dwarf + FGK-type binaries are the masses of both stellar components as well as their orbital period. Whereas the mass of the main sequence star and the orbital period can be obtained from optical photometry and spectroscopy, *measuring the white dwarf mass can only be done in the FUV*. *HST* has observed ~ 25 white dwarf + FGK binary candidates, confirming a white dwarf component in most of them, however, a population study that is sufficiently large to sample the full parameter space of stellar mass and orbital period requires a dedicated survey that is beyond the limited resources that are left to *HST*. *UVEX* will enable a population study that spans the full parameter range in stellar mass and orbital period, which is essential to establish tight observational constraints on the branching ratio of these systems with respect to their future evolution (Figure 3).

Low-resolution ($R \sim 1500$) spectroscopy covering 1130–1800Å is essential, as the Stark-broadened photospheric Ly α is sensitive to both the temperature and the surface gravity of the white dwarf, and, in conjunction with a mass-radius relation, provides a measurement of the mass. Detection of emission lines, primarily C IV 1550Å, will be a signature of ongoing mass transfer (e.g., Parsons et al. 2015). The main-sequence masses and orbital periods can be established from optical data, and hence those two components of the parameter space can be mapped out in advance of the *UVEX* survey. However, the properties of the white dwarf will be unknown prior to the *UVEX* spectroscopy. The *UVEX* spectroscopic sample can then be used to extrapolate to the full, unbiased all-sky population established from the *UVEX* imaging, which in turn will put tight con-

straints on the low-frequency gravitational background of double-degenerates descending from white dwarf + FGK binaries, as well as on rates of the various subtypes of thermonuclear supernovae.

4.5. *Evolution of Angular Momentum of Stars Across the HR Diagram*

The typical story of a star’s life begins with the Jeans collapse of a molecular cloud, before eventually contracting onto the Zero Age Main-Sequence (ZAMS). Conservation of angular momentum would then suggest that ZAMS stars have measurable rotation rates stemming from the initial angular momentum of their respective parent molecular clouds. However, observations show that there is a strong separation between fast and slow rotating stars at a temperature of ~ 6200 K. This separation, commonly referred to as the Kraft break, represents a rough boundary between stars with radiative envelopes and stars with convective envelopes (Kraft 1967).

The Kraft break highlights the significance of convective envelopes to angular momentum evolution in stars as they are essential to powering dynamo action, which generates the self-sustaining magnetic field that steals angular momentum via interaction with stellar winds (Weber & Davis 1967). This connection ties a star’s rotation to both its magnetic field and its age, both of which are notoriously difficult to characterize. In general, magnetic activity and age are quantified in terms of angular momentum using rotation-activity relations and gyro-chronology respectively.

Empirical rotation-activity relations come in several forms, one of which is a comparison of ultraviolet emission to rotation period. Stelzer et al. (2016) attempted to derive a UV rotation-activity for M dwarfs using *GALEX* photometry and *Kepler* rotation periods to better understand fully convective dynamos, but was limited by a lack of observations and commented that follow-up UV observations would be a powerful constraint for a M dwarf rotation-activity relation. Additionally, Dixon et al. (2020) found rotation-activity relations for giants using *GALEX* and APOGEE, but also suffered from a lack of fast rotating stars.

With significantly improved angular resolution and greater sensitivity than *GALEX*, *UVEX* presents an opportunity to derive well constrained UV rotation-activity relations. This is especially true as an increasing number of stellar rotation periods are becoming available from large-scale time-series surveys. ESA’s approved *PLANetary Transits and Oscillations of stars* (*PLATO*) mission, with a targeted launch date in 2026, will support *UVEX* in this science by delivering ultra-

precise optical light-curves for more than 2 million FGK dwarfs and subgiants and nearly 300,000 M dwarfs (Montalto et al. 2021).

Finally, it should be possible to associate large numbers of these stars, with space-based rotation and activity measures to regions of the Galaxy with well estimated ages, including the recently identified stellar “strings” that represent coherent stellar populations spanning large regions of the Galaxy (e.g., Kounkel et al. 2020). This will allow the development of robust rotation-activity-age relations for stars across the Hertzsprung-Russell (HR) diagram, and in turn allow the mapping of stellar ages across large swathes of the Milky Way.

5. THE MAGELLANIC CLOUDS & THE MILKY WAY

In this section, we focus on where *UVEX* will make transformative contributions to the areas of Galaxy Archaeology in the Milky Way, dust mapping and dust physics, and the evolution of single and binary stars at low metallicities⁹ in the LMC and SMC. The LMC and SMC are particularly important as hosts of large populations of low-metallicity single and binary stars. As we discuss in §5.2, the formation, evolution, and death of low-metallicity massive stars is poorly understood despite playing an outsized role across astrophysics from driving cosmic reionization (e.g., Robertson et al. 2015a) to being the precursors of explosive transients (e.g., Smith 2014a), including gravitational wave sources (e.g., Abbott et al. 2016). The dedicated *UVEX* photometric and spectroscopic survey of the Magellanic Clouds will provide qualitatively new constraints on the physics of these incredibly important metal-poor single and binary stars.

This section is organized as follows. §5.1 summarizes the current landscape of imaging and spectroscopy in the LMC and SMC, and describes the important role *UVEX* will play. §5.2 describes how *UVEX* will qualitatively advance our knowledge of stellar winds in low-metallicity massive stars. §5.3 details how a combination of deep and cadenced *UVEX* imaging, along with targeted spectroscopy, will uncover and characterize stripped stars, and provide order-of-magnitude improvements in our knowledge of binary star evolution at sub-Solar metallicities. Finally, §5.4 and §5.5 highlight how *UVEX* data products piggybacking from the all-sky survey and LMC/SMC hot star spectra will provide new constraints on dust maps and dust physics, as well as en-

⁹ As noted in §4, we adopt metallicity ranges of 10-20% Z_{\odot} for the SMC and 40-50% Z_{\odot} for the LMC.

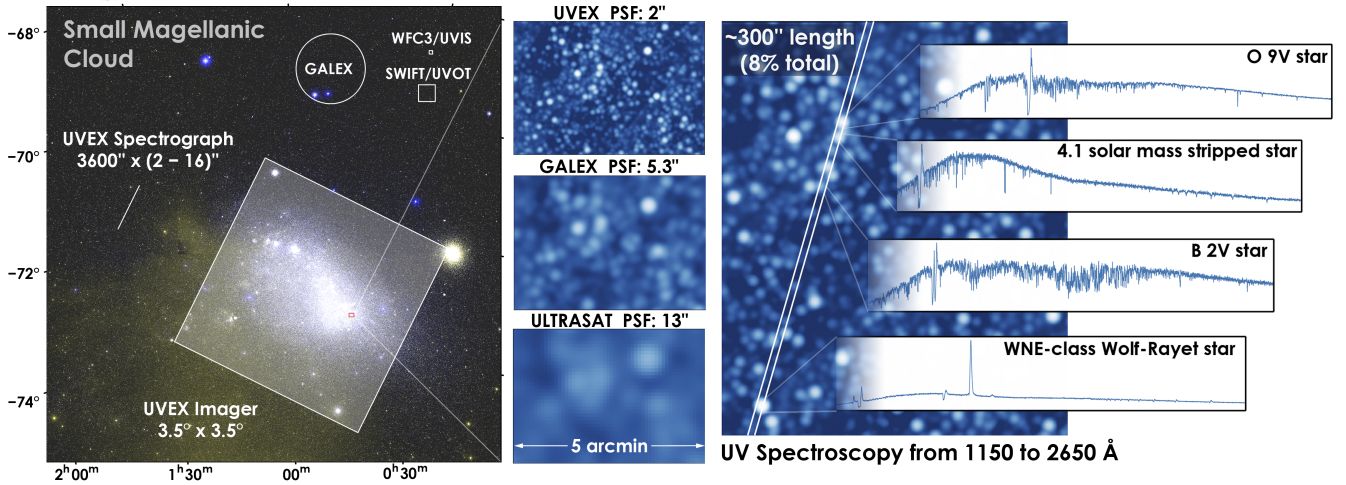


Figure 9. The *UVEX* survey of the Magellanic Clouds illustrated. Left: The *UVEX* field of view overlaid on an optical image of SMC. Select other UV facility footprints are shown for comparison. At 12 sq. deg, *UVEX* will be able to image the main bodies of the LMC and SMC in just seven pointings. *UVEX* will visit the LMC and SMC weekly over its prime mission to obtain deep and cadenced imaging as well as spectroscopy for > 1000 hot stellar systems. Middle: A simulated image in a central portion of the SMC illustrating the spatial resolving power of *UVEX*. The PSF of *UVEX* ensures it will be able to resolve stars in all but the most crowded regions; a dramatic improvement over other UV facilities. Right: Simulated *UVEX* spectroscopy for a handful of objects that *UVEX* will observe during its prime mission. The SNR and spectral resolution of *UVEX* are comparable to *HST*/COS G140L.

able the measurement of accurate stellar metallicities for ~ 300 million stars in the Milky Way. Finally, §5.6 illustrates how *UVEX* has the potential to constrain the evolution of massive stars with metallicities below that of the SMC.

5.1. The *UVEX* LMC and SMC Survey Overview

5.1.1. Imaging

The Magellanic Clouds have long been targets of deep, wide-area, and cadenced imaging surveys in the optical and near-IR. Concerted optical and near-IR efforts have provided a detailed view of the stellar contents of the LMC and SMC (e.g., Udalski et al. 2000, Zaritsky et al. 2002, Zaritsky et al. 2004, Cioni et al. 2011, Nidever et al. 2017), while observations in the mid- and far-IR reveal much about the nature of evolved stars, dust production, and the ISM at low-metallicities (e.g., Meixner et al. 2006, Meixner et al. 2013). Upcoming surveys (e.g., Rubin, *Euclid*) will provide an unprecedented deep and cadenced inventory of LMC and SMC stars in the optical and near-IR (i.e., with sub-arcsecond angular resolution and depths $m \gtrsim 25$).

Missing among these exquisite datasets is a matching, modern UV imaging survey of the LMC and SMC. Though several UV facilities have imaged the LMC and SMC, none are well-matched to properties of modern optical and near-IR datasets. *GALEX* surveyed the LMC and SMC only in the NUV band (Simons et al. 2014). Its angular resolution ($5''$ PSF) and limiting

depth ($m_{\text{NUV}} \sim 21$) is far shallower and coarser than the optical and near-IR imaging. *Swift*/UVOT ($\sim 2.5''$) is limited to $m_{\text{UV}} \sim 19$ for point sources and only available in NUV bands (Hagen et al. 2017). *HST* has the sensitivity and angular resolution in the UV to match (or exceed) modern optical and near-IR LMC and SMC imaging (e.g., Sabbi et al. 2013), but its small FOV makes it unrealistic to survey the entirety of the LMC and SMC. Moreover, *HST* is also limited to NUV wavelengths. Other UV missions, such as *ULTRASAT* ($13''$ PSF), do not have characteristics that are suitable for resolved stellar populations in the LMC and SMC.

As illustrated in Figure 9, *UVEX* has the sensitivity, wide FOV, and angular resolution to provide the missing UV coverage for resolved stars in the LMC and SMC. Moreover, with two UV filters, *UVEX* imaging will help tightly constrain the physical properties of the hottest stellar systems while mitigating the effects of extinction.

UVEX will undertake the first cadenced FUV and NUV imaging survey of the main bodies of the LMC and SMC. As described in §5.3, the depth ($m_{\text{UV}} > 25$; i.e., $\sim 100\times$ deeper than *GALEX*) will enable the detection of the faint products of binary interactions (i.e., stripped stars) and the *UVEX* cadence will provide for the detection and characterization of orbital properties for a wide range of astrophysical objects.

UVEX will resolve stars outside of the densest LMC and SMC star-forming regions. Typical stellar densities in the central regions of the LMC (excluding dense

clusters) are expected, on average, to decrease from ~ 1 star per arcsec² at $u \sim 24 - 25$ magnitude in the very near UV (u -band) and blue optical (g -band) (e.g., [Nidever et al. 2017](#)) to ~ 0.5 stars per arcsec² in NUV, and $\lesssim 0.5$ stars per arcsec² in FUV. The decrease in stellar density is due to the steep dropoff in UV flux for most stars and the rise in UV flux for rarer hot stars. The significant decrease in stellar crowding in the UV has been empirically demonstrated with *HST* in M31 ([Dalcanton et al. 2012](#)). Given these stellar densities, the angular resolution *UVEX* will be able to resolve the majority of hot stars in the LMC and SMC, aside from centers of the densest star-forming regions.

Figure 10 illustrates the spatial resolution of *UVEX* in a region on the outskirts of 30 Doradus. 30 Doradus is the most prominent, and crowded, star forming region in the Local Group. The differences in resolving power are obvious. As seen by *ULTRASAT*, this stellar field appears as a single object. Even *GALEX* only coarsely resolved the image. *UVEX* clearly reveals details of the resolved stellar populations in one of the higher density regions in the LMC. Other regions in the LMC and SMC are typically less crowded in the UV than this example, meaning the *UVEX* imaging would resolve the vast majority of stars in the Magellanic Clouds. With its large FOV, it will only take seven *UVEX* fields to survey the high density main bodies of the LMC and SMC deeper than the all-sky survey and the planned weekly cadence Magellanic Cloud observations will enable a wide range of UV time domain stellar physics (see §5.3). The *UVEX* all-sky survey will include the LMC and SMC stellar halos, Magellanic stream, bridge, and other low stellar density features. *UVEX* will provide the first FUV and NUV resolved star imaging of the entire Magellanic Cloud system.

5.1.2. Spectroscopy

Spectroscopic surveys of massive stars in the LMC and SMC are far less complete and more heterogeneous than imaging surveys. The largest systematic spectroscopic survey of the LMC is the VLT/Tarantula survey which obtained multi-epoch modest resolution optical spectroscopy of ~ 800 OB type stars in the Tarantula star-forming region of the LMC (e.g., [Evans et al. 2011](#)). Despite including only a single star-forming region and being over a decade old, this survey accounts for the majority of our knowledge of massive star properties (e.g., spectral type, binarity) in the LMC. In the SMC, combined efforts with the VLT and 2DF spectrograph have obtained optical spectra for ~ 300 massive stars (e.g., [Evans et al. 2004](#), [Evans et al. 2006](#)). Other optical

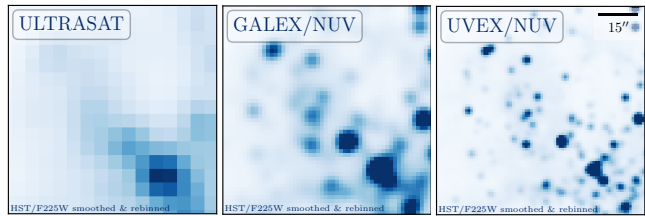


Figure 10. The spatial resolution of *UVEX* compared to select UV facilities. This *HST* UV image on the outskirts of 30 Doradus (from program GO-11360) has been convolved with the PSF of each facility. This stellar field is unresolved by *ULTRASAT*, marginally resolved by *GALEX*, and resolved by *UVEX*. As other regions in the LMC and SMC are less crowded, *UVEX* will reveal the detailed distribution of stars without being significantly affected by crowding throughout most of the LMC and SMC.

spectroscopic efforts are generally smaller and/or focus on specific sub-classes of massive stars.

UV spectroscopy of massive stars in the LMC and SMC are essential for understanding stellar winds of massive stars at sub-Solar metallicity (see §5.2). However, compared to optical data, UV spectroscopy in the LMC and SMC is sparse. The challenge and expense of obtaining UV spectra at the distances of the LMC and SMC have limited most studies to handfuls of stars per publication. The two most prominent systematic surveys are of R136, the cluster within 30 Doradus in the LMC. [Massey & Hunter \(1998\)](#) acquired UV spectra of 65 stars with *HST*, while [Crowther et al. \(2016\)](#) obtained spectra of 57 OB stars. There are fewer UV spectra of massive stars in the SMC (e.g., [Walborn et al. 2000](#)).

Though it has taken tremendous effort to assemble the above, and other, spectroscopic datasets in the LMC and SMC, they only represent a small fraction of the entire massive star content. Estimates place the number of OB type stars in the LMC and SMC at $\sim 30,000$ (based on recent star formation rates, counting resolved stars; e.g., [Harris & Zaritsky 2004](#), [Harris & Zaritsky 2009](#)). Of course, progress in understanding metal-poor massive star physics does not require spectra of every possible massive star. But far more are needed than are currently available.

Two ongoing and upcoming efforts stand to, at least partially, remedy the paucity of massive star spectra in the LMC and SMC. The first is the *Hubble* UV Legacy Library of Young Stars as Essential Standards¹⁰ (ULLYSES; [Roman-Duval et al. 2020](#)). This program will combine new and archival *HST* UV spectra in the LMC

¹⁰ <https://ullyses.stsci.edu>

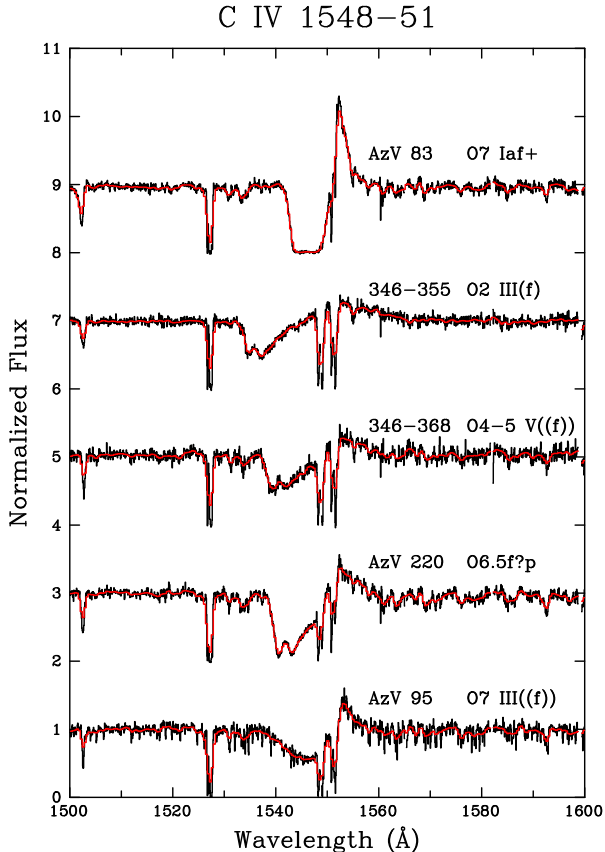


Figure 11. Example spectra showing the C IV doublet in O-type stars in the SMC. STIS/E140M observations (Walborn et al. 2000) are shown in black. The same spectra smoothed to *UVEX* resolution are shown in red. Because key features of the UV resonance lines (e.g., terminal velocities, peak intensities) are so prominent, they are preserved at the resolution of *UVEX*. The low metallicity of the SMC means these wind features are among the weakest and least pronounced. The UV line fidelity is equally well-preserved for stronger winds typically found in the higher metallicity LMC (Crowther et al. 2016).

and SMC to form the first spectral atlas of metal-poor massive stars. This large effort is being accompanied by a VLT survey that will provide high resolution optical spectroscopy for all ULLYSES targets. ULLYSES is the first systematic program targeting UV spectra in the Magellanic Clouds. However, as we discuss in §5.2, it should be viewed as an important first step of an effort that needs more data.

The second effort is from the 4MOST consortium. The 1001MC survey will target several thousand massive stars in the LMC and SMC with low-resolution optical spectroscopy (Cioni et al. 2019). Another 4MOST effort proposes to monitor $\sim 20,000$ massive stars in the LMC

and SMC over the course of 5 years with medium resolution spectroscopy with the goal of determining binarity through radial velocity variations (Sana & Shenar 2019). 4MOST will be on sky by the mid-2020s. Multi-epoch spectral constraints on binary star characteristics (e.g., binary fraction, mass ratio, orbital configuration) from 4MOST are likely to be too late to guide substantial new *HST* UV spectra in the LMC and SMC. However, 4MOST data will be well timed relative to *UVEX*, which will uniquely provide the stellar wind measurements.

Figures 9 and 11 show examples of the types of spectra that *UVEX* will provide for hot massive stars in the LMC and SMC. As we discuss in §5.2, *UVEX* spectroscopy of 1000 massive stars in the LMC and SMC will be the legacy dataset that anchors our knowledge of low-metallicity massive star winds and evolution for the next decades.

5.2. Winds and Mass Loss in Massive Metal-Poor Stars

Stellar winds are key components of massive star evolution. Winds drive mass loss, which affects a star’s lifetime, structural parameters (e.g., temperature, luminosity), radiation field, and how it ultimately dies (e.g., Smith 2014a, Vink 2021 and references therein). The abundance of metals strongly affects a massive star’s dominant electron scattering opacity, which affects it both structurally (e.g., the size and mass of a star) as well as the strength and speed of its winds, such that lower metallicities and opacities have weaker winds.

In massive stars, stellar winds and their associated mass loss are driven by radiation pressure onto numerous absorption lines of ionized metal species in the outer atmosphere. However, the precise scaling of this dependence remains uncertain and hotly debated theoretically (e.g., Vink & Sander 2021, Björklund et al. 2021) and is challenging to settle observationally due, in large part, to a paucity of UV spectra at low-metallicities. Changes in this relationship have profound implications for stellar evolution: Figure 12 illustrates how the metallicity dependence of massive star winds affect the masses of black holes and the masses of compact objects, such as precursors of gravitational wave sources. The strength of the wind, star’s metallicity, and, as discussed below, binary configuration greatly influences the mapping of initial stellar mass to final evolutionary state.

P-Cygni profiles in the UV are the gold standard for measuring stellar winds and mass loss rates in massive stars (e.g., OB stars; see Hillier 2020 and references therein). They have been extensively used to study massive stars winds in the Galaxy for decades (e.g., Groenewegen et al. 1989; Prinja et al. 1990). The UV hosts

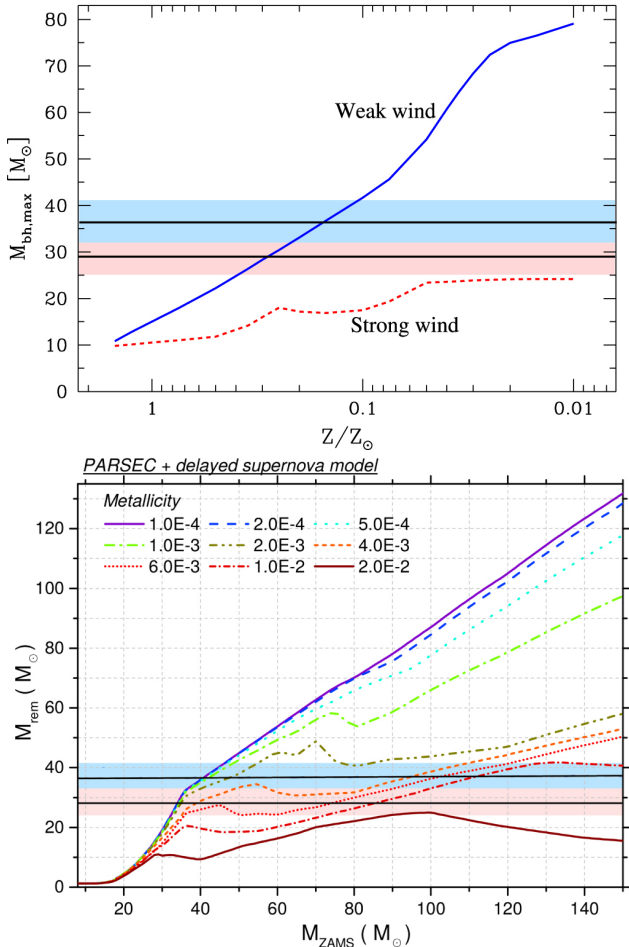


Figure 12. Adapted from Abbott et al. (2016). See also: Belczynski et al. (2010) and Spera et al. (2015). The winds of massive metal-poor stars have a dramatic effect on the fate of the star. Top: The dependence of maximum black hole mass on metallicity, with $Z_{\odot} = 0.02$ for the old (strong) and new (weak) massive-star winds (Belczynski et al. 2010). Bottom: Compact-remnant mass as a function of zero-age main-sequence (ZAMS; i.e., initial) progenitor mass for a set of different (absolute) metallicity values (Spera et al. 2015). Poor knowledge of wind driven mass loss is among the largest sources of uncertainty in this mapping. The masses for GW150914 are indicated by the horizontal bands. Improved constraints on the winds of massive metal-poor stars are crucial for the emerging era of multi-messenger astrophysics.

a number of resonance lines (e.g., C IV $\lambda\lambda 1548, 1552\text{\AA}$; Si IV $\lambda\lambda 1394, 1403\text{\AA}$, N V $\lambda\lambda 1238, 1242\text{\AA}$) that are sensitive to lower mass-loss rates than H α and can constrain the outflow velocity (e.g., Hillier 2020). The UV is also rich in iron lines, enabling direct determinations of massive star metallicity (e.g., Hillier 2020).

At sub-Solar metallicities, our knowledge of massive star winds and mass loss is limited (e.g., Smith 2014a). While the LMC and SMC are close in proximity and host

many low-metallicity, massive stars, acquiring UV spectra for large numbers of these stars has been challenging due to their apparent faintness. The most substantial work has been done with *HST*, resulting in UV spectra of a few dozen massive stars in the LMC and SMC (e.g., Massey & Hunter 1998, Walborn et al. 2000, Crowther et al. 2016). These spectra anchor modern wind scaling relations, which are known to be uncertain by a factor of ~ 3 (e.g., Smith 2014a, Vink & Sander 2021). This level of uncertainty has substantial implications for the final fate of massive stars (e.g., whether they explode or not), the mass of the resultant black hole, and properties of compact objects, as illustrated in Figure 12 and discussed extensively in Smith 2014a.

One important reason for this uncertainty is the paucity of UV spectra at low-metallicities. Existing UV spectra in the LMC and SMC have shown that mass-loss rates and wind velocities at a given stellar temperature and luminosity span a wide range of values (e.g., Walborn et al. 2000, Hillier et al. 2003). A likely culprit for these variations appears to be binarity and/or binary evolution (e.g., Crowther et al. 2016).

In an effort to increase number statistics and homogeneity, ULLYSES is an *HST* director’s discretionary program that combines new and archival STIS and COS UV spectra of ~ 300 massive stars in the LMC and SMC (Roman-Duval et al. 2020). It will create the first large UV spectral library of sub-Solar metallicity massive stars. ULLYSES provides an important platform for improving our understanding of winds and mass loss (and their variations) in sub-Solar metallicity massive stars. Complementary ground-based optical spectra with the VLT ensure an exquisite multi-wavelength dataset.

However, even with ~ 300 spectra, ULLYSES will only sparsely sample the upper HR diagram. For single stars, mass, metallicity, rotation rate, and phase of evolution are considered primary determinants of massive star winds. ULLYSES will sample approximately ten stars for each reasonable permutation of these parameters. The dimensionality and complexity of the problem grows when binarity is included. At least 50% of massive stars are in binaries and the mass ratios and separation, in tandem with single star parameters listed above, can drive winds through mass transfer, Roche lobe overflow, and/or common envelope ejection (e.g., Sana et al. 2012a). By design, ULLYSES primarily targets single stars in order to provide benchmarks in absence of additional complexity due to binarity (Roman-Duval et al. 2020).

Given the (i) large variations in wind parameters at fixed stellar property (§5.1; e.g., Crowther et al.

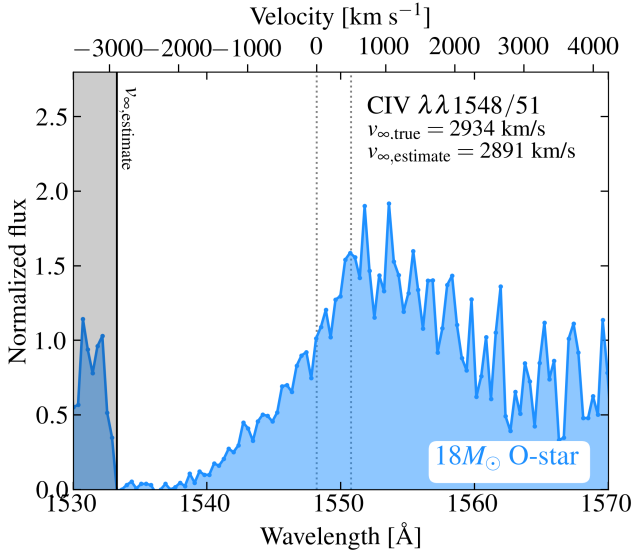


Figure 13. The simulated *UVEX* spectrum ($SNR = 10$ at the C IV doublet) of a typical LMC metallicity O-star spectrum with an average wind velocity, zoomed in on the C IV resonance line. By fitting for the blue edge of the C IV P-Cygni profile, we recover the wind velocity to within a few percent. *UVEX* will enable the accurate determination of massive star wind speeds for 1000 hot, massive single and binary stars in the LMC and SMC.

2016); (ii) importance of binarity to so many stellar end states (e.g., Figure 12, Sana et al. 2012a); and (iii) the sparse (but substantially improved) sampling provided by ULLYSES, it is imperative to improve the state of UV spectra for low-metallicity massive single and binary stars.

UVEX will substantially expand on the foundation established by ULLYSES. During its two year prime mission, *UVEX* will obtain UV spectroscopy of 1000 OB stars in the LMC and SMC. The high throughput, modest spectral resolution, and broad wavelength coverage of *UVEX* are ideal for filling out areas of the HR diagram in which ULLYSES is known to be sparse, such as binary stars. *UVEX* will provide over three times as many UV spectra as ULLYSES, ensuring the robust statistics needed to quantify variations in stellar wind properties across the HR diagram and at fixed stellar parameters (e.g., luminosity, temperature, metallicity). Crucially, it will also provide the UV spectra necessary to establish the link between binary configuration and stellar winds, a connection that is known to be important, but is essentially unconstrained empirically (e.g., Crowther et al. 2016). By the time *UVEX* is on sky, 4MOST will have acquired multi-epoch optical spectral for thousands of massive stars in the LMC and SMC (e.g., Cioni et al. 2019, Sana & Shenar 2019). Spec-

troscopic targets for *UVEX* will be selected based on a wealth of optical spectra and time series optical and *UVEX* imaging, ensuring *UVEX* spectra covers all relevant stages of single and binary massive star evolution.

The terminal wind velocity and mass loss rate of a massive star are most readily measured from the P-Cygni profile of UV resonance lines (see Hillier 2020 and references therein). The most prominent of these lines is C IV $\lambda\lambda 1548, 1552\text{\AA}$. Identifying the blue edge of the P-Cygni profile yields the terminal wind velocity, while fitting the shape of an unsaturated profile can provide the mass loss rate. Wind speeds are generally so high ($> 1500 \text{ km s}^{-1}$) that even modest resolution UV spectroscopy is suitable to characterize them.

Figure 13 shows an example of how *UVEX* will be able to accurately recover the terminal wind velocity for a typical massive O star in the LMC. Even with weaker winds (e.g., later spectral types, lower metallicity), *UVEX* will accurately recover the wind velocities to better than 20%, on par with wind velocity constraints provided by *HST* (e.g., Crowther et al. 2016).

5.3. Stripped Stars

5.3.1. Background

A third of all massive stars are expected to lose their hydrogen-rich envelopes via mass transfer or common envelope ejection (e.g., Sana et al. 2012a), leaving the hot and compact helium core exposed (i.e., a “stripped star”). Stripped stars are hot (30,000–100,000 K) and the majority of their radiation is emitted at ionizing wavelengths. Their strong ionization fields make them potential contributors to comic reionization (e.g., Stanway et al. 2016, Götberg et al. 2019, Götberg et al. 2020a, Secunda et al. 2020).

Stripped stars are a critical, but poorly understood, phase in many binary star evolutionary pathways. For example, as Figure 14 shows, two stripped stars are thought to be necessary to create a merging binary neutron star (e.g., Tauris et al. 2017, Vigna-Gómez et al. 2020, Ye et al. 2020). Moreover, when in close orbit with another companion, stripped stars can also themselves be sources of gravitational waves in the wavelength regime of *LISA* (e.g., Nelemans et al. 2004, Wu et al. 2020, Götberg et al. 2020b).

Modeling helium stars and envelope stripping started half a century ago (e.g., Kippenhahn & Weigert 1967) and is now included in the stellar evolution code MESA (Paxton et al. 2015). These models indicate that stripped stars have comparable properties over a wide range of mass. They are all hot, small ($< 1R_{\odot}$), compact ($\log_{10} g \sim 4.8 - 5.5$), helium-rich ($X_{\text{He},s} \sim 0.5 - 1$), and hydrogen-poor ($X_{\text{H},s} \sim 0 - 0.5$). A main dif-

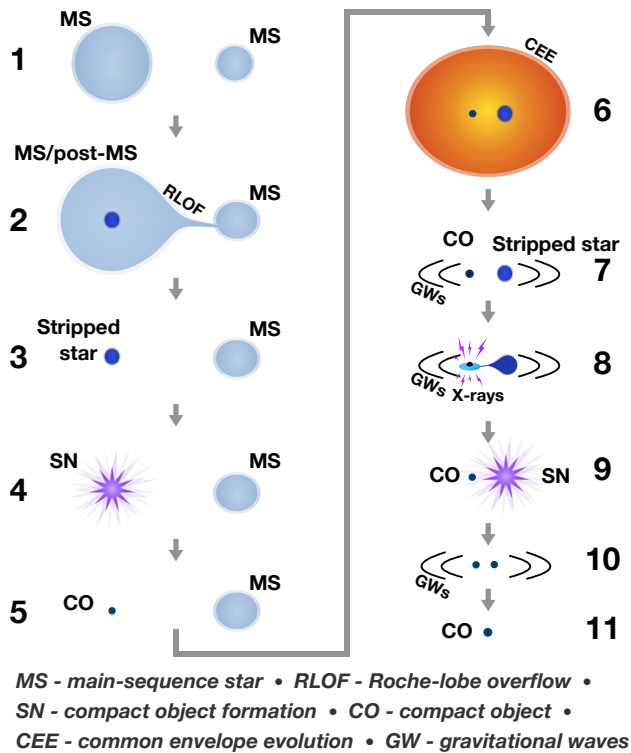


Figure 14. Adapted from Götberg et al. 2020b (see also: Tauris et al. 2017, Vigna-Gómez et al. 2020). A cartoon of a binary evolution sequence, commonly thought to be the main channel for the formation of merging neutron stars. Few of these steps have been observationally confirmed, let alone measured statistically. *UVEX* will be particularly useful for steps 3, 5, 7, and 8.

ference is that they can span a range of luminosities ($\log_{10} L/L_{\odot} \sim 1-5$) based on their mass ($0.37-10M_{\odot}$; Götberg et al. 2018). Stripped stars are products at all initial masses, as binary star interactions are mass independent. Stripped stars are fairly long-lived. Because envelope-stripping typically finishes soon after central hydrogen depletion (i.e., the main sequence evolution) of the donor star, a star spends the remaining $\sim 10\%$ of its lifetime as a stripped star.

Only a handful of population synthesis models include any binary star evolution. Those that do (e.g., to estimate black hole and/or neutron star merger rates, the effect of binaries on the integrated light of galaxies) use approximate physics for envelope-stripping via mass transfer and common envelope ejection (e.g., Hurley et al. 2000, Hurley et al. 2002). The BPASS models significantly moved the field forward with the inclusion of interacting binaries (e.g., Han et al. 2007, Eldridge

et al. 2008, Eldridge & Stanway 2009, Eldridge et al. 2017), but much of the adopted binary star physics is not well-constrained and thus the predictions are highly uncertain. For example, underlying model grids are not available for weak wind, hot, and helium-rich stars. Instead, stripped stars in this regime are typically modeled as black-bodies, existing scaled main sequence star models, or scaled Wolf-Rayet star models. While understanding the contribution of stripped stars to integrated galaxy properties is in the early stages, signs so far are that they can be significant contributors at ionizing wavelengths (e.g., Götberg et al. 2018, Götberg et al. 2019).

Observations of stripped stars are extremely limited, particularly at intermediate masses ($\sim 2-10M_{\odot}$). Stripped stars are so hot that majority of their emission is through ionizing photons; they are faint at optical wavelengths. It is only at UV wavelengths that the presence of a stripped star becomes apparent. Accordingly, to date, only one intermediate-mass stripped star is known in the entire Milky Way: the $\sim 4M_{\odot}$ quasi-Wolf-Rayet star in the system HD 45166 (Steiner & Oliveira 2005, Groh et al. 2008), despite $\sim 10^5$ stars that are predicted to exist (Figure 15; Götberg et al. 2019). Wang et al. (2021) performed an impressive search for stripped companions to Be-type stars by cross-correlating spectral models of O-type stars with observed UV spectra. They discovered ten stripped companions to early Be-type stars. The flux contribution is small, meaning that the stripped companion is a lower-mass subdwarf and that the systems experienced little mass transfer. These systems are not supernova, nor neutron star nor black hole, progenitors as their components probably had initial masses of $\sim 5-8M_{\odot}$.

Some Wolf-Rayet stars could, in principle, be intermediate-mass stripped stars. However, it is unclear if their hydrogen-rich envelopes were stripped via binary interaction or by their own strong stellar winds. For example, Shara et al. (2017) and Shara et al. (2020) measured the rotation rates of O-type companions to Wolf-Rayet stars, which is relevant for understanding whether mass transfer (which induces rotation) stripped the Wolf-Rayet stars. The derived rotation rates are similar to what has been measured for single O-type stars (Ramírez-Agudelo et al. 2013, 2015). Some of the binaries have quite short periods, just tens of days, which could suggest that the Wolf-Rayet stars were stripped via binary interaction. The ~ 4 hour period of the Wolf-Rayet X-ray binary Cyg X-3 (van den Heuvel & De Loore 1973, van Kerkwijk et al. 1992) suggests that the Wolf-Rayet star was stripped by the compact object, most likely via common envelope ejection. This

general approach is challenging and unlikely to lead to conclusive results in most cases.

There are even fewer constraints on stripped stars at sub-Solar metallicities. In the Magellanic Clouds, Massey et al. (2014), Massey et al. (2015), and Massey et al. (2017) found ten helium-rich stars with modest stellar winds that also appear fainter than regular sub-Solar metallicity Wolf-Rayet stars. They have been dubbed WN3/O3 stars after the emission features which resemble a WN3-type star and the absorption features that resemble an O3-type star. They appear to be older objects than typical Wolf-Rayet stars and their spectra match what is expected for a weaker-wind type helium star (Smith et al. 2018). However, their binarity remains to be determined, leaving their status as stripped stars unclear.

5.3.2. Stripped stars with UVEX

Stellar population models that include stripped stars predict that $\sim 5 \times 10^4$ stripped stars should exist in the Magellanic Clouds (see Figure 15; Götberg et al. 2019). These stripped stars have low metallicities, which, as discussed above, are more commonly associated with a range of transients and compact objects. Distances to stripped stars in the LMC and SMC are well-known; unlike the Milky Way in which distances are uncertain, as many stripped stars are too faint for *Gaia*. The lack of any known stripped stars in the LMC or SMC is likely due to the lack of high-fidelity UV coverage: they are faint at optical wavelengths and therefore easily hidden by a companion star, but bright at UV wavelengths.

Using the “UV excess” method (Götberg et al. 2018), *UVEX* should uncover $\sim 5,000 - 10,000$ stripped stars in the LMC and SMC that can be unambiguously separated from the main sequence (i.e., the stripped star systems will be bluer). These stars will span the full mass range ($0.37-10M_{\odot}$), providing an important new handle on the stripped star population and the physics of binary star evolution.

UVEX has several unique characteristics that will enable the detection of large stripped star populations. First, it has sufficiently high angular resolution ($\sim 2''$ PSF) to resolve individual stars in all but the most crowded star formation regions (e.g., 30 Doradus) in the LMC and SMC. Second, its exquisite sensitivity enables very deep imaging. Separating the lowest mass stripped stars ($0.37 M_{\odot}$) from the main sequence via the color excess method requires a color precision of $NUV - g \leq 0.1$ (Götberg et al. 2018) at $m_{NUV} = 25$. Moderately deep optical imaging with DECam (Nidever et al. 2017) will enable the identification of intermediate and massive stripped stars. When combined with deep Rubin imag-

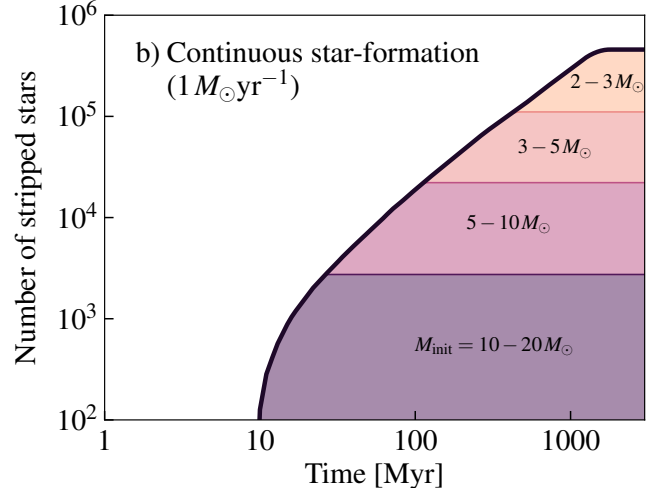


Figure 15. From Götberg et al. (2019). The expected number of stripped stars in a Solar metallicity, continuously star-forming population with a star formation rate of $1 M_{\odot} \text{ yr}^{-1}$ (i.e., the Milky Way). The population of stripped stars are color-coded by initial progenitor mass: $10-20 M_{\odot}$ (purple); $5-10 M_{\odot}$ (pink); $3-5 M_{\odot}$ (salmon); $2-3 M_{\odot}$ (peach). Scaling by recent star formation rate (Harris & Zaritsky 2004, Harris & Zaritsky 2009), the LMC and SMC are expected to host $\sim 50,000$ stripped stars, of which $\sim 5,000-10,000$ will be detectable via photometric UV excess enabled by *UVEX* imaging.

ing, *UVEX* will uncover stripped stars of all possible masses in the LMC and SMC. Though extinction in the LMC and SMC is modest (e.g., Zaritsky et al. 2004), the addition of the FUV band will help to mitigate mild degeneracies between temperature and extinction.

Other UV imaging of the LMC and SMC is not sufficient for detecting the stripped star population. *GALEX* and *Swift* imaging are both 100 times shallower and each have a much coarser PSF ($3-6''$). *HST* has both the sensitivity and depth to detect stripped stars, but is limited by its small FOV. Based on the relative FOVs and the expected number of stripped stars in the LMC and SMC (Götberg et al. 2018), *HST* is expected to host ~ 0.3 stripped stars per view of field, while a single *UVEX* field will host ~ 1400 .

Beyond identification, targeted *UVEX* follow-up spectroscopy will yield wind velocities for ~ 100 stripped stars in the LMC and SMC. Winds from stripped stars affect, for example, how much hydrogen is left over after mass transfer. In turn, this determines how much the star can swell after central helium depletion. With stronger winds, stripped stars lose the hydrogen layer and many of them cannot swell to large sizes. With weaker winds, more hydrogen remains and the stripped stars can swell to large sizes, affecting both the progenitor of supernovae and whether the star can interact

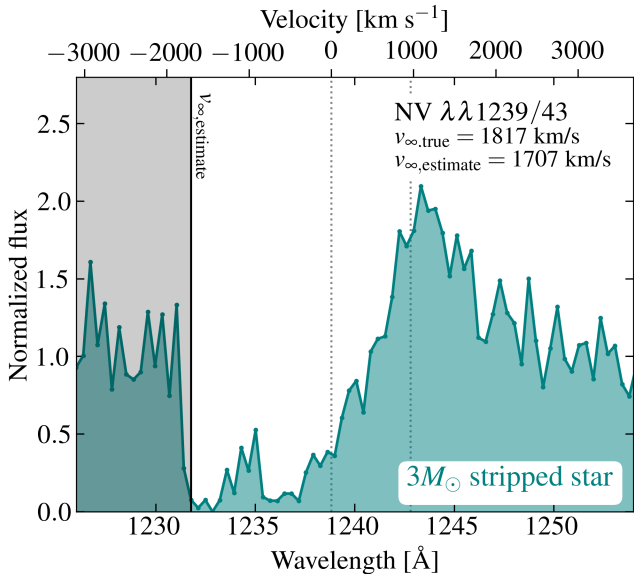


Figure 16. The simulated *UVEX* spectrum ($SNR = 5$ at the N V doublet) of a $3M_{\odot}$ stripped star with an expected typical wind velocity zoomed in on the N V resonance line. By fitting for the blue edge of the N V P-Cygni profile, the wind velocity can be recovered to within $\sim 10\%$; 20% for the weakest wind cases. *UVEX* will enable the accurate determination of massive star wind speeds for ~ 100 stripped stars in the LMC and SMC.

again with its companion. Late interaction can give rise to binaries that are tight enough to merge within a Hubble time, gravitational radiation in the *LISA* band, and bright X-ray binary phases (Götberg et al. 2020b).

There are several wind sensitive features in the FUV: N V 1239/1243, He II 1640, C IV 1549/1551, N IV 1719, O V 1371, O VI 1038. Many of these are expected to occur in P-Cygni line profile shapes, which can be used to accurately measure wind speeds when saturated (e.g., Crowther et al. 2016). P-Cygni profiles are also sensitive to the wind velocity profile (Castor & Lamers 1979). Comparing collisionally excited lines with recombination lines gives a handle on the wind clumping (see Vink 2021). The strength of the emission lines in combination with the other wind parameters constrains the wind mass loss rate. There exist wind sensitive lines in the optical, such as $H\alpha$ and He II 4686, but when winds are weak, they are likely to have absorption profiles, while there still may be emission or P-Cygni profiles in the FUV.

As shown in Figure 16, modest SNR ($SNR = 5$ at the N V 1239/1243 doublet) and modest resolution *UVEX* FUV spectroscopy enables the accurate recovery of wind velocity in a stripped star using the N V P-Cygni profile. Other lines may also help improve wind constraints, but the minimum requirement for *UVEX* is to make use of

this NV feature, as it is most prominent, even in the case of weak winds, low-mass loss rates, and/or the expected carbon deficiency in many stripped stars.

5.3.3. Photometric variability

Stripped stars in the LMC and SMC are expected to give rise to various types of light curve variability due to binarity. Stripped stars with main-sequence companions will often be detectable through eclipses. The anticipated cadence of *UVEX*'s Magellanic Cloud survey will provide sensitivity to eclipsing binaries with orbital periods $P_{\text{orb}} \lesssim 100$ days, probing both systems formed via common envelope evolution and systems formed by stable mass transfer (e.g., Han et al. 2002). Stripped star + main sequence binaries are generally dominated by the small, hot stripped star in the UV, and by the larger, cooler companion in the optical (e.g., Götberg et al. 2017, Schootemeijer et al. 2018). Eclipses are thus deep in the UV and shallow in the optical.

Dark companions, such as neutron stars and black holes, do not cause eclipses, but they can still be detected through ellipsoidal variation and Doppler beaming (e.g., Masuda & Hotokezaka 2019). The amplitude of the expected variability is strongest at close periods, such that systems with orbital periods $P_{\text{orb}} \lesssim 1$ day are most likely to be detected. Because most of the stripped star's light is emitted in the UV, *UVEX* will be sensitive to stripped star + compact object binaries too faint to be characterized with optical light curves.

Figure 17 shows example light curves of two hypothetical stripped star binaries that could be detected with *UVEX* in the LMC. We assume a cadence of 1 visit per week, with 900 s total integration time in each visit. We assume extinction $A_V = 0.5$ mag, with a Cardelli et al. (1989) extinction law. The left panel shows a stripped star + main sequence binary (e.g., step 3 in Figure 14) with a $2 M_{\odot}$ stripped star ($R = 0.5 R_{\odot}$; $T_{\text{eff}} = 60,000$ K) and a $7 M_{\odot}$ main sequence companion ($R = 4.1 R_{\odot}$; $T_{\text{eff}} = 20,000$ K). Eclipses are much deeper in the UV than in the optical because the stripped star contributes a larger fraction of the light there. Although such a system could still be recognized as a binary from the optical eclipses (and indeed, many eclipsing massive binaries in the LMC have already been studied with OGLE (e.g., Moe & Di Stefano 2013, Moe & Di Stefano 2015), only the UV light curves reveal the nature of the system and allow the physical parameters of the two stars to be determined unambiguously. Light curves from future facilities in the blue optical (e.g., LSST in the u band) will be complimentary to *UVEX* data in characterizing these binaries, but the FUV is

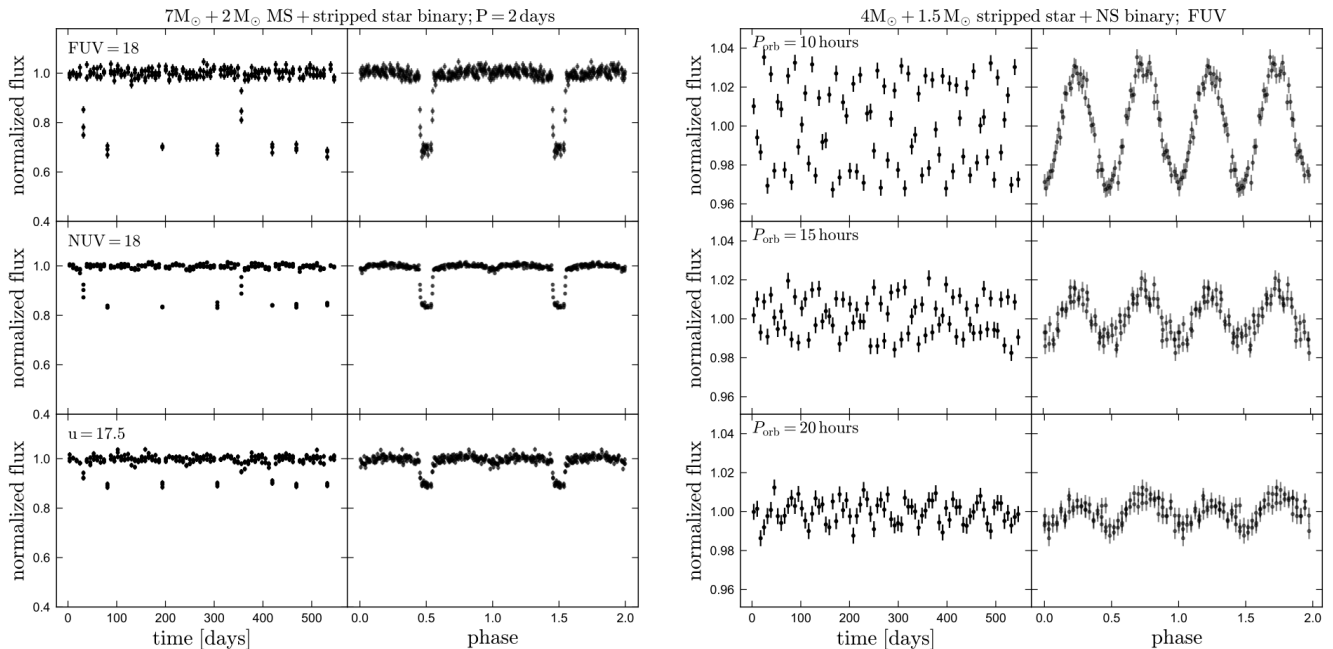


Figure 17. Predicted light curves for two types of binaries containing stripped stars detectable with *UVEX* time-series photometry in the Magellanic Clouds. Left two panels show an eclipsing binary containing a $7M_{\odot}$ main-sequence star and a $2M_{\odot}$ stripped star. Deep eclipses are apparent in the UV, where the stripped star contributes almost half of the total light. Shallower eclipses are apparent in the optical (e.g. Rubin/LSST *u*-band), but these would be misinterpreted as being due to a normal main-sequence companion without the UV data. Right panels show a $4M_{\odot}$ stripped star with a neutron star companion at different orbital periods in the FUV; the predicted variability is due to a combination of ellipsoidal variability and Doppler beaming. Such a system will evolve to become a binary neutron star.

critical for distinguishing hot stripped-star companions from much more numerous normal-star companions.

The right panel of Figure 17 shows the predicted light curve of a detached stripped star + neutron star binary (e.g., step 7 in Figure 14). Here we model a more massive stripped star ($M = 4M_{\odot}$; $R = 0.9R_{\odot}$; $T_{\text{eff}} = 75,000\text{K}$, as might be formed from a star with initial mass $12 - 15M_{\odot}$). Such a binary would likely evolve to become a binary neutron star within ~ 10 Myr. Although the neutron star contributes no light in our modeling, its gravitational effects lead to detectable variability in the UV. At short periods, the dominant effect is ellipsoidal variability (i.e., a time-varying geometric cross section of a tidally distorted star); at longer periods, Doppler beaming dominates. These effects are only likely to be detectable at short periods ($P_{\text{orb}} \lesssim 1$ day), but this is precisely the regime in which the progenitors of binary neutron stars and kilonovae are expected to be found.

5.4. Dust

5.4.1. Milky Way dust maps

Many areas of extragalactic science require high-precision maps of dust extinction and reddening at high Galactic latitudes. Maps based on far-IR (FIR) dust

thermal emission are widely used (e.g., Schlegel et al. 1998, Planck Collaboration et al. 2014), but suffer from a number of systematics. More concretely, these maps only trace dust extinction indirectly, and systematic errors can be introduced by incorrect modeling of dust temperature, spectral index, or column density, or by variations in the ratio of dust extinction at optical wavelengths to thermal emission in the FIR. In addition, dust maps based on FIR emission are contaminated by large-scale structure (through dust emission in distant galaxies; see Chiang & Ménard 2019), which is of particular concern for cosmology.

Dust maps based on optical and near-IR stellar photometry (e.g., Marshall et al. 2006, Green et al. 2015, Juvela & Montillaud 2016) more directly measure dust extinction and reddening, and are thus less affected by these systematics. However, dust maps based on stellar photometry typically achieve lower signal-to-noise ratios than FIR emission-based maps at high Galactic latitudes, where the sky density of stars is lower and per-star extinction is lower.

At high Galactic latitudes, it is therefore critical to observe stellar photometry in the UV. The UV colors of stars are extremely sensitive to small amounts of dust, and can thus boost the SNR of per-star reddening mea-

measurements. Recent work using *GALEX* photometry in combination with LAMOST spectroscopy has mapped extinction at high Galactic latitudes (Sun et al. 2021). *UVEX* will expand the number of stars with UV photometry by a factor of ~ 5 relative to *GALEX*, enabling the creation of dust extinction maps with higher resolution and/or higher signal-to-noise.

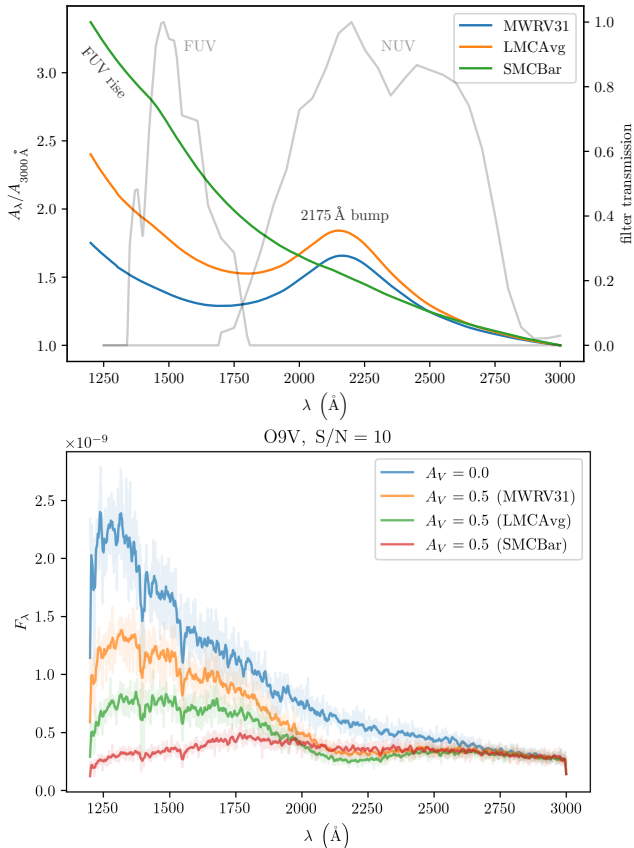


Figure 18. Top: Three representative dust wavelength-extinction relations, from the Milky Way ($R(V) = 3.1$), the LMC and the SMC bar. NUV/FUV-band transmission curves are over plotted. Extinction in the NUV band is primarily sensitive to the strength of the 2175 Å bump, while extinction in the FUV band is primarily sensitive to the slope of the far-UV rise. Bottom: The effect of different dust extinction laws on an O9V-star spectrum, observed at a native signal-to-noise ratio of 10 (light curves), and then smoothed to *UVEX* resolution to show that coarse features are clearly discernable. The lack of a 2175 Å bump and strong far-UV rise in the SMC bar extinction law are readily apparent.

5.4.2. LMC and SMC

Dust extinction laws exhibit striking variations depending on dust chemistry and the interstellar environment (Figure 18). A well-known example is variation in

the dust extinction curves along different sight lines in the SMC (Gordon et al. 2003).

The origin and extent of variations in dust extinction is poorly understood. This is particularly true at UV wavelengths. While the optical extinction law is well-characterized by a single parameter, $R(V)$, the UV extinction law exhibits more variability, which is only weakly correlated with $R(V)$ (Peek & Schiminovich 2013). In the UV, the NUV-band extinction is sensitive to the strength of the 2175 Å bump, thought to be carried by PAHs or graphite grains (Draine 2003), while the FUV-band extinction is sensitive to the slope of the far-UV rise, driven by very small grains (Mishra & Li 2015).

The gold standard for measuring dust properties is UV spectroscopy. Because shorter wavelength light is more easily scattered by dust, the amount of extinction as a function of wavelength, along with other variation (e.g., the 2175 Å bump) are the empirical anchors for our knowledge of the UV extinction laws. Within the Galaxy, the UV extinction law, and its relation to dust physics, has been measured from UV spectroscopy from samples of a few hundred stars (e.g., Fitzpatrick & Massa 2007, Fitzpatrick et al. 2019, Massa et al. 2020). Far less is known about UV extinction laws at sub-Solar metallicities. The commonly used LMC and SMC dust curves are determined from averaging over a small number of sight lines, which exhibit substantial variance.

UVEX spectroscopy of 1000 hot OB type stars in the LMC and SMC will provide qualitatively new insights into the UV extinction curve at sub-Solar metallicities. For example, the average SMC UV extinction curve exhibits no 2175 Å bump. However, the bump is present in a handful of sightlines with UV spectroscopy in the wing of the SMC (Cartledge et al. 2005, Li et al. 2006). The precise carrier of the 2175 Å bump has not yet been determined, though PAHs are a candidate (Li 2020). A census of the precise properties (amplitude, central wavelength and width) of this feature in a variety of interstellar environments (e.g., metallicity and interstellar radiation field) will limit the range of possible physical models of interstellar dust at low metallicity (e.g., Draine 2003, Hensley & Draine 2021). By piggybacking off of *UVEX* spectroscopic surveys of O-stars (see Figure 18) in the LMC and SMC, we can expand this sample by ~ 1000 stars. Because dust affects the broad UV spectrum, even fairly low-SNR (> 10) and low-resolution ($R \sim 1300$) spectra obtained by *UVEX* are well-suited for measuring variations in the UV dust extinction curve in the SMC and LMC.

5.5. Metallicity Mapping in the Milky Way

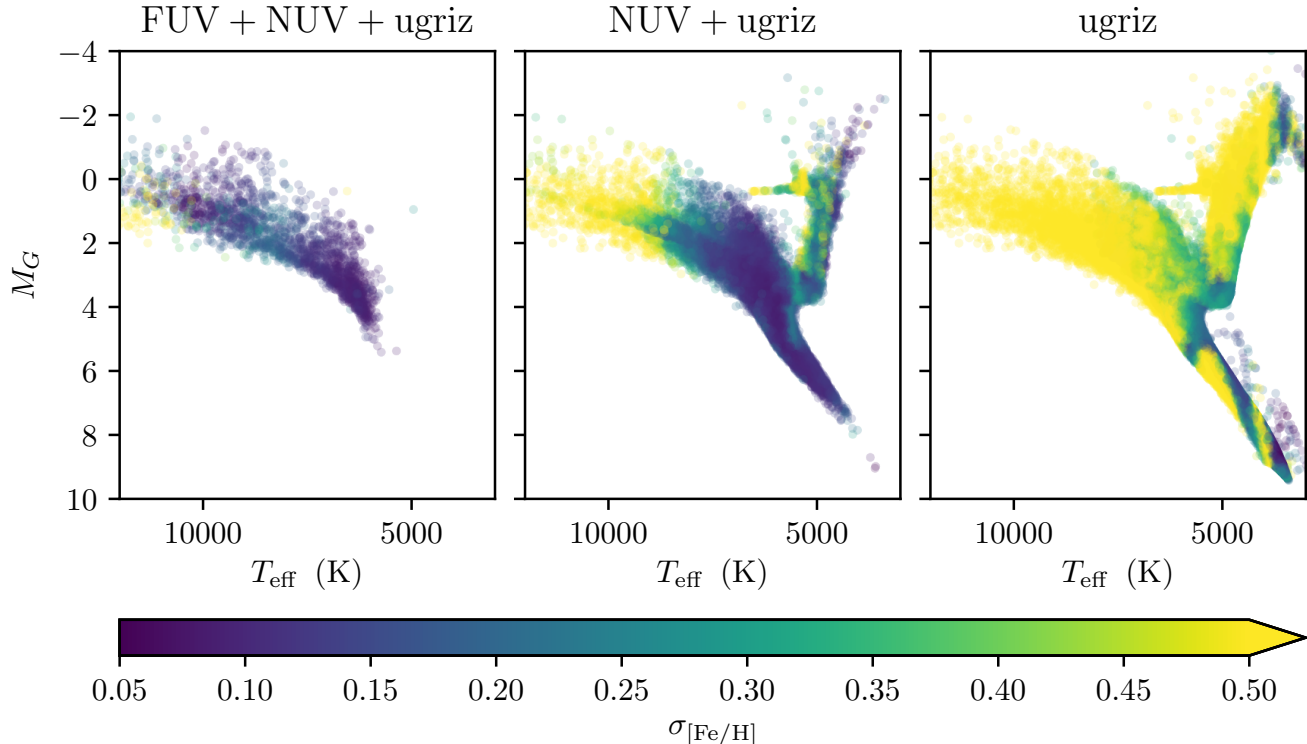


Figure 19. Cramér-Rao bounds on the uncertainties (i.e., the theoretical precision) in $[\text{Fe}/\text{H}]$ obtained using photometry different combinations of *UVEX* and LSST bands, assuming photometric uncertainties of 0.02 mag. Though *UVEX* detects fewer low-temperature stars than LSST, it will achieve lower metallicity uncertainties in $[\text{Fe}/\text{H}]$, particularly for hot (and therefore preferentially young) stars.

The resolved stellar populations of the Milky Way encode its formation history. The stellar halo of the Milky Way, in particular, hosts a wide variety of substructure (e.g., streams, globular clusters, disrupted dwarfs) accumulated through a combination of *in situ* star formation and accretion (e.g., Helmi et al. 1999; Helmi 2008; Bland-Hawthorn & Gerhard 2016). A key diagnostic for unraveling the formation history of the Milky Way is stellar metallicity. Metallicities of individual stars can be used to identify substructures and infer chemical enrichment processes. Many metallicities are derived from iron lines in optical spectroscopy. Dedicated surveys (e.g., APOGEE, LAMOST, GALAH, 4MOST, *Gaia* radial velocity survey; e.g., Deng et al. 2012, De Silva et al. 2015, Majewski et al. 2017) will provide stellar metallicities for ~ 30 million stars over the coming decade, a small fraction of the >1 billion Milky Way stars surveyed by *Gaia* as spectroscopic surveys are limited to fairly bright stars.

Photometric metallicities offer access to a much larger population of stars. Measuring a photometric metallicity usually involves combining UV/*u*-band imaging with an optical band. UV wavelengths are particularly metallicity sensitive (e.g., Balmer break, iron line blanketing

in the mid-UV) when combined with the optical. Using the UV color excess method (Carney 1979), SDSS mapped metallicity of a volume-complete sample of two million F/G dwarfs in the Milky Way disk and halo (Ivezić et al. 2008), with typical uncertainties of 0.2 dex in $[\text{Fe}/\text{H}]$. In particular, at constant optical color (for example, $g - r$), the $u - g$ color is sensitive to metallicity. These tomographic maps of Milky Way stellar metallicity were a boon to Galactic archaeology, allowing identification of chemically distinct subcomponents within the Milky Way. By comparing with LSST optical colors in the Southern Hemisphere and with PS1 in the North, *UVEX* photometry will allow an even more sensitive determination of stellar metallicity. This is because $NUV - g$ stellar colors are far more sensitive than $u - g$ to metallicity. Because *UVEX* is shallower than LSST *u*-band, it will observe fewer stars than LSST. However, *UVEX* will obtain much more precise metallicities per star, particularly for hot stars (see Figure 19). Our simulations show that *UVEX* is expected to obtain NUV photometry of ~ 300 million Milky Way stars, probing a significant fraction of the entire Galaxy (see Figure 20).

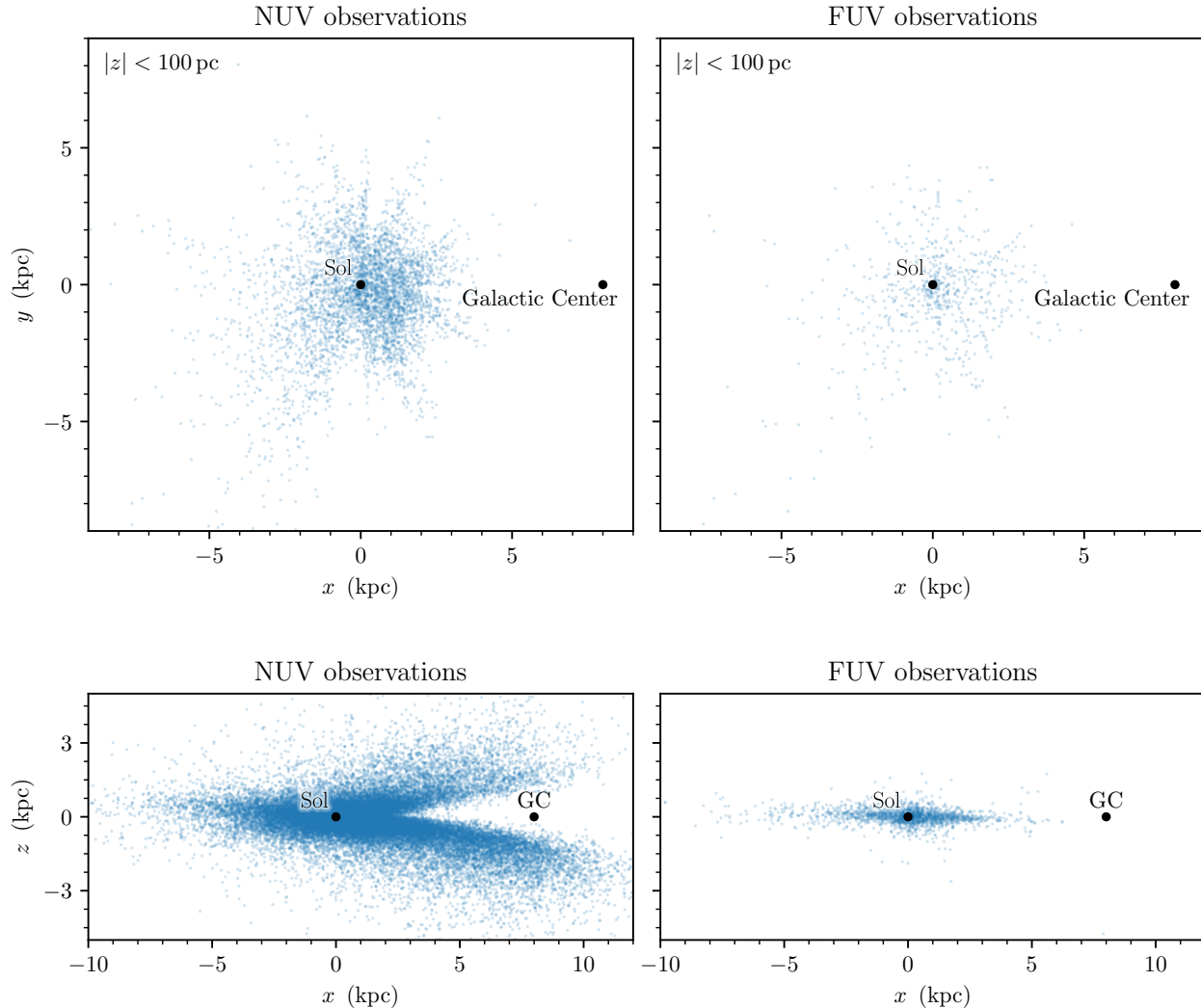


Figure 20. Expected spatial distribution of Milky Way stars observed by *UVEX*. The top panels show a bird’s-eye view – centered on the Sun – of stars within 100 pc of the mid-plane of the Galaxy that would be observed in the NUV (left) and FUV (right) bands. The bottom panels show the distribution of stars that would be observed in these two bands, projected onto the (x, z) -plane (in Cartesian Galactic coordinates, centered on the Sun). As can be seen from these panels, *UVEX* would observe stars throughout a large volume of the Milky Way, extending several kiloparsecs along sight-lines that do not pass through the inner Galaxy.

5.6. Lower-metallicity Massive Stars in the Local Group

Despite their importance to wide-ranging next generation astrophysics (e.g., as discussed in §5.2 and illustrated in Figure 12), stellar models remain essentially entirely theoretical below the metallicity of the SMC. The requirement of deep spectroscopy for individual resolved massive stars severely limits the environments to which this stellar calibration work can be applied. Early results from WLM and IC 1613 identified these galaxies as likely SMC-like in stellar abundances, stymieing the first attempts to measure mass loss rates at lower

metallicity (e.g., Bouret et al. 2015). While challenging at $\gtrsim 1$ Mpc, the dwarf irregulars Leo A (e.g., Cole et al. 2007), the Sagittarius DIG (Garcia 2018), and Sextans A (Camacho et al. 2016, Garcia et al. 2019a) harbor populations of massive stars that are likely our best hope of calibrating stellar models below the SMC. As for stars in the SMC and LMC, the UV is crucial to characterizing these stars and their winds (Section 5.2). But while *HST* has begun the work of collecting spectra for these fundamental targets, the resolution, SNR, and wavelength coverage are of varying utility for characterizing winds and photospheric abundances; and many potential other targets await a dedicated UV survey.

UVEX has the capabilities to fulfill the promise of these metal-poor dwarf irregular galaxies for massive star model constraints. First, the all-sky photometry will immediately provide the most complete picture of unobscured sub-SMC massive stars in the Local Group, where *GALEX* is severely limited by crowding and *HST* NUV coverage is incomplete (Figure 21). Compared to previous work restricted to optical selection, deep *UVEX* imaging will substantially improve the census of luminous blue stars in these galaxies especially for very hot metal-poor stripped binary products.

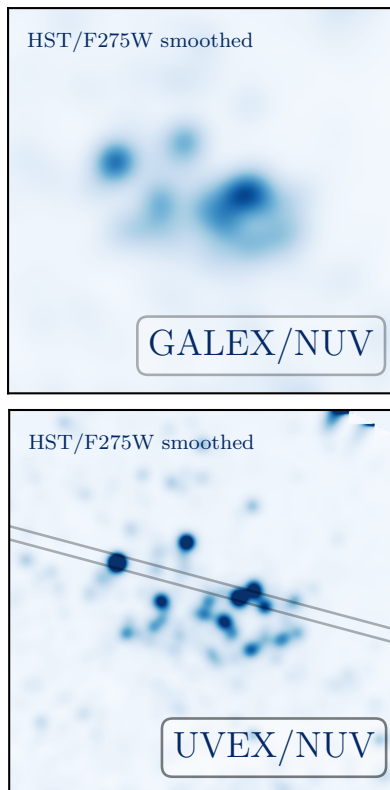


Figure 21. *UVEX* will provide access to individual massive stars in the distant, low-metallicity dwarf irregular galaxies such as Sextans A ($D \sim 1.2$ Mpc). Both full-field imaging from the all-sky survey and deep spectroscopic follow-up of the most UV luminous stars will yield unique constraints on young stellar populations below the metallicity of the SMC.

UVEX spectroscopy would allow for the completion of the first systematic investigation of stellar wind strengths at sub-SMC metallicity. Exposures of order 3–30 ks will be sufficient to provide detailed constraints on the resonant wind complexes and photospheric indices discussed in §5.2, enabling unique measurement of wind terminal velocities and mass loss rates unavailable from the optical. Approximately ten targets without UV data have already been identified with extant published op-

tical spectroscopy (7 O to early-B giants in Sextans A from Camacho et al. 2016 and Garcia et al. 2019a; 2–3 OB stars in SagDIG from Garcia 2018). *HST* will deliver UV spectra over part of the needed wavelength range for a total of 12 OB stars below SMC metallicity (8 in Sextans A, 3 in Leo A, and 1 star in Leo P), though *UVEX* could also be recruited to improve upon the resolution, coverage, and signal-to-noise of these spectra where they may be insufficient to measure robust wind properties (e.g., Garcia et al. 2019b). Though not part of the prime mission, in total, a spectroscopic survey with *UVEX* would at a minimum more than double the sample of sub-SMC massive stars with UV wind constraints.

6. GALAXY FORMATION

One of the primary motivators in extragalactic astronomy is to understand how galaxies form and evolve over cosmic time. This is an enormous enterprise that has spanned decades, engaged hundreds if not thousands of astronomers world-wide, and occupied major fractions of observing time on the ground and in space. While much is known, next generation of surveys could revolutionize our understanding of the field, if and only if they exploit the full power of the electromagnetic spectrum. UV imaging and spectroscopic surveys are an essential component of this revolution. This is because the UV measures star formation rate (SFR) averaged over a timescale which is matched to evolutionary changes in galaxies, ~ 100 Myr. Optical probes such as $H\alpha$ are noisy averages of only ~ 10 Myr, while IR traces reprocessed UV radiation in massive, metal-rich galaxies. UV is uniquely sensitive to the lowest mass, lowest metallicity systems that are virtually dust-free (Fisher et al. 2014) and represent analogues to the first galaxies (Figure 22). UV cleanly probes small amounts of residual star formation in otherwise passively evolving galaxies, essential for understanding how and why galaxies quench individually and collectively (Figure 23). UV spectroscopy probes key elements like Carbon whose metallicity is poorly constrained. UV spectroscopy can also provide the first measurements of $\text{Ly}\alpha$ escape in nearby galaxies, and of $\text{Ly}\alpha$ emission from the circumgalactic medium (CGM) that represents the majority of the baryonic universe and may be the *Deus ex Machina* of galaxy formation and evolution. In this section, we discuss three potential applications of a UV imaging and spectroscopic survey mission: Galaxy Formation, Galaxy Evolution, and Galaxy-Halo Co-evolution.

6.1. Galaxy Formation: Finding and Understanding the Youngest, Lowest Mass, Lowest Metallicity Galaxies in the Local Universe

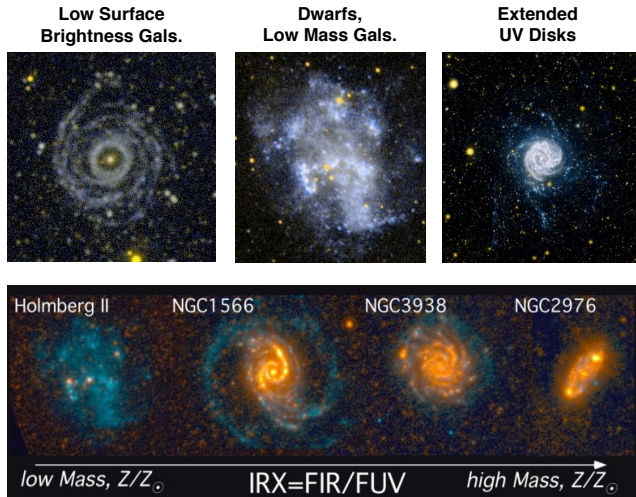


Figure 22. Low mass star forming galaxies are highly visible in the UV, because their metallicity and extinction are low, and the UV sky is dark.

Our knowledge of galaxies and galaxy halos is based largely on studies of those with masses comparable to or larger than the Milky Way ($M \sim 5 \times 10^{10} M_{\odot}$). However, the properties of these galaxies (e.g., Solar metallicity, dusty) are not well-matched to the low-mass ($M \sim 10^5 - 10^9 M_{\odot}$), low-metallicity (1-50% solar) systems that dominate the hot, metal-poor early universe, are thought to power cosmic reionization ($6 \lesssim z \lesssim 20$), and are believed to be the majority of galaxies in the local universe. Although low-mass, low-metallicity (LMLZ) systems are central to a broad range of astrophysics, they are among the least explored galaxy frontier, because only a small fraction of the large expected LMLZ galaxy population is known at any redshift and the birth, evolution, and death of stars at low-metallicities is poorly understood.

A definitive study of local LMLZ galaxies is key to understanding the processes of galaxy formation, stellar evolution and death, and the formation of compact objects in metal-poor environments. UV heating and radiation pressure from massive metal-poor stars and the explosive deaths of metal-poor single and binary stars regulate star formation in ways that are different from the Milky Way (Dessart et al. 2017a) and may be responsible for IMF variations and bursty, chaotic star formation in many known LMLZ systems. With reduced opacities, low-metallicity stars can grow to and maintain larger masses and sizes, and many more interact in binary systems (Karachentsev & Kaisina 2019; Krumholz 2014). In close binaries, lower-opacity winds reduce mass loss rates (Meurer et al. 2009a; Lee et al. 2009a) which leads to significant, but poorly understood

changes to stellar evolution such as fewer red supergiants (Weisz et al. 2012a), enhanced production of single and binary black holes (Sana et al. 2012b), and a broader diversity of SNe types.

Deep *UVEX* all-sky imaging, along with upcoming O/IR surveys (e.g., Rubin, Euclid), will help uncover millions of nearby ($D \leq 100$ Mpc; $z \leq 0.03$) LMLZ galaxies that are predicted to exist and measure their basic properties (e.g., mass, age, star formation rate, dust). Targeted *UVEX* spectroscopy of the youngest, strongest star-forming LMLZ systems will provide crucial rest-frame UV nebular emission templates needed to interpret observations of the first galaxies in the early Universe. The unique and powerful capabilities of *UVEX* will define the LMLZ frontier for decades to come.

6.1.1. Finding the Low-Mass Galaxy Population in the Local Universe

With an all-sky survey $\geq 50\times$ deeper than GALEX, *UVEX* will find the missing local population of low-metallicity, low-mass galaxies. Key questions that will be addressed include: Where are the local low-mass, low-metallicity galaxies? What are their properties? How do they vary with environment?

Our current census of the nearby LMLZ galaxies is highly incomplete. Within 100 Mpc ($z \leq 0.03$), theoretical matching of stellar and dark matter halo masses predicts the existence of ~ 10 -200 million LMLZ galaxies. Yet only $\sim 20,000$ LMLZ galaxies are known in this volume (Robertson et al. 2015b; Elahi et al. 2018), far fewer than even the most conservative theoretical estimates.

Finding local LMLZ galaxies is challenging. They are intrinsically faint and spread across the sky, tracing the local cosmic web from low-density filaments and voids to high-density groups and clusters. Their properties appear to vary with environment: star-forming and gas-rich dominate the field, while groups and clusters host more diverse populations. But these conclusions are based on small, incomplete samples.

Mapping the nearby LMLZ population requires a wide-area, sensitive UV imaging survey. Degeneracies in age/metallicity/dust/redshift mean that O/IR colors (e.g., from Rubin, *Euclid*) alone cannot distinguish local LMLZ galaxies from more massive higher-redshift ($z > 2$) interlopers (Figure 24). Due to redshift and intergalactic gas absorption, massive background galaxies have little flux in rest-frame UV bands, whereas local LMLZ field galaxies have little dust and are predominantly star-forming (Tully et al. 2016, 2019), making them UV bright. Moreover, joint analysis of GALEX+SDSS data shows that the UV is essential for

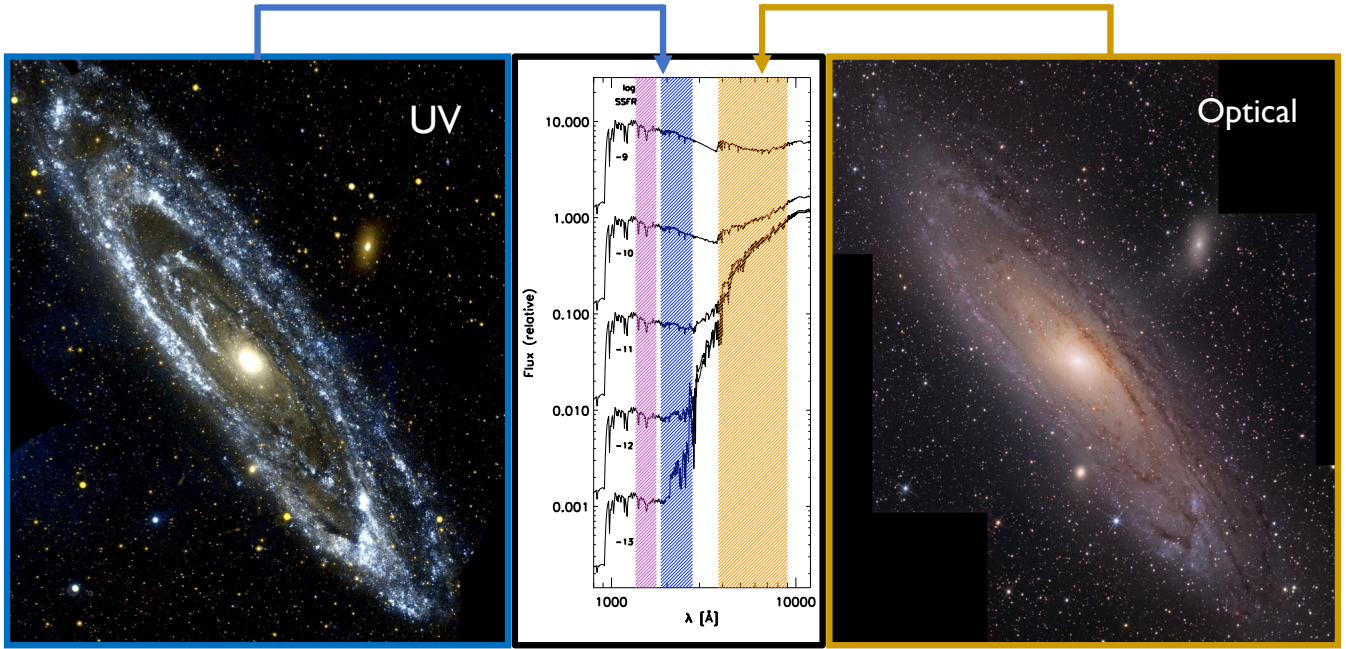


Figure 23. Optical traces ~ 1 -5 Gyr of star formation history, UV traces 100-300 Myr, and can measure small amounts of residual star formation (SSFR) superimposed on old stellar populations [image credits: M31 optical: Adam Block/NOAO/AURA/NSF; UV: GALEX/JPL/NASA].

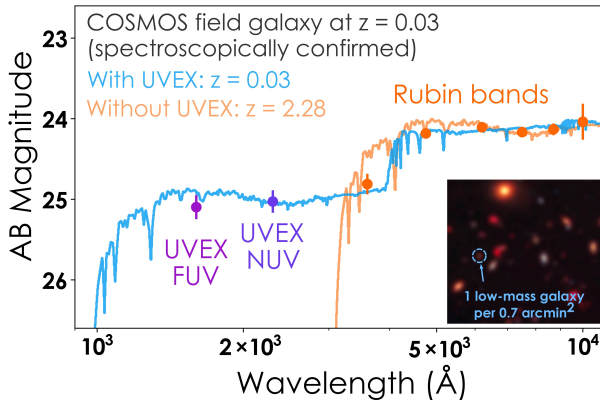


Figure 24. UVEX imaging picks out low-mass, $z \sim 0.3$ galaxies by providing the crucial UV photometry needed to differentiate the Balmer break for a low- z system (blue) from the Lyman break in far more numerous high- z galaxies (orange)

measuring basic properties (e.g., mass, age, star formation rate) of nearby LMLZ galaxies (Nuza et al. 2014).

UVEX will identify millions of LMLZ galaxies within a 100 Mpc volume down to $M_* \sim 10^6 M_\odot$, when combined with optical imaging from Rubin and Northern-hemisphere counterparts (e.g., UNIONS, DESI Legacy Survey). This large sample is essential for anchoring

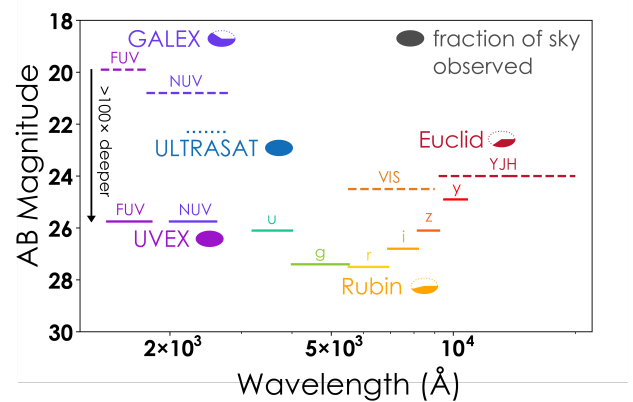


Figure 25. UVEX will provide deep, two-band UV data to complement planned deep, wide-field ($> 10,000 \text{ deg}^2$) optical and near-IR surveys by Rubin and Euclid.

the stellar-halo mass relation, providing the 3D maps of the low-mass, low-density Universe (probing poorly surveyed filaments and voids), enabling the first large-scale study of how the lowest-mass halos evolve as a function of environment, and finding the most extreme examples (lowest metallicity and youngest) for follow-up. For example, if low mass galaxies continue to form, the probability of finding one within 10 Myr of formation is ~ 10

Myr/10 Gyr, or 1/1000. Thus we require a very large sample to isolate the rarest and most interesting forming galaxies.

Adequately sampling rare LMLZ galaxies, and studying large-scale cosmic structures requires surveying the entire extragalactic sky (i.e., 20,000 deg²). A typical 10⁶ M_⊙ star-forming galaxy has $M(UV) = -10$ mag (AB). Detecting such galaxies to 100 Mpc, and constraining star formation rates requires $SNR \geq 5$ to a depth of $m_{UV} = 25$ in both FUV and NUV.

Figure 25 shows the estimated depth of the *UVEX* all-sky UV survey (in a typical high-latitude extragalactic field), highlighting both its generational improvement and its complementarity to modern wide-area O/IR surveys. *UVEX* reaches 4-5 mag fainter than the GALEX wide area surveys over the entire extragalactic sky. GALEX reached $m_{UV} \sim 25$ over only 80 deg², far too small an area to obtain a global census of low-mass systems (Bruch et al. 2021a). The HST FoV is far too small to undertake the needed survey. Many LMLZ galaxies are too faint ($m > 24$) for optical spectroscopy, while because of the bursty star formation histories narrow-band imaging (e.g., H α) is a less reliable tracer of star formation in many LMLZ galaxies compared to the UV.

6.1.2. Nebular Emission in the Lowest Mass, Lowest Metallicity Systems

UVEX will diagnose low- z , low metallicity galaxies dominated by radiation from hot stars, and polluted by early generations of SN. This is essential to the quest to understand the first galaxies at high redshift. Key questions that will be addressed include: What is the radiation environment created by the first generation of stars? What are the feedback processes in high- z star forming regions at very low metallicity?

What we learn from ALMA, JWST, and the ELTs about the first galaxies and their stars will come from integrated nebular emission lines. Emission lines are powerful diagnostics of the baryonic processes that shape galaxy evolution (e.g., star-formation history, supernova feedback, ionizing radiation field). However, interpreting emission lines from the first galaxies is challenging due to a lack of local anchors. The extremely low metallicities, strong radiation fields, and high star formation rates of the first galaxies are not captured in typical nearby calibration samples of resolved stars (e.g., Milky Way, SMC) or integrated light observations of most nearby low-metallicity dwarf galaxies.

To understand these high-redshift environments we need integrated spectral templates of extremely low-metallicity, strongly star-forming, young nearby galaxies. These spectra will anchor the stellar population synthesis models used to interpret observations of primor-

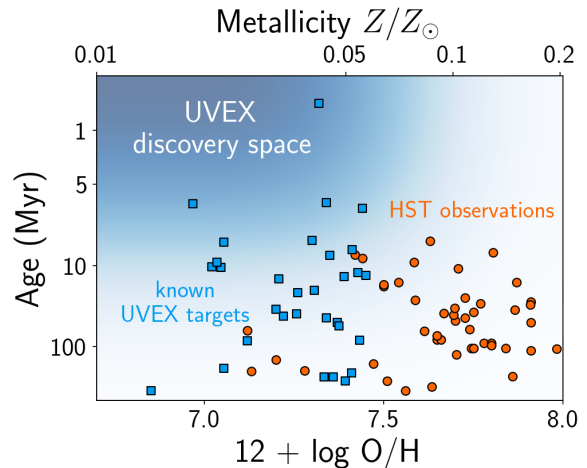


Figure 26. *UVEX* will obtain spectra of the lowest-metallicity galaxies in the local universe. Orange dots are measurements from HST, blue squares indicate the known sample selected for *UVEX* followup. HST can still make some progress in the lighter shaded blue regions but probing the darker blue region requires *UVEX*.

dial galaxies. Rest-frame UV spectra are particularly urgent, as they contain several key diagnostic nebular lines such as He II, O III], Si III], and C III], all of which are being detected in high-redshift observations. The most powerful constraints include the C/O ratio (sensitive to the star formation history, supernova feedback, and age) and C III] / O III] / C IV] / He II (sensitive to the shape of the ionizing spectrum).

HST has opened this field by obtaining UV spectra of several dozen local, strongly star-forming, modestly low-metallicity systems. However, HST has only been able to cover a fraction of the needed age-metallicity parameter space (Figure 26) as the available detector/grating combinations on HST/STIS and COS have throughputs that fall precipitously past $\sim 1950\text{\AA}$, limiting studies to a handful of local LMLZ systems. In contrast, *UVEX* is optimized for sensitivity and resolution across the range from 1500-2000 \AA , making it ideal for acquiring the sorely lacking UV spectra in low-redshift LMLZ galaxies.

6.1.3. The Extremes of Star Formation: Tests of Fundamental Baryonic Structure Formation Processes

In order to understand a fundamental astrophysical process such as star formation, it is critical to vary key parameters to extremes in order to explore how the process changes. In particular, the lowest mass, lowest metallicity, and lowest gas density regimes of star formation probe the impact of mass, metallicity, and density on this process. UV is unique in its ability to trace star

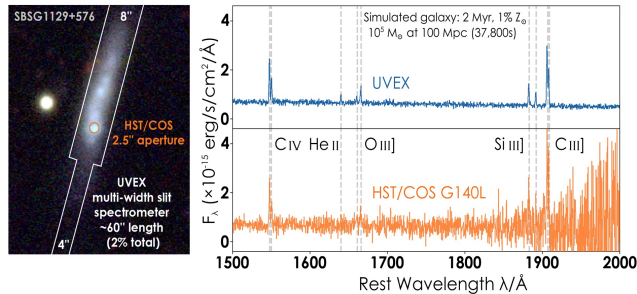


Figure 27. The UVEX spectrograph is optimized for observing nebular emission lines over the crucial wavelength range. Left, a gri image of the local extremely metal-poor galaxy showing HST/COS and UVEX spectroscopic apertures. (right) A simulated UVEX spectrum of a 1% Z_{\odot} low-mass galaxy at 100 Mpc compared to HST/COS for similar integration times..

formation in low mass, low metallicity, and low density regimes, providing key tests of star formation scaling laws, the IMF, and the root cause of low baryon efficiency and low metallicity in the lowest mass galaxies.

For example, GALEX discovered that many galaxies have “Extended UV” (XUV) disks (Thilker et al. 2005; Thilker et al. 2007; Lemonias et al. 2011), extended regions of low-density gas and star formation unlike the bulk of most disk galaxies. These extended regions may be produced by on-going accretion of gas from the IGM, and if so could be used to study the effects of IGM accretion on galaxy growth. XUV disks and low surface brightness galaxies are laboratories for studying the extreme low end of the Schmidt-Kennicutt (SK) star formation scaling law (Kennicutt 1998). GALEX showed (Wyder et al. 2009; Bigiel et al. 2008) that there is a sharp transition in the power-law SK dependence of SFR density with gas density. Star formation continues, but the dependence is much steeper, suggesting a physical transition perhaps produced by the lack of dust and resulting low H_2 formation rate and $H_2/H\text{ I}$ fraction (Krumholz 2013). A deep UVEX survey would provide a definitive sample of low-mass galaxies and XUV disks, allowing the study of the most extreme examples. Follow-up of these with long-slit UV spectroscopy would constrain stellar populations, star formation rate and history, metallicity, and dust content. Long-slit spectroscopy would probe H_2 fluorescent emission from the Lyman and Werner bands (Martin et al. 1990), a measure of the equilibrium balance between H I and H_2 in photodissociation regions.

The initial mass function (IMF) has been assumed to be universal based on relatively limited data. The high-mass end of the IMF may be particularly sensitive to key processes, since these low-probability objects require the

most massive molecular clouds to form without the negative feedback of stellar winds. A powerful constraint on the high-mass end of the IMF comes from comparing $H\alpha$ and UV luminosity, since the former traces the highest mass stars and the latter traces high-intermediate mass stars. GALEX provided strong but not definitive evidence for a top-lite IMF in low mass galaxies (Lee et al. 2009b; Meurer et al. 2009b). The challenge in interpretation is that the burstiness of star formation history in low mass galaxies produces a noisy $H\alpha/UV$ ratio which could be biased (Weisz et al. 2012b). $H\alpha$ and UV respond differently to dust extinction (Calzetti et al. 2000) also adding uncertainty and possible bias (Seibert et al. 2005; Johnson et al. 2007a; Johnson et al. 2007b; Salim & Narayanan 2020). However, with a large, homogeneous, multi-wavelength sample it should be possible to simultaneously solve the SFH, dust, and IMF problem using the connect-the-dots approach for SFH (cf., §6.2) and recent techniques to constrain extinction and extinction laws (Salim & Narayanan 2020).

The lowest mass galaxies are also the least successful at making stars (lowest baryon-to-dark matter ratio) and at making (or keeping) metals. Since galaxies are as a whole inefficient at making stars, low mass systems are perfect laboratories for uncovering the processes which prevent efficient star formation and metal retention, determining the low-mass end of the baryon-to-dark matter efficiency relation (Moster et al. 2013) and the mass-metallicity relation (Tremonti et al. 2004). As we discuss below, it should be possible to use a differential constraint on SFH, in combination with measurements of $Ly\alpha$ emission in low mass galaxy halos to track the ebb and flow of star formation in low mass systems, and relate this to the feedback driven outflows which are believed to be the root cause for the low baryon efficiency and metallicity of low mass galaxies.

A spectroscopic subsample of low mass galaxies and low density star formation regions will provide critical calibration of the photometric sample. With fast UVEX long-slit spectroscopy it will be possible to measure UV spectra in low surface brightness conditions where star formation is below the canonical threshold. Spectroscopy provides critical diagnostics of stellar age, metallicity, feedback, and the IMF (Figure 28).

6.2. Galaxy-Halo Co-Evolution

6.2.1. The Galaxy “HR-Diagram”

A fundamental tool for probing galaxy evolution is the UV-optical color-magnitude diagram (UVOCMD; Figure 29). The extinction-corrected UVOCMD is truly a galaxy “HR-diagram” (GHR), because the optical/NIR magnitude traces stellar mass (M_*), and the UVO color

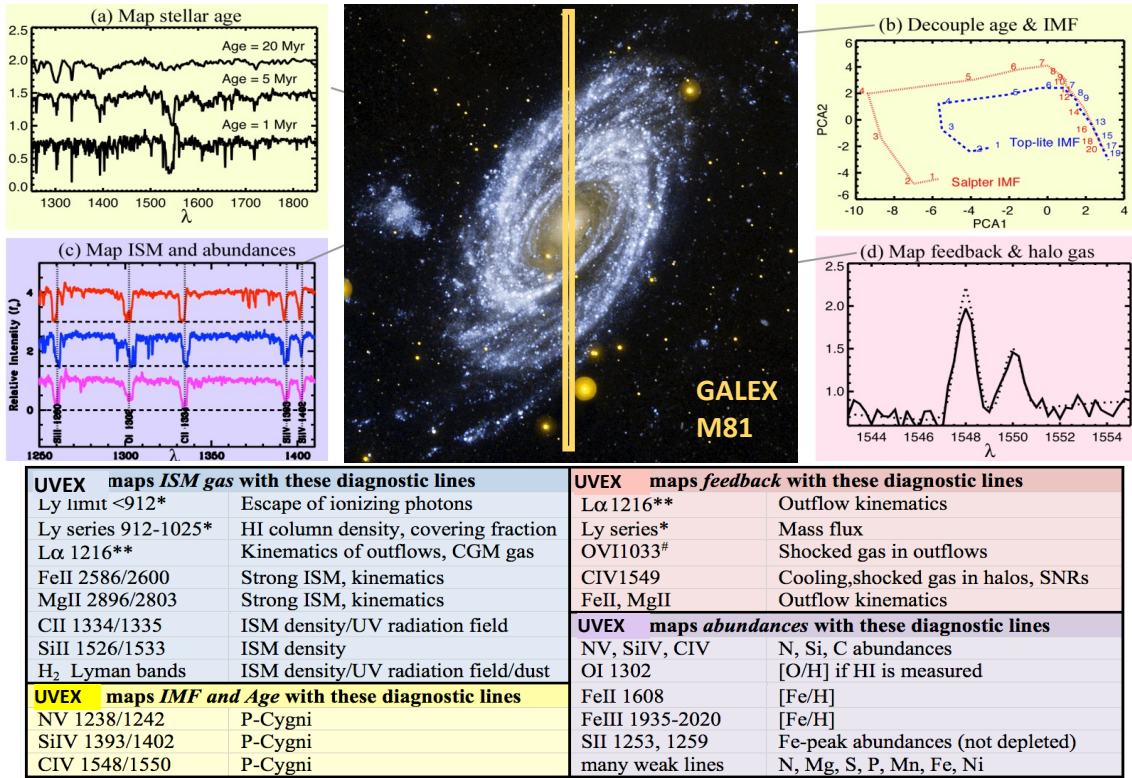


Figure 28. UV spectroscopy provides key physical diagnostics of galaxies, including metallicity (notably carbon), IMF, stellar age, presence of feedback. UVEX long-slit spectroscopy will provide exquisite spectra of nearby and distant galaxies in the FUV and NUV.

(e.g., NUV-r) traces specific star formation rate (sSFR) to remarkably low levels. On-going star formation moves galaxies to the right. New star formation bursts move galaxies up, while quenching moves them down. Thus we can trace on this diagram the key processes driving galaxy evolution. The rate that galaxies move on the GHR diagram is determined by the processes driving evolution, as with stars largely the availability of fuel. Bursts are caused by the delivery or threshold exceedance of new (“cold”) gas, while quenching results from the removal of cold gas. By “cold” we usually mean gas whose cooling time is much less than a Hubble time, typically $T < 10^6$ K.

The GALEX mission and other NASA Great Observatories provided a huge leap forward in our understanding of galaxy formation and evolution. We now know that the galaxy distribution can be described to first order as bimodal (i.e., either red or blue), with a population of transitional galaxies in the so-called “Green Valley” between the actively star-forming blue cloud galaxies and the passively evolving red sequence systems (Wyder et al. 2007; Schiminovich et al. 2007; Martin et al. 2007a; Martin et al. 2007b). The UVOCMD that first identified this bimodality and the intermediate green phase

can also be extended beyond the low redshift galaxies observed by GALEX into higher redshift regimes to help explore evolution over time. As large populations of galaxies at higher redshifts have been added to the UVOCMD from more recent surveys (e.g., Ilbert et al. 2013), we can now state that the mass fraction of galaxies in the red sequence vs. the blue sequence has grown by a factor of at least ~ 3 since $z \sim 1$. This indicates that there is a global evolution across time that we are only just beginning to understand and characterize. With the next generation of UV and multi-wavelength surveys, we will directly measure the evolution of galaxies across the GHR. By doing this, we will be able to answer three key questions: 1) What equilibrium processes create the star formation “main-sequence”? 2) What processes drive galaxies out of equilibrium leading to star formation “quenching”? and 3) How do galaxy halos and galaxies co-evolve, and how does this co-evolution govern galaxy evolution?

6.2.2. The Star Formation Main-Sequence (SFMS)

Star forming galaxies form a tight “main-sequence” with SFR proportional to stellar mass (Noeske et al. 2007; Wyder et al. 2007; Salim et al. 2007), but we do

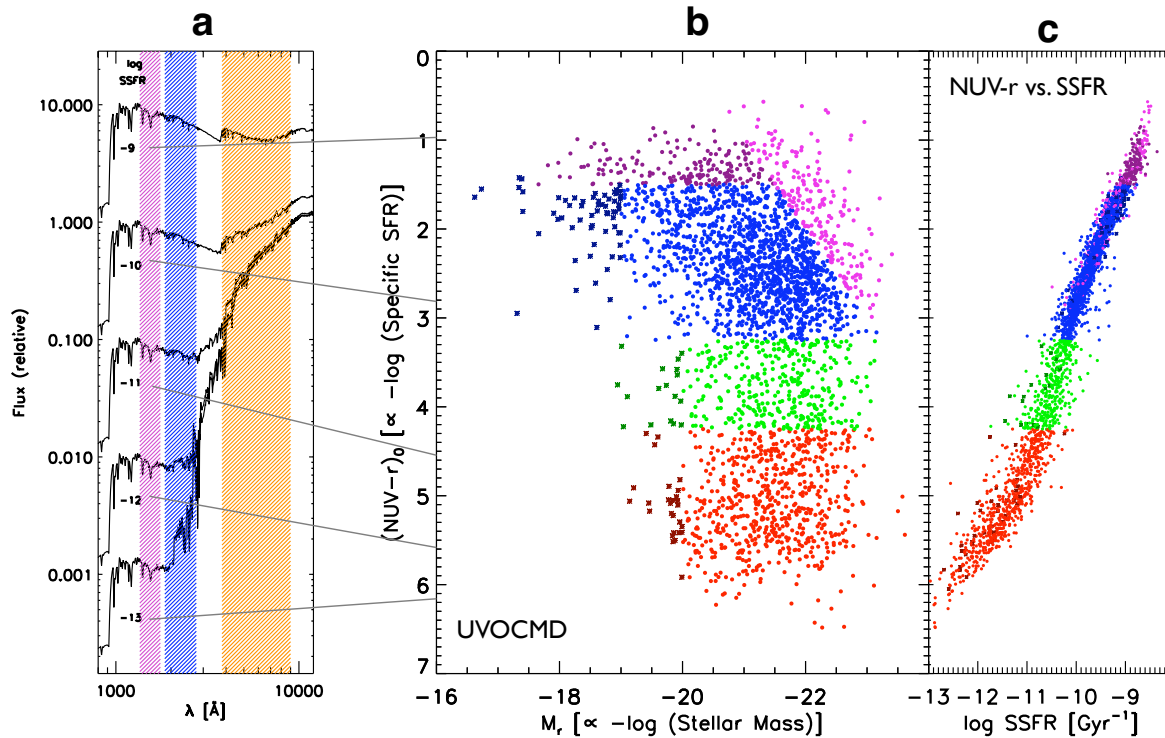


Figure 29. Galaxy HR Diagram constructed from mass-tracing optical/NIR color and FUV or NUV color. a) Old population with superimposed star-forming population with different specific star-formation rates (SSFR). b) Distribution of galaxies on the GHR showing the relation between star forming (main sequence) galaxies [blue], galaxies bursting above the SFMS [purple], transition galaxies [green], and quenched galaxies [red]. c) Tight correlation apparent between the extinction-corrected NUV-r color and SSFR.

not understand why. We need to understand the processes driving returns to equilibrium when galaxies are perturbed by mergers/accretion/gas exhaustion. These include galactic winds/fountains, accretion of new gas, and adjustments in the star formation efficiency in SF regions. A large sample of SF galaxies can be split into subsamples, e.g., mass, deviation from MS, and environment. The combination of FUV/NUV and optical/IR photometry and targeted spectroscopy allows determination of recent SF history, which probes deviations and returns to equilibrium.

Key to this investigation are the power of combining integral and differential constraints on evolution, which can only be accomplished with very large and homogeneous photometric samples spanning the UVOIR. The growth of stellar mass in galaxies is an integral constraint, while the SFR history is a differential constraint (Madau & Dickinson 2014). The UVOCMD vs. redshift is an integral constraint, while a measure of the flux of galaxies across the UVOCMD provides the next level of differential constraint (Martin et al. 2007a; Martin et al. 2017; Darvish et al. 2018; de Sá-Freitas et al. 2021). By combining GHR integral and differential constraints with galaxy-halo connection methods (e.g., Halo Occu-

pation Distribution [HOD]), we can take a step towards the ideal of “watching” galaxies evolve by weaving together statistically the snapshots we observe. Because stellar and dark halo mass can only increase with time, and because the integral and differential constraints are linked by a continuity equation, we can begin to assemble an ensemble of individual galaxy star formation histories, and correlate these with halo mass and environment. We call this approach “Connecting the Dots” (CTD). This approach will provide a powerful new constraint on galaxy formation and evolution models and numerical simulations.

How does this work in the case of the SF main sequence? The best way to diagnose equilibrium processes is to observe them out of equilibrium, where they will be maximally subject to the return-to-equilibrium processes. If we consider galaxies on, below, and above the SF main sequence, the integral constraint comes from how many galaxies are in each bin vs. redshift. The differential constraint comes from how fast galaxies are moving between these states. The distribution in bursting “Star Formation Acceleration” ($SFA \equiv d(\text{NUV} - H)/dt \sim d(\text{SSFR})/dt > 0$) and quenching ($SFA < 0$) gives the relative fraction vs. the speed

of these processes. Fast bursting could be produced by mergers, slow bursting by changes in gas accretion. Fast quenching could be produced by galactic winds evacuating the gas, while slow quenching by starvation of gas (accretion strangulation by hot gas or ram pressure/tidal stripping of satellites). Therefore the spread in SFR and the distribution in SFA give strong constraints on the equilibrium processes on the SFMS.

We do not know whether the lowest mass galaxies exhibit a SFMS, and what the dispersion around the relation is. It might be the case that very low mass galaxies have long periods of quiescence punctuated by SF bursts, as is suggested by resolved stellar photometry of nearby dwarf galaxies (Weisz et al. 2014a; Weisz et al. 2014b; Weisz et al. 2014c; Weisz et al. 2015). *UVEX* will supply the necessary sample to determine the star formation history in the lowest mass galaxies in the universe. UV observations provide a direct measurement of SFR in these low mass galaxies because of their low mass, metallicity, and dust extinction.

6.2.3. Cosmic Quenching

Cosmic quenching has shut down star formation by more than an order of magnitude since $z \sim 2$. Quenched galaxies exist at all masses but dominate the high mass population. The fundamental evolutionary process, quenching of star formation transforms main sequence star forming galaxies into passively evolving galaxies, is still only poorly understood. Why do most high mass galaxies quench? Why do some intermediate and low mass galaxies quench, while others do not? What are the physical processes responsible for quenching: merging, starvation/strangulation, stripping, feedback? How does quenching depend on halo mass, environment, position in the cosmic web, central/satellite identification? What causes rejuvenation in quenched galaxies?

The approach discussed in the previous section, CTD on the GHR diagram, allows us to measure the flux of galaxies from the SFMS to the red sequence (quenching through the green valley, $SFA > 0$) and the flux of galaxies experiencing periods of rejuvenation (bursting, $SFA < 0$). The speed of quenching and bursting is determined by the physical processes at work, such as strangulation (slow) and mergers/AGN winds (fast). Combining the integral and differential constraints will test whether we have fully accounted for the evolutionary tracks of galaxies across the GHR. The distribution of SFA vs. position on the GHR, vs. environment (e.g., local density), AGN presence, and central/satellite status will provide powerful new constraints on models and simulations of galaxy quenching. The FUV and NUV provide the maximum leverage to study quench-

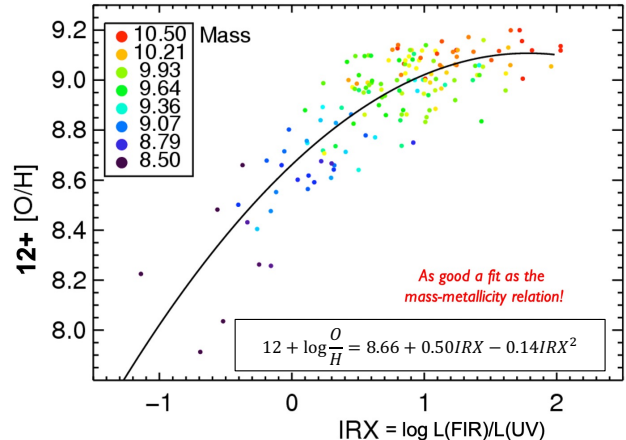


Figure 30. Metallicity is traced by IRX (IR/UV luminosity ratio) with a correlation tighter than the mass-metallicity relation.

ing because the UV traces SFR even for very low SSFR galaxies, where quenching has already begun. In other words, they magnify the green valley, where galaxies in transition reside.

6.2.4. Galaxy Metallicity

The mass-metallicity relation is a fundamental scaling relation of galaxies. The global metallicity is an archival record of the star formation, gas inflow and outflow, and merger history of a galaxy. Combining a metallicity history with a SF history of galaxies as a function of mass, SFR, and environment will paint a comprehensive picture of galaxy formation and evolution. Understanding the low mass metal deficit, ascribed to feedback, is key to our understanding of galaxy evolution. The poorly constrained carbon abundance distribution is central to our understanding of the formation of molecular clouds, stars, and life. We discussed above how this could be measured spectroscopically.

UV extinction (UVX) is a surprisingly good proxy for metallicity (Martin et al. 2007a; Martin et al. 2007b; Wyder et al. 2007), as we show in Figure 30, and can be determined by either measuring the IR excess ($IRX = L(IR)/L(UV)$) or SED fitting of UVOIR photometry. Metallicity represents a third dimension in the GHR diagram, given that it traces a completely independent integral of the gas inflow, enrichment, and outflow cycles that are tied by different relations to the star formation history. If we add UVX as a third empirical dimension to the UVOCMD, and accumulate a large enough statistical sample to robustly sample a 3D distribution, we can obtain even more powerful constraints on the combined star formation and gas enrichment history.

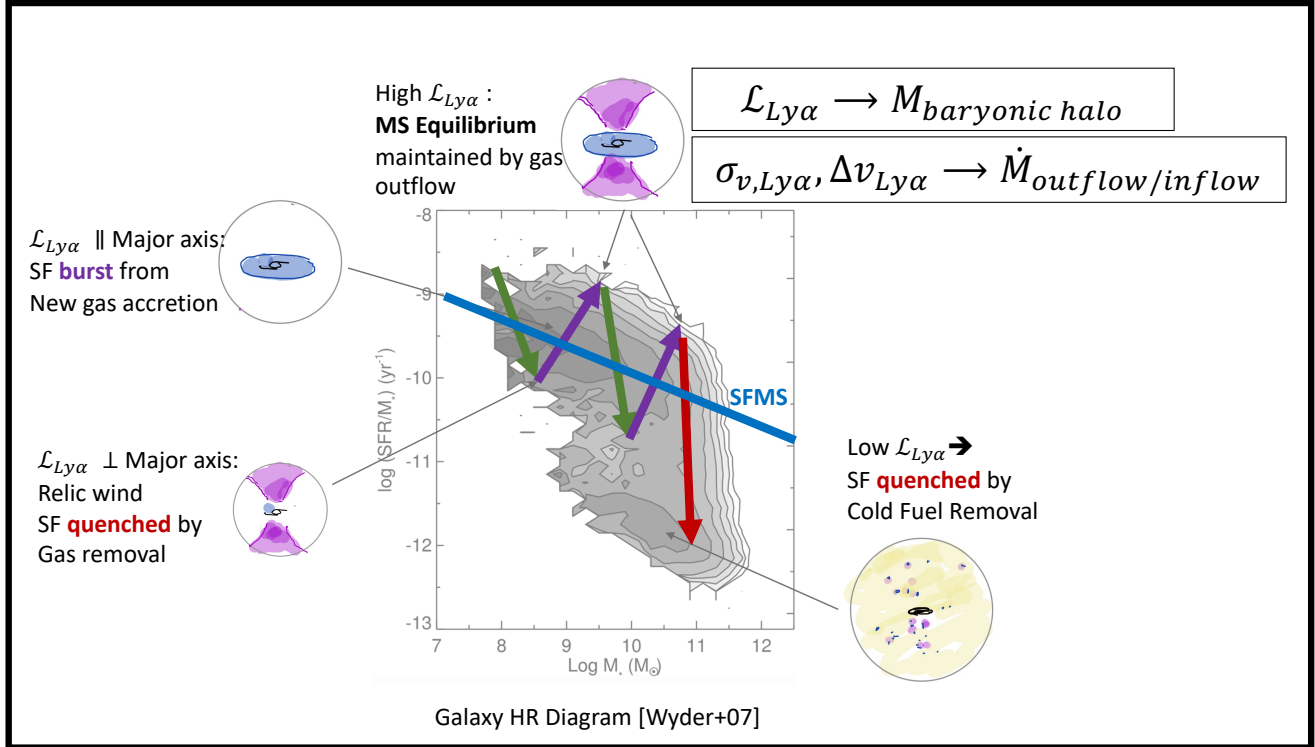


Figure 31. Galaxy HR Diagram related to baryonic halo traced by $\text{Ly}\alpha$. Halo $\text{Ly}\alpha$ luminosity gives baryonic halo mass, and line profile gives mass flux in outflows or inflows through the halo. UVEX traced SFR and SFA give recent bursting/quenching history.

6.2.5. Galaxy-Halo Co-Evolution

Galaxy formation and evolution is governed by the flow of gas, metals, and energy into and out of the halo. Galaxy evolution is really galaxy-halo co-evolution. Most of the baryons in the universe are located in the halos of galaxies (Circum-Galactic Medium) and the IGM (Tumlinson et al. 2017). The baryons required for star formation in galaxies are delivered through the halo and returned there by galactic winds. Thus, the star forming main sequence, the mass-metallicity relation, and the causes of cosmic quenching may ultimately be tied to the flow of gas in the halo. A census of this halo gas vs. galaxy mass, star formation history, and environment is required to understand the co-evolution of galaxies and their halos.

$\text{Ly}\alpha$ is the most sensitive tracer of halo gas in emission. $\text{Ly}\alpha$ halos can be measured photometrically by stacking analysis of galaxies with redshifts at the peak of the FUV band (compared to neighboring redshifts). Because of the long-slit and fast spectrograph design, deep UVEX spectroscopic observations will detect $\text{Ly}\alpha$ halos in 20,000 galaxies in targeted and blank fields for comparison and calibration, and provide information about kinematics, inflows, and outflows. $\text{Ly}\alpha$ halo measurements will be stacked on galaxy properties on

the GHR diagram in order to determine global scaling laws between halos and galaxies (Figure 31). The key observables are the $\text{Ly}\alpha$ luminosity (L_α), line profile (width, mean), and mass to light ratio (M/L_α). For example, low mass galaxies that are above and below the star forming main sequence can be compared in M/L_α to determine the role of halo gas flows in maintaining main-sequence equilibrium. Quenching galaxies may show lower M/L_α than galaxies of the same mass on the SFMS. Metal lines (O IV, O VI, N V, C IV, C III, Si IV) may also be detected from warm baryonic halos.

7. COSMIC EXPLOSIONS

Supernovae (SNe; Branch & Wheeler 2017) play a major role in the structure and evolution of galactic ecology and, unsurprisingly, they constitute a vibrant research area of modern astrophysics. Stellar explosions inject energy, momentum and newly synthesized metals into the interstellar medium. With the recent discovery of kilonovae resulting from double neutron star coalescence (e.g., Margutti & Chornock 2020 for a review), astronomers now have a better understanding of how SNe contribute to the buildup of the periodic table.

We identify three main frontier areas in the field of stellar explosions. In most cases, SNe that are not of thermonuclear origin leave a stellar residue in the form

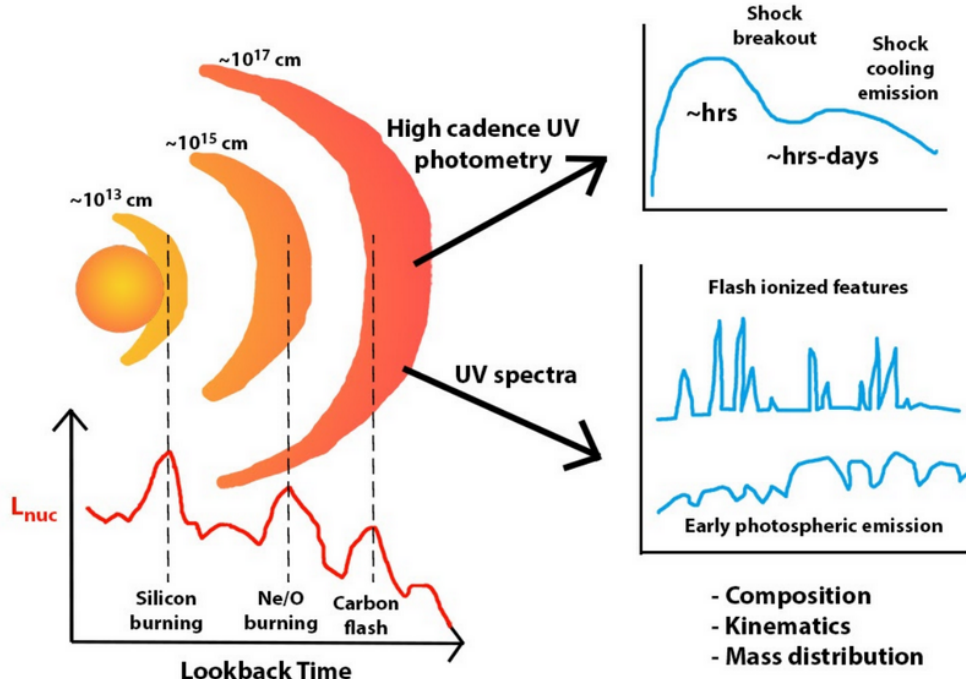


Figure 32. Cartoon showing the mapping between the last nuclear burning stages before core-collapse, (lower left plot), the ejection of shells of material by the progenitor as a result of instabilities developed in this process, and the observables (i.e., UV light-curves and spectra; plots on the right). Rapid turn around UV spectroscopy of infant explosions in the hours after core-collapse (Fig. 34) can uniquely reveal the composition, kinematics and mass distribution of shells of material ejected during the last moments of life of the progenitor star. In this way, UV observations can reveal details about core burning instabilities that would not be otherwise accessible.

of neutron stars and black holes. The natal properties of neutron stars – rotation and strength of magnetic field – appears to range over many orders of magnitude. Newly formed black holes can be born spinning slowly and dominated by fallback or spinning rapidly and generating tremendous amount of power via accretion of stellar debris. In either case, in some fraction of the events the central object injects power following the explosion (e.g., luminous magnetar or power generated by an accreting black hole), and the resulting supernova is distinct and bright. In fact, the spinning accreting black hole is an accepted model for gamma-ray bursts (GRBs; e.g., see Woosley & Bloom 2006; Hjorth & Bloom 2012; Cano et al. 2017 for reviews of GRB-SNe) and the magnetar model is a popular explanation for super-luminous SNe (SLSNe; see below) and might be behind some observational manifestations of “Fast and Blue Optical Transients” as well (FBOTs; see below).

Next, the structure and chemical composition of stars at the time of explosion, and their very recent mass-loss history in the final $\sim 0.1 - 100$ years before stellar death are among the least understood aspects of stellar evo-

lution (e.g. Smith 2014b) and have direct consequences on the explosability of a star (e.g., Janka 2017 and references therein). Specifically, a major open question is if the physical origin of instabilities that act in the final moments of stellar life (at $\delta t < 1$ yr) and that originating from deep down the stellar core (e.g., Quataert et al. 2016, Fuller & Ro 2018, Morozova et al. 2020, Leung & Fuller 2020; Wu & Fuller 2021; Figure 32) can trigger the most extreme episodes of mass loss in massive stars across the mass spectrum that we have just started to uncover with observations (for some examples see, e.g., Pastorello et al. 2013; Margutti et al. 2014; Smith 2014b, Margutti et al. 2017, Bruch et al. 2021b, Strotjohann et al. 2021; Jacobson-Galán et al. 2021). Extreme mass loss timed with core-collapse might play an important role in defining the thermal UV-optical emission of the emerging (motley, perhaps) class of FBOTs (Drout et al. 2014, Arcavi et al. 2016, Pursiainen et al. 2018, Ho et al. 2021a). From a different perspective, the non-thermal emission of long GRBs and FBOTs represents one of the few real-time observational manifestations of the compact object formed in core-collapse: the properties of

their relativistic or sub-relativistic jets directly link back to those of the newly-formed neutron star or black hole (Margutti et al. 2019, Ho et al. 2019a, Ho et al. 2019b, Ho et al. 2020a, Coppejans et al. 2020, Perley et al. 2019, Perley et al. 2021a).

Finally is our limited knowledge of which stars are progenitors of Hydrogen-poor supernovae (which together comprise >50% of SNe by volume, Li et al. 2011), including normal core-collapse explosions and SLSNe (e.g., Quimby et al. 2013, Chomiuk et al. 2012). Finally, the origin of SNe of Type Ia, which have been vastly employed as cosmic ladders to reveal the accelerating Universe (Riess et al. 1998) continues to be shrouded (e.g., Maoz et al. 2014).

In summary, the past decade has uncovered a dizzying range of new phenomena but our understanding is poor. This lack of understanding is significant, as it further impacts the estimates of the initial stellar mass function in galaxies and star formation through cosmic time (e.g., Smith 2014b and references therein). Stated succinctly, *linking stellar progenitors to SN types and to their compact object remnants is a fundamental goal in modern astrophysics.*

It is clear that further progress requires observational guidance. Below we outline an ambitious program to be undertaken with *UVEX* which is designed to advance our understanding of the phenomena and physics of the frontier areas discussed above. We set the stage by first summarizing the unique diagnostic value provided by UV spectroscopy (§7.1). We then discuss the key progress that will result from focused UV spectroscopic studies of the most common types of SNe (§7.2). We conclude with how the all-sky *UVEX* survey will naturally allow for exploration of exotica, in particular the most luminous and also the rarest events (§7.3).

7.1. *The unique role of UV spectroscopic observations of Cosmic Explosions*

Following the explosion the debris is very hot. The peak emission naturally cascades from high energy to low energy as time goes by. The first radiation able to escape the explosion is the shock breakout (Waxman & Katz 2017 for a recent review), which peaks in the UV on timescales of \approx hours for many extended stellar progenitors (e.g., Campana et al. 2006; Bersten et al. 2018). The next phase of UV emission can arise from two distinct phenomena: (i) the SN shock interaction with a companion star (e.g., Kasen 2010, Liu et al. 2015); (ii) the SN shock interaction with the very nearby circumstellar medium (CSM), which was sculpted by the recent mass loss by the progenitor star before stellar death (e.g., Smith 2014b; Chevalier & Irwin 2011; Chevalier &

Fransson 2017 and references therein). For massive stellar explosions, scenario (ii) applies. The gas then rapidly expands and cools, shifting the peak of the emission towards increasingly longer wavelengths. This combines with the higher line blanketing at lower temperatures to quickly suppress the UV flux within a few days after the end of the interaction phase. This final phase of declining UV emission (and progressively emerging optical emission) from the shock heated ejecta can thus be studied by using ground-based observations (see the temporal evolution of the UV and r-band light-curves from a red supergiant star explosion in Figure 33).

Our focus here is on the second phase of UV emission. Because of the much larger velocity of the SN shock compared to any pre-explosion mass ejections ($v_{shock} \sim (10 - 1000)v_{ej}$, e.g., Chevalier & Fransson 2017), the SN shock effectively acts as a time machine, and a UV spectroscopic sequence during the earliest ($\delta t < 48$ hours post-explosion) stages offers a unique opportunity to probe the mass-loss history and chemical composition of the exploding star in the last years of evolution. This phase is rich with diagnostics (mass and composition of the ejecta; mass and radius of the pre-explosion ejected shell or shells, etc.). The short-lived nature ($\delta t \lesssim 48$ hours) of the UV emission from the explosion's shock interaction either with the companion or with confined CSM shells deposited in the environment by the dying star in the years before explosion, coupled with the current complete lack of UV spectroscopic facilities with rapid repointing capabilities, makes this an assuredly fertile field for both detailed studies and exploration.

The HST ToO response time is $\delta t > 48$ hours after trigger submission, which clearly prevents very early UV spectroscopy of transients of any kind (Figure 33, gray arrows in the main panel). Previous HST and *GALEX* spectra of normal core-collapse SNe were usually taken at least one week after explosion, when the SN ejecta had cooled and the UV emission was suppressed relative to the optical (e.g., Baron et al. 2000; Gal-Yam et al. 2008; Marion et al. 2014). In the case of persistent interaction with an extended CSM, UV spectra at later times provided unique insight into the CSM abundances and properties (e.g., Fransson et al. 2005, 2014; Ben-Ami et al. 2015).

Obtaining rapid-response broadband UV spectroscopic sequences is beyond the capabilities of current missions. To date, the best observed core collapse event is SN 1987A, which exhibited a drop by a factor of 2000 in the FUV flux over the first 5 days after IUE observations commenced 1.5 days after explosion (Pun et al. 1995). In the subsequent decades, no compara-

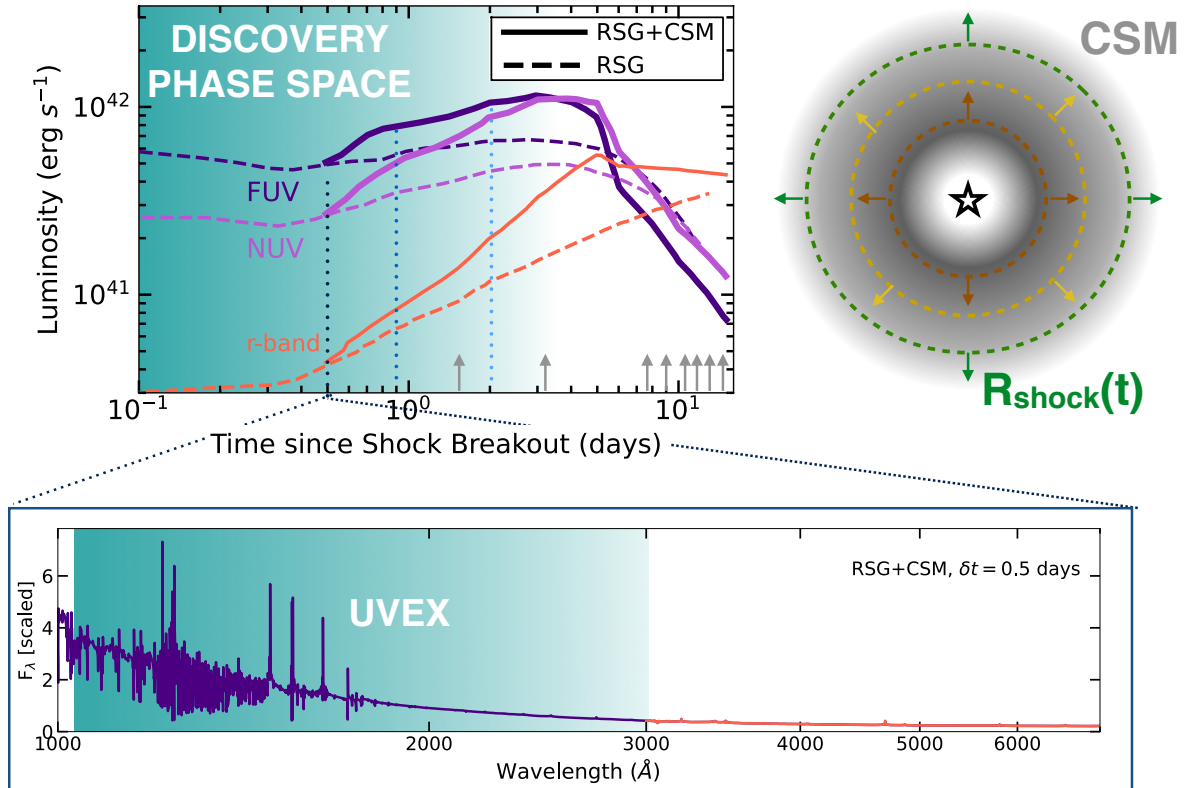


Figure 33. For most stellar explosions, the very early emission peaks in the UV. The explosion of a red supergiant (RSG) star surrounded by a dense shell of circumstellar medium (CSM, grey shell in the upper right cartoon) is a bright source of FUV (dark purple solid line) and NUV emission (light purple solid line). As the explosion’s shock propagates into the CSM (green, gold and brown dashed lines in the cartoon) it ionizes the material that recombines producing a rich UV spectrum (lower panel) that carries direct information on the unknown chemical composition of this material. At early times the optical emission is significantly fainter (see the r-band light-curve in the upper-left panel) and has less prominent spectral features, as shown in the lower panel (red line). Dashed lines in the upper-left panel: FUV, NUV and r-band light-curves of the same RSG explosion without a thick CSM. The presence of CSM directly manifests as a more luminous UV display and different spectrum (Figure 34). Grey vertical arrows: epochs of acquired UV spectra of SNe, including the International Ultraviolet Explorer (IUE) observations of SN 1987A which started 1.5 days after the neutrino burst (Pun et al. 1995) and the earliest Hubble Space Telescope (HST) spectra, which were acquired ~ 3.3 days after the estimated time of first light of SN 2020fqv (Tinyanont et al. 2021). *UVEX* will thus explore a completely pristine part of the parameter space and will provide the characterization of stellar explosions of all types (from ordinary to rare explosions) in their earliest hottest phases. Simulated spectra from Dessart et al. (2017b).

ble UV spectral sequence has been acquired because of the slow response time of HST. The earliest HST UV spectrum of a SN yet obtained was 3.3 days after explosion (Tinyanont et al. 2021). The Swift/UVOT slitless grism has rapid-response NUV capability, but has limited sensitivity and low resolution, with spectra that do not extend to the feature-rich FUV (Romig et al. 2005; Bufano et al. 2009). *UVEX* will uniquely fill this observational gap. As we detail in the next section, at early times optical spectra are relatively featureless (see the UV-optical spectrum displayed in Figure 33), and rapid optical spectroscopy does not access enough bright emission lines to constrain parameters (see e.g., Groh 2014,

their Section 4, for the case study of SN 2013cu, a SN with arguably the best optical flash spectroscopy, and yet an unconstrained stellar progenitor type because of the lack of UV spectroscopic coverage).

UVEX, with its ToO capabilities and highly-sensitive low-resolution spectrometer, is perfectly matched to realize the vision described above. *UVEX* spectroscopic observations of stellar explosions will map for the first time the chemical composition, kinematics and location of the innermost layers of CSM of normal (§7.2) and exotic (§7.3) stellar explosions, providing information that would not be otherwise available. In the case of Type Ia SNe, *UVEX* observations have the potential to un-

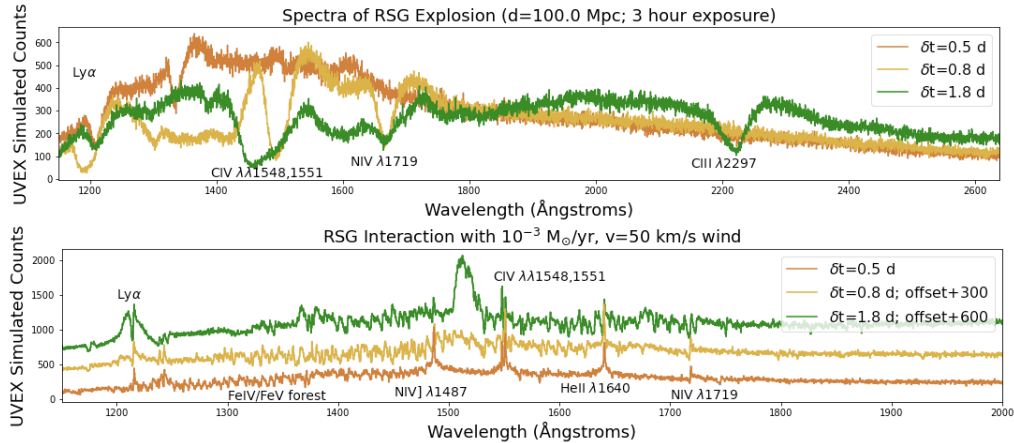


Figure 34. Simulated multi-epoch early *UVEX* spectra of the RSG explosions of Figure 33. We assume a representative distance of 100 Mpc and a *UVEX* exposure time of 3 hours. *Upper panel:* RSG explosion without CSM. *Lower panel:* RSG explosion embedded in thick CSM created by large pre-explosion mass-loss with rate of $10^{-3} M_{\odot} \text{ yr}^{-1}$ and ejected with velocity of $v_w = 50 \text{ km s}^{-1}$. The presence of dense CSM in the explosion’s surroundings completely changes the spectroscopic appearances of the SN (and increases the fraction of flux in the UV, Fig. 33). In both cases (with or without CSM), the UV spectrum undergoes very rapid evolution during the first few days after the explosion, and allows us to constrain the kinematics, chemical composition and ionization stage of the emitting material. At these epochs the optical emission is significantly fainter. Simulated spectra taken from Gezari et al. (2008a) and Dessart et al. (2017b).

veil the nature of the companion stars to exploding CO-WDs. Very early UV spectroscopy thus qualifies as a direct probe of the immediate explosion’s environment and progenitor system.

We end this section by directly addressing the question: “Why cannot we address this with observations at other wavelengths?” We will first discuss X-ray and radio observations of stellar explosions and then address the use of very fast (i.e. “flash”) spectroscopy of SNe.

Radio and X-rays: Radio and X-ray observations that map the thermal and non-thermal emission from the explosion’s shock interaction with the circumstellar medium (CSM) are directly sensitive to the CSM density profile and can be used (and have been widely used! e.g., Kulkarni et al. 1998; Berger et al. 2002; Chevalier & Fransson 2006; Soderberg et al. 2006b; Corsi et al. 2016; Margutti et al. 2017; Chevalier & Fransson 2017) to reconstruct the mass-loss history of the progenitor system before stellar death. The limitations of this approach are as follows: (i) radio and X-rays provide no information on the chemical composition of the material, which is key to understand the evolutionary stage of the progenitor at the time of stellar death; (ii) radio and X-rays do not provide information about the expansion velocity of the CSM (or any kinematics), which is another key parameter to reconstruct how the material was lost to the surroundings by the star in the last year of evolution and thus pin down the physical process behind the mass ejections; (iii) radio and X-rays provide no information on the ionization state of matter around the exploding star, which contain precious in-

formation about the physical properties of the ionizing source of radiation (i.e. on the break-out/shock interaction radiation); (iv) in the case of a very dense CSM, the radio emission may be free-free absorbed (for emission measure $\gtrsim 10^{29} \text{ cm}^{-5}$) and the X-rays produced by the shock heated gas may be reprocessed into the UV band (for column density $\gtrsim 10^{24} \text{ cm}^{-2}$).

Optical Spectroscopy: In the past few years, optical “flash spectroscopy” (i.e. very early optical spectroscopy of transients in the first hrs-days since explosion) has been established as a new tool of investigation (e.g., Gal-Yam et al. 2014; Bruch et al. 2021b). Optical flash spectroscopy provides information about the chemical composition and density of the environment around the exploded star. However, the limitations of this approach are as follows: For FBOTs, sub-luminous GRBs and transients powered by shock interaction (with either the CSM or a companion star) the optical pass band will miss the peak of the SED of the thermal emission (which will be in the UV) at early times. As we detail below, at very high temperatures ($T > 20,000 \text{ K}$), resonant lines of the relevant highly ionized atomic species are present in the FUV, compared to the weaker features visible in the optical spectrum (Figure 33, lower panel; Figure 34). These UV lines will provide better diagnostics of the ionization state of the CSM and its extent, and hence the properties of the source of ionizing photons (e.g. Groh 2014; Boian & Groh 2020).

7.2. UV spectroscopic studies of “ordinary” SNe

Recent observations of outbursting behavior in stars before core-collapse have shaken the traditional understanding of mass loss in evolved massive stars (e.g., [Smith 2014b](#) for a recent review). A combination of pre-explosion optical imaging and post-explosion optical spectroscopy have demonstrated that a large fraction of massive stars, spanning all known classes (from ordinary IIP supernovae to rare broad-lined Ic SNe), undergo major instabilities in the years preceding stellar death that spew dense shells of material into the surrounding environment (e.g., [Ofek et al. 2010](#), [Ofek et al. 2014](#), [Margutti et al. 2014](#), [Margutti et al. 2017](#), [Milisavljevic et al. 2015](#), [Ho et al. 2019c](#), [Bruch et al. 2021b](#), [Tartaglia et al. 2021](#), [Strotjohann et al. 2021](#)). In some cases the amount of expelled matter can reach $\gtrsim 1 M_{\odot}$, completely changing the observable properties of the resulting transient. This was not predicted on theoretical grounds and challenged currently known physical mechanisms that drive mass loss in evolved massive stars ([Smith 2014b](#)). One leading model suggests that these mass ejections can result from nuclear burning instabilities in the final stages of stellar evolution ([Quataert & Shiode 2012](#); [Fuller & Ro 2018](#); [Wu & Fuller 2021](#); [Figure 32](#)).

To advance our understanding of the physics behind these mass ejections it is necessary to know the chemical composition, ionization stage and kinematics of the ejected material. However, our current knowledge of these three key physical properties of the pre-explosion ejecta is unfortunately limited to the information that can be extracted from *optical* spectroscopy. For young hot objects, the optical is relatively poor in bright emission lines (mostly He II 4686 and a few more lines; [Gal-Yam et al. 2014](#)). As a result, fundamental properties of the progenitor star and the physical conditions that lead to enhanced mass loss followed by the explosion are unconstrained. For example, even in the case of the extremely well-monitored SN 2013cu, for which exquisite optical spectroscopy was acquired starting as early as 15.5 hr after collapse ([Gal-Yam et al. 2014](#)), state-of-the-art modeling of these optical spectra by [Groh \(2014\)](#) could not distinguish between a luminous blue variable or a yellow hypergiant progenitor star due to the dearth of bright emission lines. Early UV spectroscopic observations are uniquely capable of diagnosing the pre-supernova ejecta chemical composition, metallicity, and velocity structure, as emphasized by [Groh \(2014\)](#).

UV spectroscopy is crucial because: (i) compared to the optical, it accesses a significantly larger number of spectral transitions, adding crucial constraints to an otherwise under-constrained problem ([Figure 33](#), lower panel; [Figure 34](#)). (ii) Virtually all young stellar ex-

plosions are bright UV emitters, with a spectral energy distribution that peaks in the UV, and a UV flux that is several times larger than the optical ([Figure 33](#), upper-left panel). (iii) UV probes resonance lines such as C IV $\lambda\lambda 1548, 1551$, He II $\lambda 1640$, and N IV $\lambda 1719$. Given their high optical depths, UV resonance lines will be detectable at significantly lower wind densities compared to the optical. These lines further allow a much more precise determination of the wind velocity structure. (iv) Finally, UV also probes highly-ionized Fe lines at $\lambda\lambda 1200\text{--}1450$, which can be used as direct probes of the close CSM metallicity, which would not be otherwise accessible (at the high temperatures no Fe transition is available in the optical).

Additionally, in the specific context of Ia-SNe, a novel way to gain insight into their progenitor systems is by studying the short-lived excess of UV emission that is expected to originate from the SN shock interaction with the companion star in the first ~ 48 hrs after explosion ([Kasen 2010](#), their [Figure 3](#)). The UV burst properties (temperature, luminosity, duration) depend on the properties of the companion star and thus provide direct insight into its nature (WD or non-degenerate star? e.g., [Brown et al. 2012](#)). *UVEX* has the potential to acquire the first UV spectra of type-Ia SNe at $\delta t < 48$ hrs and constrain the nature of their progenitor systems. To date, due to limitations of current observing facilities, the earliest UV spectroscopic observation of a type-Ia SN has been acquired at $\delta t \approx +5$ days since explosion with the HST ([R. J. Foley](#), private communication), well after the end of any emission from shock interaction with the companion.

To conclude, the acquisition of the first UV spectroscopic sequences of stellar explosions at very early times by *UVEX* will thus open an entirely new window of investigation on stellar death. *UVEX* will acquire rapid, high-cadence, UV spectroscopic sequences of the youngest stellar explosions identified by ground-based surveys (in 2028 we expect a large number of surveys to be operational, including ASAS-SN, BlackGEM, LS4, ATLAS, ZTF PS-1 and 2, LAST, an upgraded EVRYSCOPE, WLAST and more) as well as SNe discovered by other spacecraft (e.g., ULTRASAT). Additionally, *UVEX* is equipped to discover $\approx 6\text{--}10$ SNe within hrs of explosion through its synoptic survey over the course of two years.

7.3. Probing the Exotica: the Rarest and most UV-luminous Stellar Deaths

In a typical core-collapse SN, the explosion is largely isotropic and the ejecta is accelerated to velocities up to about 10 percent of the speed of light—the consequence

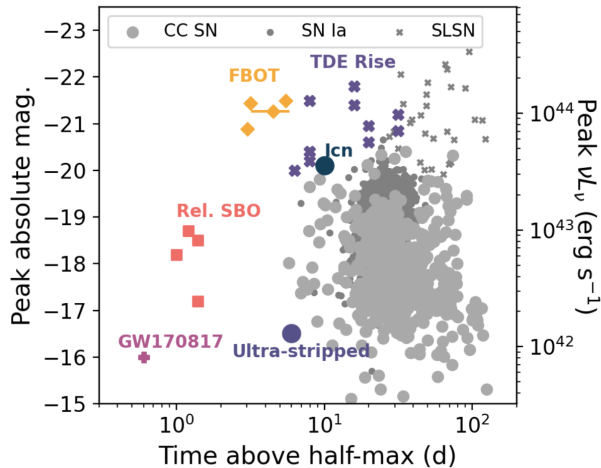


Figure 35. The luminosity vs. duration of optical transients highlighting classes of relativistic explosions that are prime targets for *UVEX*: Fast and Blue Optical Transients (“FBOTs”; yellow diamonds), events powered by relativistic shock breakout (“Rel. SBO”; red squares), as well as ultra-stripped SNe, counterparts to GW sources (here exemplified by GW170817, purple plus sign), the new class of Icn SNe and Tidal Disruption Events (“TDEs”; purple crosses). We place these transients in the context of Ia SNe, CC SNe, and SLSNe from the ZTF Bright Transient Survey. References: Perley et al. (2019); Fremling et al. (2020); Margutti et al. (2019); Coppejans et al. (2020); Ho et al. (2020a); Perley et al. (2021a). Modified from Ho et al. (2021a).

of a neutrino-mediated spherical shock produced following core bounce (e.g., Janka 2017). However, since the late 1990’s it has been realized that some massive stellar explosions are driven by a distinct mechanism involving the production of relativistic jets by a *central engine*: a rapidly-spinning neutron star or a black hole. The most extreme examples are long-duration gamma-ray bursts (GRBs; Piran 2004; Hjorth & Bloom 2012; Cano et al. 2017): extremely rare explosions involving ultra-relativistic (Lorentz factor $\Gamma > 100$) jets and almost exclusively discovered by high-energy satellites. However, the discovery of “low-luminosity” GRBs (or “X-ray flashes”; Galama et al. 1998; Kulkarni et al. 1998; Campana et al. 2006; Soderberg et al. 2006b; Liang et al. 2007), and observations of relativistic explosions with no associated detected GRB by wide-field surveys at other wavelengths (Soderberg et al. 2010; Cenko et al. 2013; Margutti et al. 2014; Milisavljevic et al. 2015; Ho et al. 2020b), suggest that GRBs are only the tip of the iceberg of a broader landscape of engine-driven phenomena spanning a wide variety of engine timescales, beaming angles, shock velocities, and CSM properties (Lazzati et al. 2012; Margutti et al. 2014; Milisavljevic et al. 2015; Gottlieb et al. 2021). This suggest that the role of jets

in end-of-life stellar explosions may be more significant than was previously appreciated by most of the astronomical community.

Of particular importance to this mission is the population of transients sometimes termed “FBOTs” (fast blue optical transients, Figure 35) and typified by the intensely-studied event AT2018cow (Prentice et al. 2018, Perley et al. 2019, Kuin et al. 2019, Margutti et al. 2019, Ho et al. 2019a), discovered in 2018. These events rise and fade on timescales of just a few days (an order of magnitude faster than a typical supernova; Ho et al. 2021a), retain very high temperatures long after peak (Perley et al. 2019, Margutti et al. 2019), and have been shown in several cases to be accompanied by very luminous radio and sub-millimeter emission, indicating an energetic and mildly relativistic shock ($v \sim 0.1\text{--}0.6c$) in a very dense circumstellar medium (Margutti et al. 2019; Ho et al. 2019a; Coppejans et al. 2020; Ho et al. 2020a, 2021b; Bright et al. 2021). Hydrogen and helium were detected in the late-time spectra of AT2018cow (Perley et al. 2019, Margutti et al. 2019), indicating an important distinction from the progenitors of GRBs, which are exclusively accompanied by H/He-poor SNe.

FBOTs are fundamentally a UV phenomena—the emission before, at, and (in many cases) after maximum light peaks in the UV (Drout et al. 2014; Pursiainen et al. 2018). However, so far they have only been discovered via ground-based optical surveys, and the only constraints from spectroscopy have come from the optical as well. The result is that even in this era of wide-field optical surveys, the discovery rate is low (~ 1 per year), and spectroscopy has been minimally constraining. Almost all of our knowledge of this class of phenomena originates from AT2018cow itself, and there are few constraints on how these events are related to FBOTs and relativistic transients more broadly. The next ten years are unlikely to change this paradigm, since even the most powerful new time-domain facilities (e.g., the Large Survey of Space and Time carried out by the Vera C. Rubin Observatory) will not be capable of recognizing similar transients at the critical, short-lived early phases of their evolution.

A dedicated UV facility would offer several advantages in the study of this event class. FBOTs are more luminous at these wavelengths, the background is greatly reduced, and UV spectral diagnostics (with the extensive set of strong resonance lines) will be far more powerful at examining the properties of the outflow and surrounding CSM compared to what can be done with optical observations alone.

By the launch of *UVEX*, the entire sky will be surveyed in the soft X-ray bands by facilities such as

Einstein-Probe (Liu 2021), transforming the study of relativistic explosions, which has been limited to the hard X-ray and gamma-ray bands. Low-Luminosity GRBs (LLGRBs, i.e. GRBs with significantly lower-luminosity γ -ray prompt emission) may represent phenomena intermediate to classical GRBs and ordinary SNe (Soderberg et al. 2006a, Liang et al. 2007, Nakar 2015, Cano et al. 2017). *UVEX* will obtain the first UV spectra of LLGRBs. The volumetric rate is uncertain, but could be between 0.1% and 1% of the core-collapse SN rate (Soderberg et al. 2006b, Liang et al. 2007). Their luminous UV emission is accessible to *UVEX* for spectroscopy out to $z = 0.06$, so we estimate between 6 and 60 candidates per year.

In addition, an entirely new class of strongly interacting SNe has been identified in the last few months: Icn SNe, i.e. SNe that show clear spectroscopic signatures of shock interaction with a He and H poor medium (Fraser et al. 2021; Gal-Yam et al. 2021; Perley et al. 2021b). Type Icn SNe join the groups of type Ibn and type IIn SNe, which show interaction with He-rich and H-rich CSM, respectively. Icn SNe descend from stellar progenitors that shed their envelopes at significantly earlier times before collapse, compared to their Ibn and IIn “cousins”. The physical nature of Icn SNe is unknown. These SNe are rare but UV-luminous (Figure 35), and thus detectable out to large volumes. *UVEX* has the potential to acquire the first UV spectra of a Icn SN and shed lights on its origin.

8. ACTIVE GALACTIC NUCLEI

Active galactic nuclei (AGN), corresponding to the phases in a galaxy’s life when its central supermassive black hole is actively accreting material, are intrinsically UV phenomena. Gravitational potential energy from infalling material becomes kinetic energy, and is then released as thermal energy from the hot accretion disk that naturally forms. Accretion disk temperature is inversely proportional to the central mass, so while emission from the accretion disks of stellar mass compact objects in the Galaxy, i.e., Galactic binaries, peak in the soft X-ray regime, emission from the accretion disks of supermassive black holes peak in the UV. Indeed, the first quasars were identified as unusually blue, quasi-stellar counterparts to radio sources (Schmidt 1963), and the so-called “Big Blue Bump” which dominates quasar spectral energy distributions (SEDs) in the spectral range from $\sim 100 \text{ \AA}$ to 3000 \AA is dominated by 10,000-100,000 K thermal emission from the accretion disk (Sanders et al. 1989).

Thermal UV emission from the accretion disk provide the source photons for two other distinguishing features

in AGN SEDs. UV emission from the accretion disk is reradiated in the IR by dust, often assumed to be in form of a torus of material that obscures the higher energy emission along certain lines of sight (e.g., Stern et al. 2005). And UV emission is Compton up-scattered into the X-ray range by the AGN corona, creating the characteristic power-law X-ray spectrum of actively accreting, unobscured AGN.

Thus, it should come as no surprise to find that UV observations play an outsized role for AGN studies. In the following, we consider the scientific potential of *UVEX* for AGN studies, with an emphasis on the discovery space enabled by sensitive, synoptic UV imaging, UV spectroscopy, and the $\geq 50 - 100\times$ increase in two-band UV imaging sensitivity enabled by *UVEX* relative to *GALEX*. The related phenomenon of tidal disruption events (TDEs) are discussed in the next section (§ 10). However, we do note that TDEs are also expected to happen in active galaxies. Ricci et al. (2021) present one dramatic candidate event, while Frederick et al. (2021) discuss optical transients in narrow-line Seyfert 1 galaxies, some of which they associate with likely TDEs. In addition, Stein et al. (2021) discuss the likely coincidence of a PeV neutrino with a TDE in an active galaxy. UV observations are a key aspect of their analysis, which shows that the EM observations can be explained with a multi-zone model: a UV-bright photosphere powers an extended synchrotron-emitting outflow in which high-energy neutrinos are produced. Their model suggests TDEs with mildly-relativistic outflows are likely important contributors to the cosmic neutrino flux, particularly at high energies, and also shows the key role that UV observations play in probing extreme AGN events, touching on AGN (§ 9), TDEs (§ 10), and multimessenger astrophysics (§ 11). Finally, from the theoretical side, McKernan et al. (2021) and McKernan et al. (in prep.) discuss how stars embedded in AGN accretion disks can lead to TDEs.

8.1. Quasar Variability

Time domain surveys have long been recognized as important tools for studying AGN. Indeed, optical continuum variability was recognized as a common feature of quasars within a year of their initial discovery (Matthews & Sandage 1963), and was quickly exploited as a means of identifying quasars, particularly those that might be missed by the UV-excess technique due to their higher redshift (e.g., van den Bergh et al. 1973). Since then, several groups have used optical synoptic studies to construct quasar samples based on their unique optical variability, thereby avoiding the inherent biases of color selection. A non-exhaustive list of such efforts in-

clude studies of SDSS Stripe 82 (MacLeod et al. 2011), MACHO (Pichara et al. 2012), OGLE (Kozłowski et al. 2013), COSMOS (De Cicco et al. 2019), and GOODS-S (Pouliasis et al. 2019). Graham et al. (2014) show how combining optical variability from CRTS with mid-IR colors from *WISE* (e.g., Stern et al. 2012, Assef et al. 2013) improves completeness and reliability of quasar selection relative to variability or color selection alone, and optical variability selection of quasars has long been heralded as one of the many promising scientific results to come from LSST (e.g., Ivezić et al. 2019).

UVEX will provide a powerful probe of quasar UV variability, a wavelength where quasars are $\sim 5\times$ more variable than at optical wavelengths (Gezari et al. 2013). This will be useful for a wide range of quasar studies, from simply identifying quasars, to correlating their UV light-curves with variability at other wavelengths, to map out the central engine and determine black hole masses, to exploring the new territory of extreme quasar variability recently opened from optical time-domain surveys. In particular, since quasar UV emission comes predominantly from the hot accretion disk, UV studies are uniquely sensitive probes of extreme events and activity close to the supermassive black hole.

Studying quasars at a wavelength where they are more variable, *UVEX* has significant promise for identifying AGN based on their variability, particularly in the low-redshift Universe where the rest-frame UV photons are detected in the observed UV bands. Of particular interest will be identifying AGN in low-mass, low-redshift galaxies, which are predominantly star-forming (Geha et al. 2012). UV color excess techniques will therefore be somewhat compromised (e.g., Latimer et al. 2019), making UV variability a powerful tool for identifying low-luminosity AGN in dwarf galaxies. Obtaining a comprehensive census of such systems is particularly exciting as a tool to understand early black hole growth and potentially answering the key open question regarding supermassive black hole “seeds” (e.g., Reines et al. 2013): how was the universe able to create billion solar mass black holes in less than a Gyr (e.g., Bañados et al. 2018)? Different models for these high-redshift seeds have different predictions for the massive black hole occupancy fraction in low-mass galaxies in the local universe (Reines & Comastri 2016).

8.2. Reverberation Mapping

Although the spatial structure of the AGN central engine cannot be directly resolved, the time-variable nature of AGN emission makes it possible to resolve the inner structure by correlating variability from different emitting regions and associating time delays with the

light travel time (Blandford & McKee 1982, Cackett et al. 2021). This method, known as reverberation mapping, uses synoptic observations to determine the geometry of the central region; spectroscopic monitoring open such studies up to dynamical studies as well (e.g., Pancoast et al. 2014). Reverberation mapping provides our largest sample of robust supermassive black hole mass measurements, supplemented with a few nearby sources, such as Sgr A*, where we can kinematically resolve the central regions (e.g., Ghez et al. 2008, Cohn et al. 2021). Panda et al. (2019) discuss photometric reverberation mapping with LSST, essentially modeling the huge sample of quasars with six-band synoptic photometry as a substitute for spectroscopic monitoring of a smaller sample, as is the current standard for reverberation campaigns (e.g., Barth et al. 2015). Providing two additional photometric bands at wavelengths where quasars are most variable, *UVEX* will be an important supplemental dataset for photometric reverberation programs.

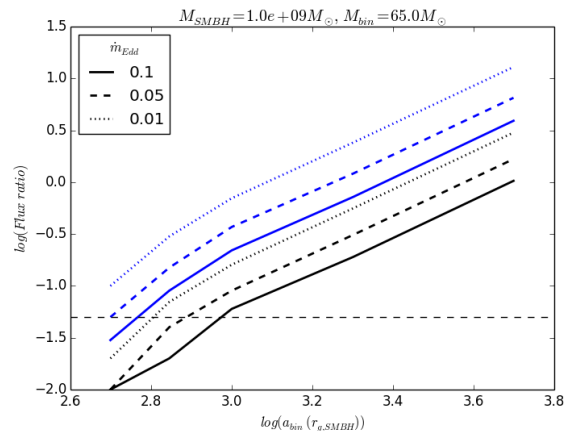


Figure 36. The merger of stellar mass black holes in an AGN accretion disk causes a bright UV flare. Plotted is the ratio of *GALEX* NUV flux (blue; similar to *UVEX* NUV) and ZTF *g*-band flux (black) from such an event relative to an unperturbed AGN disk. These curves are for a $10^9 M_\odot$ SMBH in an AGN accreting at a range of Eddington ratios: $\dot{m}_{\text{Edd}} = 0.1$ (solid), 0.05 (dashed), and 0.01 (dotted), and assume that the merging black holes have a total initial mass of $65 M_\odot$, 5% of the mass is lost to gravitational waves from the merger, and a kick velocity of 100 km s^{-1} for the resultant, merged black hole. Ratios are plotted for a range of binary distance a_{bin} from the SMBH, in units of the SMBH gravitational radius, $r_{\text{g,SMBH}} \equiv GM_{\text{SMBH}}/c^2$. The horizontal dashed line corresponds to a flux increase of 5%. The flux increase is larger at shorter wavelength. From McKernan et al. (2019).

8.3. Stellar Mass Black Hole Mergers

One exciting, though controversial, possibility is that a significant fraction of black hole merger gravitational wave events occur within AGN accretion disks and are detectable in EM (e.g., [Graham et al. 2020a](#)). Stellar mass black holes are expected to be common in galactic nuclei due to mass segregation, and accretion disk gas will dissipate angular momentum, causing more massive embedded objects to in-spiral more rapidly than less massive ones. This provides a natural explanation for asymmetric mass mergers ([McKernan et al. 2020](#)), such as GW190814 which consisted of a $23 M_{\odot}$ black hole coalescing with a $2.6 M_{\odot}$ compact object ([Abbott et al. 2020b](#)), as well as black holes more massive than $35\text{--}70 M_{\odot}$, the maximum black hole mass expected from a supernova ([Woosley 2017](#)), such as GW190521 which consisted of an $86 + 66 M_{\odot}$ black hole merger ([Abbott et al. 2020c](#)). As shown by Figure 36, from [McKernan et al. \(2019\)](#), the disk gas provides baryons that are expected to produce a UV flare due to the merger, assuming either a short diffusion time or a thin AGN accretion disk. Jetted emission from a rapidly spinning, merged black hole can also yield UV photons, implying that *UVEX* will be a powerful tool for studying counterparts not only to neutron star merger events (discussed in § 11), but also to black hole merger events.

8.4. Supermassive Black Hole Binaries

Time-domain surveys have recently identified a population of quasars with apparently sinusoidal, periodic light-curves ([Graham et al. 2015a](#), [Graham et al. 2015b](#), [Charisi et al. 2016](#)). With the important caveat that many candidate periodic sources are claimed on the basis of problematic statistical analyses (e.g., see discussion in [Vaughan et al. 2016](#) and [Barth & Stern 2018](#)), actual sustained periodic or quasi-periodic variability is likely a signature of a binary supermassive black hole (SMBH) system with a sub-parsec separation. For example, [D’Orazio et al. \(2015\)](#) showed that the periodicity of PG 1302-102 can be explained by relativistic Doppler boosting and beaming of emission from the mini-accretion disk around a secondary SMBH as it orbits a more massive primary at velocities of a few tenths the speed of light with a separation of ~ 2000 AU (i.e., ~ 0.01 pc). This model predicts a strong inverse correlation between variability amplitude and wavelength ([Xin et al. 2020](#)), which *UVEX* will test.

8.5. Flaring AGN

UVEX will also be important for studying AGN with unusual, extreme optical light-curves, such as flaring AGN. For example, [Graham et al. \(2017\)](#) reported on

a systematic search for major flares in AGN in the Catalina Real-time Transient Survey as part of a broader study into extreme quasar variability. Requiring flares that are quantitatively stronger than normal, stochastic quasar variability, [Graham et al. \(2017\)](#) identified 51 extreme events from a sample of $> 900,000$ confirmed and high-probability quasar candidates. The events typically lasting 900 days, with a median peak brightening of $\Delta m = 1.25$ mag. The sample show a range of flare morphologies, with some being more symmetric, while others evolve with fast-rise followed by a slower, exponential decay. While a subset of the sources appear consistent with microlensing (e.g., [Lawrence et al. 2016](#)) or self-lensing (e.g., [D’Orazio & Di Stefano 2018](#)), [Graham et al. \(2017\)](#) attribute the majority of the events to explosive stellar-related activity in the accretion disk, such as super-luminous SNe, TDEs, and mergers of stellar mass black holes. Given the range of potential phenomena, and that the flares are likely associated with events close to the central engine in the UV-luminous accretion disk, *UVEX* observations will be critical for refining our understanding of these events, and ultimately using them to improve our understanding of the extreme and poorly understood physics of AGN accretion disks.

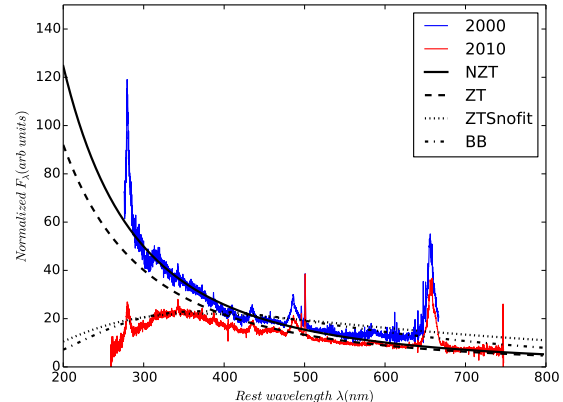


Figure 37. Example of a changing-look AGN, SDSS J110057.70-005304.5, in which the UV emission from the AGN collapsed ([Ross et al. 2018](#)). The authors explore models where the source has non-zero torque (NZT model; solid line) at the inner, stable circular orbit (ISCO; [Afhordi & Paczyński 2003](#)), and suggest that the spectrum is best explained by shutting down emission from the inner $\sim 200r_g$ of the accretion disk (ZTSnofit model; dotted line). See [Ross et al. \(2018\)](#) for details.

8.6. Changing-Look Quasars

UVEX will also be important for studying AGN with unusual, extreme optical light-curves, such as “changing-look quasars” which rapidly rise or drop in optical brightness (e.g., LaMassa et al. 2015, Ross et al. 2018, Stern et al. 2018, Graham et al. 2020b). Though a range of selection criteria and wavelength ranges have been used to identify such sources, changes in the innermost accretion disk occurring on the thermal or cooling/heating front timescale seem to be the most plausible explanation for the year-scale variability typically observed in changing-look quasars. For example, Ross et al. (2018) present one example of a changing-look AGN where the UV emission has collapsed (Figure 37). The authors argue that the most likely explanation is that some triggering event caused the inner accretion disk to cool, and thus dim, though other models have been favored for other events (e.g., Guo et al. 2016). With few such events studied, particularly at the key UV wavelengths which likely dominate the state changes, *UVEX* will have an important role to play in determining the timescales, characteristics, and spectral changes associated with changing-look quasars.

9. TIDAL DISRUPTION EVENTS

It is now well established that supermassive black holes (SMBHs) are a ubiquitous presence in the nuclei of almost all galaxies (Magorrian et al. 1998; Kormendy & Richstone 1995; Ho 2008). In fact, the remarkably tight correlation between the masses of central SMBHs and the mass, luminosity, and structure of their host galaxies (Ferrarese & Merritt 2000; Gebhardt et al. 2000; Graham et al. 2001; Marconi & Hunt 2003) suggest coeval formation and growth over cosmic time. Despite these advancements, the formation mechanism of the primordial seeds from which SMBHs grow through accretion and mergers is yet unknown. The demographics of SMBHs in low-mass galaxies may place the most promising constraints (Volonteri & Natarajan 2009). Unfortunately, however, the low-mass end of the SMBH mass function is more difficult to detect, due to the smaller gravitational sphere of influence and lower Eddington luminosity of the black hole, which both scale linearly with SMBH mass. Tidal disruption events (TDEs) provide the most promising method to detect and weigh black holes below $10^8 M_\odot$, where scaling relations between black hole mass and galaxy mass are poorly constrained.

A TDE will occur when an unlucky star’s orbit passes close enough to a central SMBH to be tidally ripped apart, and the resulting stellar debris is slowly consumed by the black hole, producing a luminous accretion flare. The physics of TDEs depend on the interplay of the stel-

lar radius and the black hole tidal radius: black holes more massive than $\sim 10^8 M_\odot$ disrupt main sequence stars inside the event horizon and thus do not produce a flare, while black holes less massive than $\sim 10^{5.4} M_\odot$ do not have a tidal field sufficient to disrupt main sequence stars. Compact stars, such as white dwarfs, can be disrupted by intermediate mass black holes (IMBHs; $\sim 10^4 M_\odot$), while red giants can be disrupted by the most massive black holes known.

TDEs are not only probes of SMBH demographics. They are also an ideal laboratory to study the physics of accretion. One of the primary parameters in accretion physics is the accretion rate. The mass accretion rate in a TDE undergoes a large variation over months to years timescales, starting as super-Eddington and gradually decreasing as a power-law with time. When it occurs around an inactive black hole, it provides a unique opportunity to study the formation and physics of an accretion disk and its associated structure. There is increasing suspicion that TDEs are sources of very high-energy neutrinos (e.g. van Velzen et al. 2021a). Finally, TDEs can be used to probe the occupation fraction of massive black holes in the nuclei of low-mass galaxies, which provides a test of competing models proposed to explain the surprising presence of SMBHs with masses $> 10^9 M_\odot$ in the first Gyr after the Big Bang (Bañados et al. 2018).

The census of TDE candidates has been steadily growing thanks to dedicated searches for nuclear transients from quiescent galaxies across the electromagnetic spectrum (see Gezari 2021 for a recent review).

9.1. *UV Properties of TDEs & Uniqueness of UVEX*

TDE candidates were first identified from the *ROSAT* X-ray All Sky Survey (Bade et al. 1996; Komossa & Bade 1999). The modest number of epochs were sufficient to establish the phenomenon from extremely soft, luminous X-ray outbursts from otherwise quiescent galaxies. The second era of TDE searches began with *GALEX*, together with joint optical observations from the ground, which led to a class of UV-selected TDEs (Gezari et al. 2008b, 2009, 2012). These TDEs are characterized by thermal emission with temperatures $T_{\text{bb}} \sim (3 - 5) \times 10^4$ K (and radius $R_{\text{bb}} \sim 10^{14} - 10^{15}$ cm) peaking in the UV – much cooler than the original TDE candidates discovered in the soft X-rays ($T_{\text{bb}} \sim 10^6$ K and $R_{\text{bb}} \sim 10^{12}$ cm). Since those studies with *GALEX*, the majority of TDE discoveries have been made in the optical. ZTF is now routinely discovering 15 TDEs per year (van Velzen et al. 2021b). Follow up with the Neil Gehrels *Swift* satellite, have shown that they are also very bright in the UV, with typical colors

of $NUV - r < -1$ mag, and peak luminosities with $-18 < NUV < -22$ mag (Gezari 2021; see Figure 38). In fact, TDEs are some of the most luminous and long-lived UV transients in the Universe (see Figure 35).

The origin of the luminous UV-bright thermal emission is still debated (see §9.4), but some UV and optically selected TDEs are also bright in the soft X-ray band, indicating that these are two emission components that likely co-exist in the same TDE system.

Owing to the brilliance and long lifetime of TDEs in the UV, *UVEX* will routinely discover TDEs. However, by 2027 the TDE landscape will be quite sophisticated and the focus will be on *large and well-defined* samples of TDEs. To this end, we will consider an exemplar survey, which will discover and characterize over a thousand TDEs. The framework to compute the discovery rate of TDEs is given in the appendix (§A). This exemplar survey will be accompanied by a spectroscopic component to systematically probe the kinematics and structure of outflows launched by TDEs, and test competing models for the origin of the UV emission (§9.4).

The resulting trove of TDEs will enable us to (1) detect the lower energy tail of thermal emission of X-ray loud TDEs (§9.2), (2) address the “missing energy problem” for optically loud TDEs (§9.3), (3) identify the mechanisms of the UV/optical thermal emission (§9.4), and (4) probe the black hole occupation fraction of low mass galaxies, and even the spin distribution of high mass black holes (§9.5).

9.2. UV Detections of X-ray Loud TDEs

The Russian-German Spektr-RG (SRG) mission is now finding TDEs at a higher rate relative to those found from optical surveys (Sazonov et al. 2021). X-ray discovered TDEs (Saxton et al. 2020) display temperatures of $T_{\text{bb}} \sim 10^6$ K and $R_{\text{bb}} \sim 10^{12}$ cm, as expected from emission near the innermost stable circular orbit (ISCO) of a black hole (BH) of $M \sim 10^6 M_{\odot}$. The black dotted line in Figure 39 (left panel) illustrates a typical blackbody inferred from soft X-ray observations. However, from angular momentum conservation, we expect the tidal debris to circularize at a few times the tidal radius $R_{\text{T}} = R_{\odot}(M/M_{\odot})^{1/3}$ (for a solar-like star), which means that the radius of the outer disk is of the order $R_{\text{out}} \sim 10^{13}$ cm. One of the exciting capabilities of the FUV sensitivity of *UVEX* will be to detect the lower energy tail of the thermal emission of X-ray loud TDEs, even for those without the additional UV/optical component.

Multi-color disk SEDs for two different choices of $R_{\text{out}} = 2R_{\text{T}}$ and $5R_{\text{T}}$ are shown in solid and dashed black line in Figure 39. For a threshold of 24 mag,

UVEX will be able to detect the emission from the outer accretion disk out to at least 610 Mpc. Quasi-simultaneous X-ray observations can be provided by all-sky X-ray surveys such as *SRG* ($\gtrsim 10^{-14}$ erg s $^{-1}$ cm $^{-2}$) and *SVOM* ($\gtrsim 10^{-12}$ erg s $^{-1}$ cm $^{-2}$), as well as by short *Swift* XRT follow-ups of *UVEX*-discovered TDEs ($\gtrsim 10^{-13.5}$ erg s $^{-1}$ cm $^{-2}$).

9.3. Late-time UV light curve of TDEs

The total radiated energies in optically-discovered TDEs are in the range 10^{50} – 10^{51} erg. This is at least one order of magnitude below the theoretically expected energy release from $0.1M_{\odot}$ of accreted mass, even considering that the accretion disk may be radiatively inefficient in the super-Eddington regime (Lu & Kumar 2018). Thus, $> 90\%$ of the expected energy has been missed by current observations — this is one of the major puzzles in TDEs.

A possible solution is that the majority of the disk mass is only slowly accreted onto the BH on a timescale much longer than a few years, provided that the accretion disk is very thin with a long viscous timescale. Without optically thick reprocessing gas at large distances, the disk emission is expected to be primarily in the UV and soft X-ray bands, as shown by the multi-color blackbody SED in Figure 39. This is supported by late-time (~ 5 yr) FUV/NUV observations of a handful of TDEs by *HST* after the optical emission has completely faded away (van Velzen et al. 2019). The observed FUV fluxes are in the range 23–25 mag, which are detectable by single-epoch (900 s) *UVEX* observation or stacking of multiple exposures. Thus, the *UVEX* all-sky survey will provide late-time FUV measurements or stringent upper limits for all $N \sim 10^3$ TDEs that will have been discovered by optical and X-ray surveys before 2028, whereas it is not feasible to monitor such a large number of TDEs with individual *HST* observations.

9.4. Confronting Observations to TDE Models

There are two competing models for how the UV/optical emission seen in some TDEs is generated.

1. **Reprocessing of Disk Emission.** In this scenario, an optically thick gas layer (most likely in the form of an outflow) at a distance of 10^{14} – 10^{15} cm absorbs the soft X-ray emission from the disk and re-emits in the UV-optical band (Metzger & Stone 2016, Roth et al. 2016, Lu & Bonnerot 2020). As the fallback rate declines with time, the density of the “reprocessing layer” drops and there is less and less absorption. Thus, the bulk of the emission is expected to shift to higher fre-

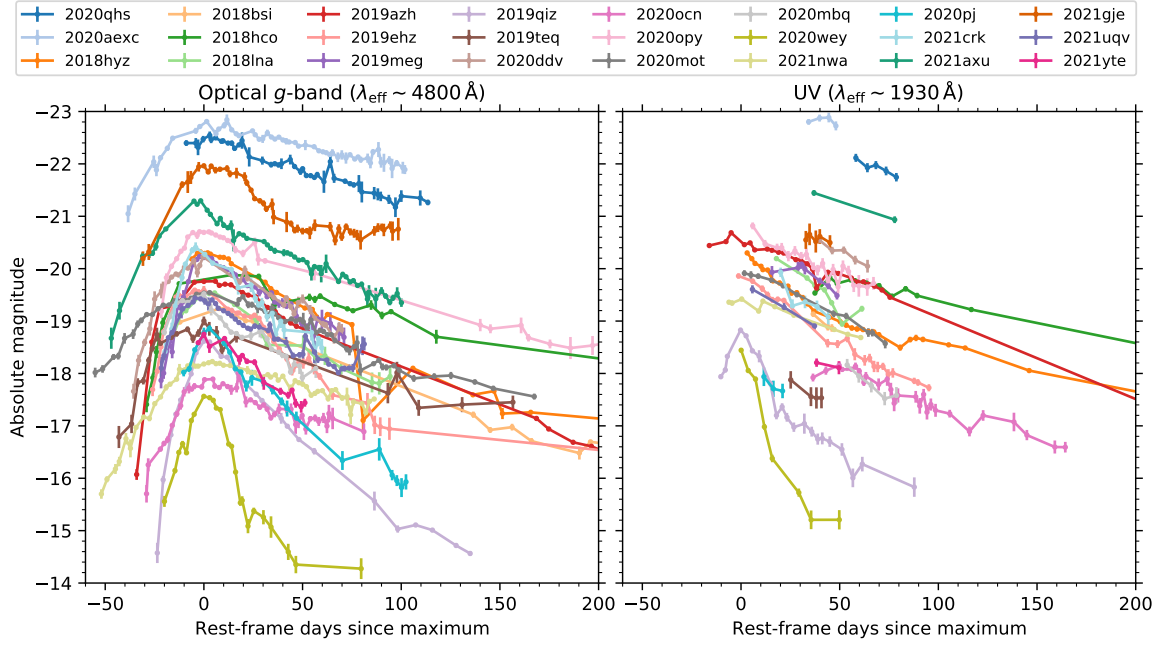


Figure 38. Optical (left panel) and UV (right panel) light curves of TDEs selected from ZTF. Since UV observations were carried out after the optical identification, only three TDEs had UV data before the peak of the light curves.

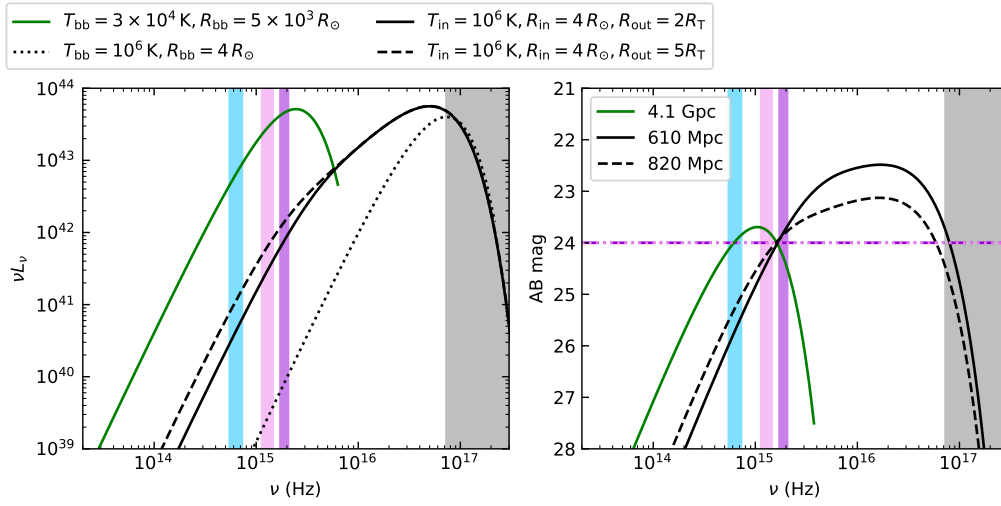


Figure 39. Left: SEDs of typical optically-discovered and X-ray-discovered TDEs. Photometric bands are marked by the vertical lines in blue (g -band), light purple (NUV), deep purple (FUV), and gray (0.3–10 keV). Right: The SEDs are now shifted to the largest distance that still meets the *UVEX* sensitivity threshold (conservatively assumed to be 24 mag), including K -correction.

quencies and correspondingly, T_{bb} **increases** and R_{bb} drops with time.

2. **Stream-stream Collisions.** An alternative scenario is that the bound stellar debris stream intersects itself (due to general relativistic apsidal precession) producing a self-crossing shock, and the kinetic energy dissipated by the shock powers the optical emission (Piran et al. 2015, Jiang et al. 2016). In this case, R_{bb} is of the order the self-

crossing radius, which stays roughly unchanged over time. As the fallback rate declines with time, the shock power drops (roughly as $t^{-5/3}$) and hence the blackbody temperature T_{bb} is expected to **decrease** with time.

While temperature evolution is a compelling discriminator between these models, the optical band is on the Rayleigh-Jeans tail (insensitive to T_{bb}) of the TDE thermal continuum, and UV photometry is required for a re-

liable measurement of the temperature evolution. However, as can be seen from Figure 38, early UV photometry is only available for a few TDEs. *UVEX* will for the first time, provide UV photometry before and after the peak, and map out the temperature evolution on timescales relevant for the circularization of the debris streams.

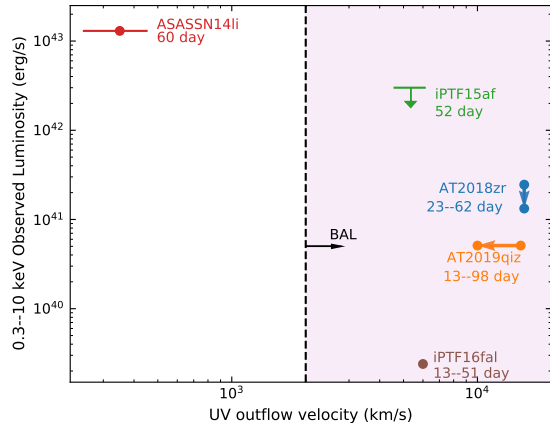


Figure 40. X-ray luminosity versus outflow velocity measured from UV spectroscopy. Among the five TDEs with published UV spectra, four exhibit broad absorption line systems (BALs; defined by $v > 2000 \text{ km s}^{-1}$).

The typical ionization parameter near the optical photosphere of TDEs is $\xi \gtrsim 10^2$. This means that most atoms lose their outer-shell electrons which are responsible for transitions in the optical band, whereas the transitions of inner-shell (K and L) electrons produce lines in the UV band. Thus, UV spectroscopy provides a unique probe of the density and velocity structures of the gas under high UV and soft X-ray fluxes.

As of now there are only five TDEs with UV spectra, ASASSN-14li (Cenko et al. 2016), iPTF16fml (Brown et al. 2018), iPTF15af (Blagorodnova et al. 2019), AT2018zr (Hung et al. 2019), and AT2019qiz (Hung et al. 2021). In four of the five sources we observe broad absorption line (BAL) systems (ASASSN-14li is the only one without). The broad absorption/emission features are thought to arise from an outflow driven by the disk accretion or stream collision.

A direct prediction of the **reprocessing scenario** is that if we observe from the funnel of the disk-driven wind, more X-rays and less prominent UV absorption features are visible. This is because most atoms are completely ionized by the high X-ray flux. On the other hand, if we observe from other angles where the X-rays are obscured by the outflow, the UV absorption features should be strong. An anti-correlation between BAL presence/strength and X-ray luminosity will be a

smoking gun for the reprocessing picture. The current sample of five TDEs with UV spectra thus far supports this picture (see Figure 40) — *UVEX* will \sim triple the sample of TDEs with UV spectra to enable significantly more robust conclusions about such an anti-correlation.

The outflow velocity of the gas in the line formation region can be measured by the P-Cygni profiles. In the case that the outflow is driven by disk accretion, one expects the outflow speed to *increase* as the accretion rate drops at later time, because the disk-wind launching radius gets closer and closer to the ISCO. In the alternative scenario where the outflow is driven by stream collision, the outflow speed stays roughly constant since the radius of stream self-crossing does not evolve with time (Lu & Bonnerot 2020).

In the past, the study of line-width evolution in TDEs is stymied by the relatively late optical discovery and the latency of HST UV ToO triggers. Up to now the earliest UV spectrum of a TDE only started at $\Delta t = +13$ day (relative to the optical peak). *UVEX* will allow us to track the velocity evolution of ≈ 20 TDEs with five spectra spanning from $\Delta t \sim -4$ days to $\sim +56$ days, which will provide a unique probe of the outflow’s origin. The current *UVEX* spectral resolution of ≥ 1600 is more than adequate to measure the outflow velocity (typically $> 10^3 \text{ km s}^{-1}$).

9.5. Probing Black Hole Demographics

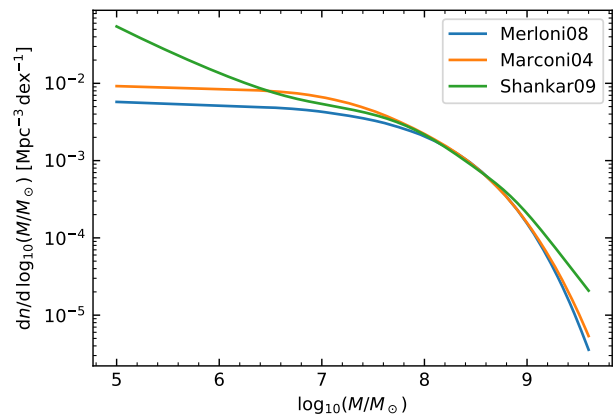


Figure 41. Three different BHMFs given in the literature (Marconi et al. 2004, Merloni & Heinz 2008, Shankar et al. 2009).

The BH mass function (BHMF) below $\sim 3 \times 10^6 M_\odot$ and above $\sim 5 \times 10^8 M_\odot$ is poorly known (see Figure 41). Our goal is to use TDEs as tracers of BH demographics. Specifically, we would like to measure the BHMF at the low mass end from $10^5 M_\odot$ to $10^6 M_\odot$, and to investigate the upper bound of M_{BH} that can disrupt a star. The

TDE rate at the low mass end is sensitive to the BH occupation fraction (Stone & Metzger 2016).

Given the relatively strong correlation between M_{BH} (inferred from the host galaxy central velocity dispersion) and t_{fb} (derived from fitting the decay timescale of the light curve; van Velzen et al. 2020; Gezari 2021; see Figure 42), one should be able to use well sampled light curves to infer the BH mass independently of host galaxy properties. This is particularly important for “intermediate mass” BHs (IMBHs), where the scaling relations between host galaxy mass and central black hole mass are poorly constrained (Greene et al. 2020). A survey cadence of $\lesssim 25$ days would be needed to track the decay of IMBH TDEs (see AT2020wey in Figure 38). Figure 43 shows that a sample of ≈ 1000 TDEs is needed to constrain the BHMf between $10^5 M_{\odot}$ and $10^6 M_{\odot}$ and to measure the shape of TDE rate suppression due to the BH event horizon.

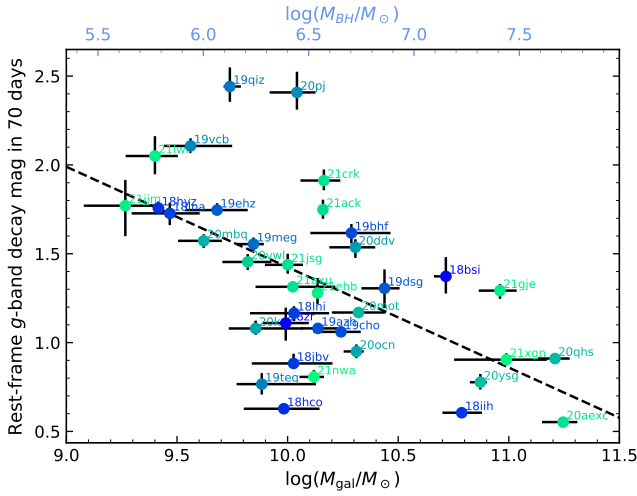


Figure 42. TDE optical decay rate as a function of host galaxy stellar mass M_{gal} . The decay is quantified by the total magnitude the light curve fades from peak to 70 days post-peak. M_{gal} is measured by modeling the host galaxy UV–MIR SED following the procedures laid out in van Velzen et al. (2021b). The upper x-axis marks rough estimates of M_{BH} using the $M_{\text{gal}}-M_{\text{BH}}$ relation from Reines & Volonteri (2015). A statistically significant correlation was found ($p = 0.0006$ for a Kendall’s Tau test), suggesting that TDEs disrupted by higher mass BHs fade slower.

The *UVEX* measurement of the TDE rate on the high M_{BH} end will potentially constrain the spin distribution of the most massive non-active BHs near $10^8 M_{\odot}$ (Kesden 2012), which has never been possible before. Generally, higher BH spins will allow TDEs to be observed from higher mass BHs. In the following, we take the simplest example of non-spinning BHs and consider two Kroupa stellar populations at ages of 100 Myr and

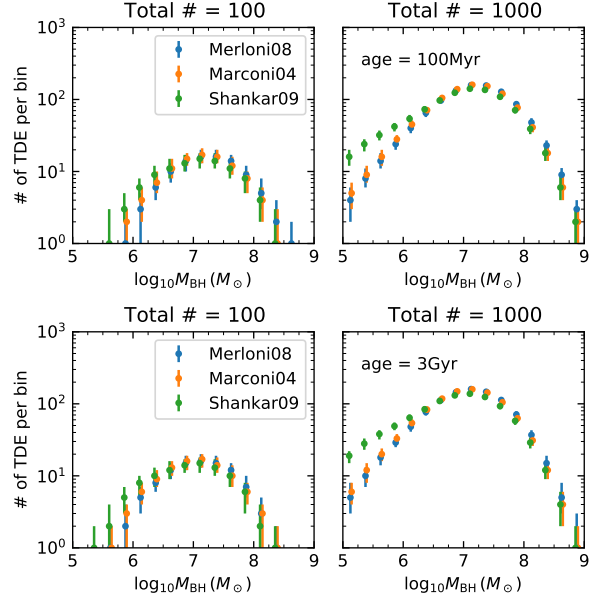


Figure 43. Observed number of TDEs as a function of M_{BH} , under different assumptions of the total number of detected TDEs, the BHMf (Figure 41), and age of the stellar population (upper panels: 100 Myr; lower panels: 3 Gyr).

3 Gyr. The mass-radius relation of the main-sequence stars at these two ages are obtained by SPISEA (Hosek et al. 2020), and we ignore red-giants and very low mass dwarfs $< 0.1 M_{\odot}$. For a given BH mass, only a fraction of the stellar population above a minimum mass will produce observable TDEs. The functions $M_{\text{max}}(m_*)$ and $g(M)$, where

$$M_{\text{max}}(m_*) = 8.9 \times 10^7 M_{\odot} m_*^{-1/2} r_*^{3/2}, \quad (1)$$

and $g(M)$ describes the suppression of TDE rate by the BH event horizon, are shown in Figure 44, assuming a likelihood of a tidal disruption for a given BH mass of

$$f_M \propto M^{-0.25} g(M) \quad (2)$$

where the factor of $M^{-0.25}$ is due to loss-cone dynamics (how stars are fed to the BH by random scattering) (Stone & Metzger 2016).

The exact $M_{\text{max}}(m_*)$ mainly depends on the age and metallicity of the star (which determine the radius and internal structure), BH spin (giving the size and shape of the event horizon) and orbital inclination, as well as other minor factors such as the exact boundary between full and partial TDEs and the rate at which stars of different masses are scattered into the loss cone.

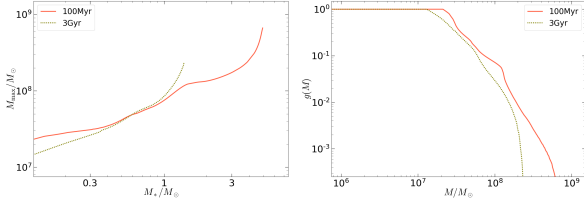


Figure 44. Left: Maximum BH mass for observable TDEs, for two stellar populations of metallicity $[\text{Fe}/\text{H}] = 0.3$ at different ages of 100 Myr and 3 Gyr. Right: The TDE rate suppression factor due to the (non-spinning) BH event horizon. Rapid spins will allow TDEs to be observed from higher mass BHs above $10^9 M_\odot$.

Then, the TDE rate as a function of BH mass M is

$$\frac{d\mathcal{R}}{dM} = \int_{L_{\min}}^{L_{\max}} dL \int_0^{D_{\max}} \Omega D^2 dD \frac{dN}{dL dM} \quad (3a)$$

$$= \frac{\Omega}{3} \int_{L_{\min}}^{L_{\max}} dL D_{\max}^3 A L^{-2.5} f_M \frac{dN}{dM} \quad (3b)$$

Following the rationale laid out in §A, we only consider events that peak at $L < 10^{44} \text{ erg s}^{-1}$. Therefore,

$$\frac{d\mathcal{R}}{dM} \propto \int_{L_{\min}}^{L_{\max}} L^{0.2} dL f_M \frac{dN}{dM} \quad (4a)$$

$$\propto f_M \frac{dN}{dM} L_{\max}^{1.2} \quad (4b)$$

Now we make the reasonable assumption that the UV luminosity L is capped at the Eddington luminosity, and therefore $L_{\max} \propto M$. Hence, we have

$$\frac{d\mathcal{R}}{d \log_{10} M} \propto M^{1.2} f_M \frac{dN}{d \log_{10} M} \quad (5)$$

Eq. (5) reflects how the detected TDEs described by Eq. (A4) distribute over different BH masses. We assume that the intrinsic scatter of the $t_{\text{fb}}-M_{\text{BH}}$ relation is 0.4 dex. Figure 43 shows the number of TDEs as a function of M_{BH} .

10. MULTI-MESSENGER ASTRONOMY: GRAVITATIONAL WAVE ASTRONOMY & HIGH-ENERGY NEUTRINO ASTRONOMY

On August 17 2017, the groundbreaking discovery of both gravitational waves and electromagnetic radiation from a neutron star merger (e.g., Abbott et al. 2017a) marked a new era in multi-messenger astrophysics (MMA). The discovery of a flaring blazar (Ice-Cube Collaboration et al. 2018) and three tidal disruption events (Stein et al. 2021; Reusch et al. 2021; van Velzen et al. 2021b) associated with high energy neutrinos opened up yet another facet of MMA.

With planned advances in sensitivity of gravitational wave (GW) interferometers, neutrino detectors and electromagnetic (EM) surveyors, we could expect several MMA events to be discovered in the years leading to the launch of *UVEX*. However, capabilities for opening the UV window into MMA will be limited because of the combination of wide field-of-view (FoV), sensitivity and rapid response time that is required. While *HST* has the sensitivity, it is neither wide-field nor does it respond fast enough. *ULTRASAT* (launch date, 2025) will have a larger FoV and rapid response, but will be much less sensitive than *UVEX* (and lacks an FUV channel), thus may only be able to pick the lowest hanging fruit (e.g., exceptionally nearby or bright sources). Fully realizing the potential for population studies enabled by the A+ sensitivity upgrades (e.g., H_0 constraints: Chen et al. 2018; connection to gamma-ray bursts: Abbott et al. 2017b) requires the higher sensitivity that will be provided by *UVEX*.

Opening a new region of the wavelength-depth-FoV phase space, particularly FUV imaging, *UVEX* could significantly impact the study of neutron star mergers, black hole mergers and supermassive black hole flares. *UVEX* will tackle open questions on where the heaviest elements are synthesized and how relativistic jets are formed by identifying and characterizing the ultraviolet emission from GW and high energy neutrino events. In this section, we discuss the science case for neutron star mergers, both binary neutron star (BNS) and neutron star–black hole (NS–BH) mergers. The science case for high energy neutrino follow-up and supermassive black hole flares is discussed in the section on Active Galactic Nuclei.

10.1. Neutron star mergers

A vast multi-wavelength data set was acquired by astronomers worldwide when GW170817 occurred. However, precious few UV photometric measurements of the EM counterpart exist, collected by the *Swift* satellite at 15 hours after merger (Evans et al. 2017). No measurements of UV light curves of kilonovae (the UV/optical/IR transient counterparts to neutron star mergers) exist at earlier times. O3 also saw the first discoveries of NS–BH mergers in GW (Abbott et al. 2021). While none of these NS–BH events revealed EM counterparts (see results from NS–BH triggers follow-up, including Goldstein et al. 2019, Gomez et al. 2019, Hosseinzadeh et al. 2019, Lundquist et al. 2019, Ackley et al. 2020, Andreoni et al. 2020, Kasliwal et al. 2020, Vieira et al. 2020, Anand et al. 2021, Oates et al. 2021), for sufficiently small mass ratios bright kilonovae are expected theoretically (Li & Paczyński 1998, Foucart 2012,

Kawaguchi et al. 2016). Thus NS–BH mergers represent an exciting prospect for future MMA observations in the *UVEX* era.

Observing the early UV emission from a kilonova is the best way to discriminate between models that describe the origin of the earliest (quasi)-isotropic emission (c.f., gamma-ray burst). These include for example shock-powered (Piro & Kollmeier 2018), nucleosynthesis-powered (e.g., Villar et al. 2017), and free neutron decay powered models (Kulkarni 2005, Metzger et al. 2015). The optical/IR emission is dominated by heating from nucleosynthesis (e.g., Drout et al. 2017, Kasliwal et al. 2017, Pian et al. 2017, Smartt et al. 2017) and cannot probe whether there was a contribution from the other two sources (Arcavi 2018). This early UV emission is a sensitive diagnostic to the properties of the remnant (e.g., lifetime of the supermassive neutron star before it collapses into a black hole; Kasen et al. 2015), system parameters (e.g., viewing angle, size of disk wind; Fernández & Metzger 2016) and jet physics (cocoon formation; Kasliwal et al. 2017, Gottlieb et al. 2018). Thus, a large sample of events need to be systematically followed up to sufficient sensitivity to meaningfully constrain the system parameters. To achieve this goal, a wide FoV, deep sensitivity and rapid response capabilities are needed. In addition, the FUV channel and UV spectroscopy planned for *UVEX* will provide new and unique information.

10.1.1. Simulation to define selection criteria, tiling and depth

Currently, the LIGO-Virgo-KAGRA GW interferometers are fully funded for A+ sensitivity for a fifth observing run (O5) in 2025–2026 (Abbott et al. 2020a). The sixth observing run (O6) is expected to be 18–24 months in duration in the years 2028–2029 and overlap with *UVEX*. In addition to LIGO Hanford, LIGO Livingston, Virgo and KAGRA, the LIGO India interferometer is expected to join the O6 run (Abbott et al. 2020a).

We undertake a detailed end-to-end simulation of the GW network performance to quantify *UVEX* measurement requirements. Our simulation assumes that all five interferometers are active in O6, but only at the funded A+ sensitivity, each with a duty cycle of 70%. The methodology is similar to that described in Petrov et al. 2021, updated to reflect population modeling results from the most recent gravitational-wave transient catalog through the end of O3, GWTC-3. Fig. 7 of the GWTC-3 paper (The LIGO Scientific Collaboration et al. 2021a) shows that the data currently support a fairly broad and flat NS mass distribution. Therefore, we adopted a distribution that is uniform from

1 to $2 M_{\odot}$. We use the GWTC-2 rate estimate of $R_{\text{BNS}} = 320_{-240}^{+490} \text{ Gpc}^{-3} \text{ yr}^{-1}$ (The LIGO Scientific Collaboration et al. 2021b) as it is quoted for a uniform mass distribution consistent with what we learned from GWTC-3.

From the sample of simulated BNS mergers in O6, we select only those targets that are better localized than 100 deg^2 . We then determine the necessary exposure times and tiling scheme to map 90% of the enclosed probability while meeting our astrophysical requirements. Our goal is to achieve the depth necessary to detect and characterize a kilonova regardless of which model is dominant (§ 10.1.2) - thus we choose a conservative FUV absolute magnitude of -12.1 mag , which corresponds to an apparent magnitude of 24.4 mag at 200 Mpc (Figure 46). We use the *UVEX* ETC to estimate the required exposure time for each event depending on the mean GW estimate of the distance to the source and the UV background at that simulated location. For the selected events, the estimated exposure time varied between 500 s and 5,250 s (with a median of 1080 s).

GW events are selected if their entire 90% localization region can be observed to the required depth within 10 ks (Figure 45). As a result of this analysis, $\sim 2.8\%$ of the events satisfy the localization, tiling, and exposure time criteria. Of these, 53% are fully within the *UVEX* field-of-regard (accounting for sun exclusion). We conclude that 35 ToO triggers are expected to pass our selection criterion during the 18 months of the GW O6 run (20 ToO triggers would pass our selection criterion using the O5 configuration).

10.1.2. Light Curve Models

Early kilonova data do not yet exist in the UV. Hence we calculate light curves for a GW170817-like event for three possible models powering the UV transient at early times.

1. The first is a semi-analytical, nucleosynthesis-powered model (Hotokezaka & Nakar 2020; also, Li & Paczyński 1998, Metzger et al. 2010), where the radiation is purely generated by radioactive decay of r -process nuclei. The model is described by 7 parameters: the mass of the ejecta (M_{ej}), the minimum and maximum velocity of the ejected material (v_{min} , v_{max}), the transition velocity between low and high opacity κ (v_{κ}), the effective grey opacity for $v \leq v_{\kappa}$ and $v > v_{\kappa}$ (κ_{low} , κ_{high}), and the power law index of the velocity distribution across the mass space (n).
2. The second model is a shock-powered analytical prescription (Piro & Kollmeier 2018), where the

kilonova is powered through shock-cooling of material surrounding the merger remnant, that has been heated by a jet depositing energy into the material. It is described by four parameters, the mass of the shock-heated material (M_{sh}), the minimum velocity of the material (v_{sh}), the initial radius of the material (R_0) and the opacity of the material (κ_{sh}).

3. For the third model we use predictions that, on top of the nucleosynthesis-powered model, there is additional radiation coming from the β -decay of free neutrons that have not been captured by nuclei through r-process (Metzger et al. 2015), with a total mass of $M_{fn} = 10^{-4} M_{\odot}$. This model is only considered in combination with the nucleosynthesis-powered model, and only affects the very early behavior of the light curve ($t \leq 6$ h).

In Table 3 we summarize the parameters for the models, and indicate the ranges within which these parameters can vary, noting that the free neutron model is fixed. Within these ranges, 90% of the peak absolute magnitude lies between $[-15.6, -12.4]$ ($[-14.5, -10.2]$) for the nucleosynthesis powered model and $[-17.8, -15.3]$ ($[-17.9, -15.0]$) for the shock-powered model in the NUV (FUV) band. In Figure 46 we show the apparent AB magnitude of all three models in the two *UVEX* filter bands, for a GW170817-like event at a distance of 200Mpc, calculated with the fiducial model parameters from Table 3. The cadence, 10,000 seconds, is determined by the amount of tiles needed to map the localization area as estimated from the GW analysis, for which we take a fiducial value of 100 deg², and a 1,000s exposure time.

Based on the model light curves, especially the fast fading shock-model and neutron-precursor model, our goal is for *UVEX* to respond within 3 hours on average for BNS/NS–BH events. Once *UVEX* is on target, it will map the localization area and repeat the sequence for 24 hours. The median number of tiles per event will be 5 (minimum is 1, maximum is 22). Thus, a median of 17 epochs in the *UVEX* light curve is expected.

The results demonstrate that *UVEX* will generate high-SNR, well-sampled light curves **in both FUV and NUV bands** for all selected events in the O6 simulation, even in the more pessimistic case where the early UV emission is powered entirely by heavy-element nucleosynthesis.

10.2. Constraints from kilonova light curves

With each detection of a kilonova, we are able to constrain model parameters that describe the outflow dur-

ing and after a gravitational wave merger. As an example, we demonstrate a simulated detection and recovery of the semi-analytical light curve model with 7 parameters (§10.1.2) in Figure 47, using the observational data shown in Figure 46 (labeled “nucleosynthesis-powered, without free neutron decay”). We show the difference in posterior distribution for an event at 100 Mpc and 200 Mpc, and note that for both scenarios we can constrain the parameters and recover the injected values. Due to the possible wide diversity in kilonova (Kawaguchi et al. 2020) and that only $\sim O(10)$ GW events will be expected to have an electromagnetic counterpart detected before *UVEX* launches, detecting and constraining individual events will still be scientifically compelling.

Our goal, however, is to utilize the large sample of over 20 kilonovae that *UVEX* provides to start constraining the underlying population distributions of kilonova properties. Currently, population studies of kilonova properties are restricted to using upper limits from non-detections of electromagnetic counterpart searches (Kasliwal et al. 2020), which have provided some loose constraints on the luminosity function, as well as put limits on the ejecta mass, lanthanide fraction and inclination angle of a few individual kilonovae. Due to the many parameters describing the merger ejecta, the large sample of kilonovae detections, that *UVEX* provides, is crucial to significantly constrain the underlying populations. With accurate estimates of the underlying distribution of, e.g., the ejecta mass, it is possible to constrain the contribution of neutron star mergers to the formation of r-process elements (Hotokezaka et al. 2018). Furthermore, there exists a fundamental connection between parameters describing the outflows and parameters describing the binary system (e.g., Krüger & Foucart 2020, Nedora et al. 2020). Constraints on population distributions of ejecta parameters can therefore provide new constraints on this connection, break existing degeneracies, and constrain ejection mechanisms during and after the merger. Finally, detecting a population of electromagnetic counterparts to gravitational wave events will allow for a few percent measurement of the Hubble constant (e.g., Chen et al. 2018, Feeney et al. 2021).

10.3. Follow-up UV Spectroscopy

Very little is known and predicted about the possible UV spectrum of a kilonova (Kasen et al. 2017, Piro & Kollmeier 2018). *UVEX* could pioneer spectroscopic observations of EM counterparts in the UV. If the position of a bright and/or nearby kilonova is identified within 12 hours of merger, *UVEX* can be switched to spectroscopy mode to obtain unprecedented UV spectra.

We input a black-body model through the *UVEX* ETC to assess feasibility. We assumed temperatures of 13,900 K at 6 hours and 9,600 K at 12 hours from the merger. We estimated that a strong enough signal (mean $S/N > 3$ per resolution element) can be achieved with 3 hr of exposure time for sources out to approximately 115–185 Mpc in the first 12 hours from the merger. Assuming the BNS merger rate from [The LIGO Scientific Collaboration et al. \(2021b\)](#) and a conservative 18-month duration for O6, we expect up to ~ 4 events to happen within 115 Mpc that can be spectroscopically characterized with *UVEX*. More distant sources that exhibit particularly blue UV emission can also be studied spectroscopically. It is likely that any line emission is blended and broadened due to the large number and high velocity of the line transitions, however direct observations are needed to verify the predictions. The temperature can be well constrained ($< 10\%$ accuracy) for all selected sources in the O6 simulation.

10.4. Summary

Based on our simulations, *UVEX* will obtain a median of 17 UV epochs within 24 hours of the merger of over 20 well-localized ($< 100 \text{ deg}^2$) neutron star mergers. Such well-sampled light curves will allow us to understand which mechanisms power the early kilonova emission, breaking the degeneracy between shock-powered, nucleosynthesis-powered, and free neutron decay powered models. This information in the early-time light curve is best gleaned from the UV and cannot be assessed at later times or longer wavelengths.

11. EXOPLANETS

With thousands of discoveries at hand, the field of exoplanets is rapidly pivoting from detection to characterization. Limited thus far by the necessary advances in technology, we have nevertheless been able to explore a small number of planets in unprecedented detail. In particular, our ability to observe and understand the atmospheres of exoplanets has increased significantly over the last decade. Understanding exoplanet atmospheres, and refining how we analyze and model them, is a crucial stepping stone towards the detection and understanding of biosignatures, which are likely to be first found in exoplanet atmosphere analyses.

Transmission spectroscopy—measuring the absorbing cross section of the planet as a function of wavelength during transit—has been one of the most productive paths of atmosphere investigation. One finding is that clouds and hazes are prevalent across all types of exoplanet atmospheres ([Wakeford et al. 2019](#), [Fu et al. 2017](#), [Iyer et al. 2016](#), [Crossfield & Kreidberg 2017](#), [Morley](#)

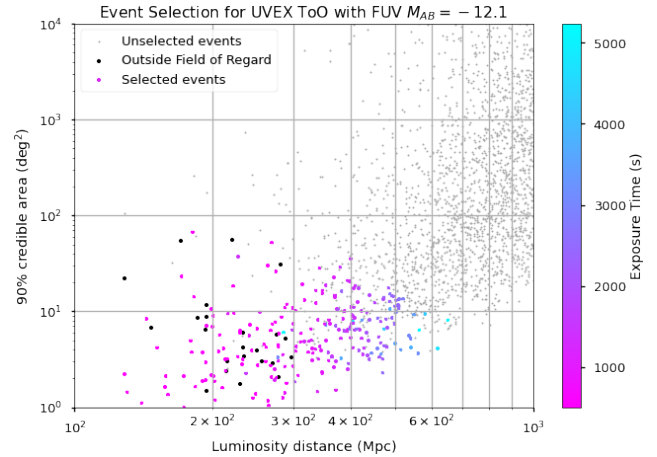


Figure 45. Simulation of Gravitational Wave triggers in the LIGO-Virgo-Kagra sixth observing run. The y-axis shows the 90% credible area and the x-axis shows the luminosity distance. Only those events with a credible area $< 100 \text{ deg}^2$ and distance such that a depth of -12.1 mag can be achieved in each pointing will be selected; selected events are color-coded by the optimal exposure time per the *UVEX* ETC. Events that are outside the *UVEX* field of regard are excluded and denoted as black points. (Note that the number of points in the simulation shown above is proportional to the number of predicted events in O6 but this scaling is not 1:1.)

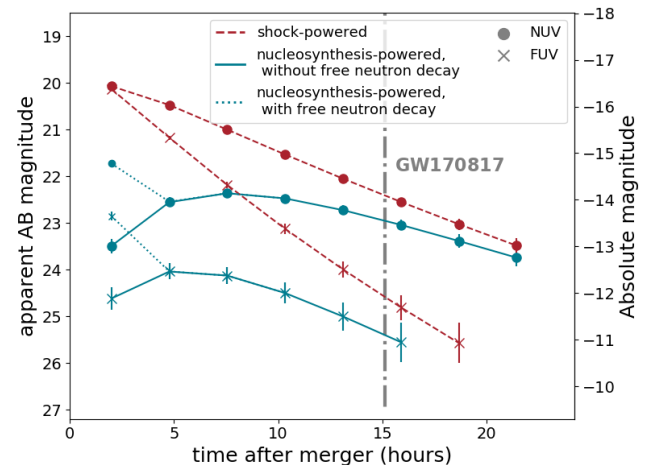


Figure 46. UV light curve predictions for a shock-powered model (dashed), nucleosynthesis-powered model with (dotted) and without (solid) a free neutron decay component. This light curve assumes a distance of 200 Mpc, exposure time of 1,000s and cadence of 10,000s (due to ten tiles needed to map the localization area). Note that 24.4 mag at 200 Mpc corresponds to an absolute magnitude of -12.1 mag, which means that the targeted *UVEX* depth of -12.1 mag is sensitive to all models in both filters.

Table 3. The parameters describing the nucleosynthesis powered and shock interaction powered models in neutron star mergers, with the allowed ranges within each parameter can vary. The fiducial values are the values used to generate the data in 46.

Parameter (Unit)	Description	Range	Fiducial value
<i>Nucleosynthesis Powered Model</i>			
M_{ej} (M_{\odot})	Ejecta mass	(0.01, 0.1)	0.05
v_{min} (c)	Minimum ejecta velocity	(0.05, 0.2)	0.1
v_{max} (c)	Maximum ejecta velocity	(0.3, 0.8)	0.4
n_{ej}	Power law index of ejecta density distribution	(3.5, 5)	4.5
v_{κ} (c)	Transition velocity between high and low κ	(v_{min} , v_{max})	0.2
κ_{high} (cm^2/g)	Effective grey opacity for $v \leq v_{\kappa}$	(1, 10)	3
κ_{low} (cm^2/g)	Effective grey opacity for $v \geq v_{\kappa}$	(0.1, 1)	0.5
M_{fn} (M_{\odot})	Free neutron mass	-	10^{-4}
<i>Shock Interaction Powered Model</i>			
M_{sh} (M_{\odot})	Shocked ejecta mass	(0.005, 0.05)	0.01
v_{sh} [c]	Shocked ejecta velocity	(0.1, 0.3)	0.2
R_0 (10^{10} cm)	Initial shock radius	(1, 10)	5
κ_{sh} (cm^2/g)	Effective grey opacity of shocked ejecta	(0.1, 1)	0.5

et al. 2015). Clouds and hazes can reduce the amplitude of spectral features, a reduction that can also independently be produced by high mean molecular weight atmospheres (Madhusudhan & Redfield 2015). The amplitudes of important molecular features, such as water, vary significantly between planets in the same class—hot Jupiters (Sing et al. 2016), warm Neptunes (Crossfield & Kreidberg 2017), and super-Earths (Southworth et al. 2017)—and understanding the origin of these variations is crucial for unlocking the physical processes that dominate these atmospheres. The degeneracy between the presence of clouds and hazes and the impact of a higher mean molecular weight atmosphere has hindered further understanding of these variations.

With the launch of the *James Webb Space Telescope*, transmission spectroscopy will be substantially boosted at IR wavelengths. The IR, with its many important molecular bandheads, is an important window into understanding the composition and structure of exoplanet atmospheres. However, at IR wavelengths the aforementioned aerosol/mean molecular weight degeneracy is severe. In addition, in order to holistically understand atmospheres and the physical processes that sculpt them, IR spectroscopy on its own is insufficient. We need to characterize exoplanet atmospheres over a much broader wavelength range, to capture physical processes that manifest at other wavelengths and to understand the entire energy budget of the planet. We also need to characterize exoplanet atmospheres over a much larger set of exoplanet parameters than has been previously accessible, such as planet size and insolation. The upcoming ESA ARIEL mission with the NASA/CASE

contribution will fill in important gaps at optical and near-IR wavelengths for a very large number of planets, partially satisfying these needs, but there remain important atmospheric processes that are only captured in the ultraviolet. Without complementary ultraviolet observations, our ability to both plan and interpret JWST and ARIEL observations will be significantly hindered. There is a broad range of atmospheric physics that can be studied with UV observations. These include Rayleigh and Mie scattering properties of cloud and haze particles (Section 11.1.1); heavy metal condensation and disequilibrium processes (Section 11.1.2); and observations of atmospheric escape in Lyman- α (e.g., Zhang et al. 2021). The former in particular presents the opportunity to identify cloudy or hazy atmospheres and break the aerosol/mean molecular weight degeneracy. Looking forward to JWST and ARIEL, being able to use ultraviolet observations to predict which planets are most likely to have measurable spectral features, and to interpret the very high quality optical and IR transmission spectra that will be obtained, will be crucial for maximizing the scientific return of these missions.

In addition to atmospheric science, understanding the ultraviolet environment of exoplanets is also crucial to understanding their habitability. Much attention has turned to rocky planets orbiting in the habitable zones of M dwarfs, as they are more readily detectable and characterizable than their analogs around FGK stars. Transit and radial velocity surveys, for instance, have optimized their filter bandpasses for M dwarf spectral energy distributions (e.g., Ricker et al. 2015, Addison et al. 2019). However, the ultraviolet radiation from

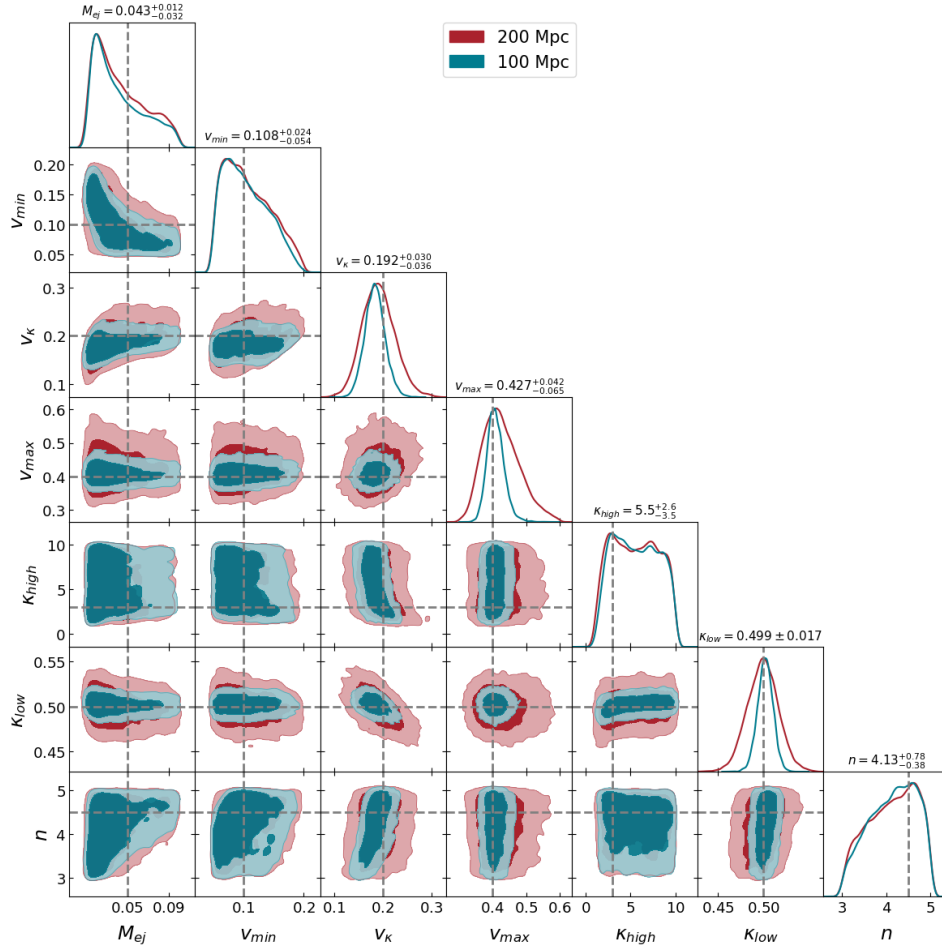


Figure 47. Posterior distribution on the parameters of the nucleosynthesis-powered model without a free neutron decay component, when inferring from simulated data from the light curve in Figure 46 at 100 and 200 Mpc.

M dwarfs is much more stochastic than that from FGK stars, with both more energetic flares and higher flare rates in general (see, e.g., Medina et al. 2020). This could have significant impact on the viability of these planets for hosting life (Estrela & Valio 2018, France et al. 2020). Understanding the ultraviolet radiation history and current insolation of rocky planets orbiting M dwarfs is another important question addressed by ultraviolet observations.

While the Hubble Space Telescope ultraviolet capabilities are operational, we can continue to construct and exploit multi-wavelength transmission spectroscopy and to investigate the ultraviolet environment of exoplanets. However, when those capabilities are gone, we will have a large gap in our ability to constrain these phenomena. In the following sections we outline two important science cases that could be performed with an exoplanet transmission survey undertaken with an ultraviolet telescope with the capabilities of *UVEX*.

11.1. A survey of exoplanet clouds, hazes, and metals

There are currently no extant or planned large-scale, systematic, ultraviolet surveys of the transiting planets that will be the target of optical and IR observations in the future. By undertaking a such a survey for the first time, *UVEX* could help answer several vital questions in atmospheric science. Two such questions are outlined below.

11.1.1. Constraining hazes in cool exoplanet atmospheres

Whereas clouds are considered to be ‘grey’, scattering stellar insolation roughly equally with wavelength, Rayleigh scattering of small haze particles in the upper atmospheres of exoplanets has a very strong wavelength dependence ($\propto \lambda^{-4}$). This leads to a much higher cross-section of a hazy planetary atmosphere at bluer wavelengths, and correspondingly deeper transit depths. The slope in the transmission spectrum as a function of wavelength can thus be used to measure the particle size of hazes forming high up in a planet atmosphere. Hazes may become more significant for planets cooler than 850 K (Morley et al. 2015, Crossfield & Kreidberg

2017), which are of particular interest to the community as they approach the conditions of habitability. Significant effort and observing time will be expended by the next generation of optical and IR missions to characterize the atmospheres of cool exoplanets, and large remaining uncertainties remain about the fraction of their atmospheres that are cloudy or hazy, and the characteristics of the extant clouds and hazes. See, e.g. Figure 2 of (Sing et al. 2016) for a sample of hot Jupiters with significantly varying transmission spectra between UV and IR wavelengths. Understanding how hazes manifest across a large range of atmospheric composition, from hydrogen- and helium-dominated atmospheres to higher mean molecular atmospheres dominated by, for instance, methane or carbon dioxide, over a range of exoplanet sizes and temperatures is crucial to breaking the aerosol/mean molecular weight degeneracy that mutes the spectral features. By measuring a large sample of UV-IR transmission spectral slopes, we can constrain trends with planet properties, which can then be compared to theoretical and experimental studies of haze production rates and compositions (e.g. Gao et al. 2017, Hörst et al. 2018, He et al. 2020)

11.1.2. *Probing metals, clouds, and rainout in hot exoplanets*

A few low-resolution observations of ultra-hot Jupiters (>2300 K) show strong absorption at UV wavelengths which far exceeds that expected from Rayleigh scattering (e.g. Sing et al. 2013, Evans et al. 2018, von Essen et al. 2019, Fu et al. 2021). The source of the absorption is not clear, and several suggestions (photochemistry, mass loss, disequilibrium chemistry) remain under consideration. Theoretical transmission spectra of hot (>1000 K) gas giant atmospheres from Lothringer et al. (2020) show strong absorption lines from heavy metal atoms and ions at near-ultraviolet wavelengths, including Fe I, Fe II, Ti I, Ni I, Ca I, and Ca II. These species had not often been included as opacity sources in transmission spectra models because of their low abundances, however, the authors show that since they have such strong absorption lines in the ultraviolet, they can significantly increase the broadband transit depths measured at these wavelengths. Indeed, evidence for heavy metal absorption has been found for some ultra-hot exoplanets at higher resolution, e.g. Fossati et al. (2010), Gibson et al. (2020), Ehrenreich et al. (2020).

Lothringer et al. (2020) demonstrate the use of a UV-optical spectral index to test if heavy metals are indeed the mystery ultraviolet opacity source for hot exoplanets. One such index is defined in their Eq. 2: $\Delta R_{p,NUV-Red} = (R_{p,0.2-0.3\mu m} - R_{p,0.6-0.7\mu m})/H_{eq}$, where $R_{p,0.2-0.3\mu m}$ is the radius of the planet as mea-

sured between $0.2-0.3 \mu m$, $R_{p,0.6-0.7\mu m}$ is the radius of the planet as measured between $0.6-0.7 \mu m$, and H_{eq} is the atmospheric scale height at the equilibrium temperature. If the hot atmospheres are in equilibrium, then $\Delta R_{p,NUV-Red}$ should increase rapidly from 3 to 9 between 1000 and 2500 K (see their Fig. 4). Between 2500 K and 4000 K, $\Delta R_{p,NUV-Red}$ will slowly decrease to 6. This predicted characteristic shape to the spectral index could be tested with a large sample of $\Delta R_{p,NUV-Red}$ measurements across the 1000–4000 K temperature range measured with *UVEX*. Further, we can test if the metals are raining out after forming clouds. If this is the case, then certain metal species should have depleted abundances in the atmospheric regions probed by transmission spectroscopy. This will lead to a shallower slope in $\Delta R_{p,NUV-Red}$ between 1000 and 2500 K.

11.1.3. *A systematic NUV/FUV survey with UVEX*

We simulated a survey of transiting exoplanets with *UVEX*. We found that we can address the two aforementioned questions and provide a legacy survey of UV exoplanet measurements with a *UVEX* survey spanning a broad range of both planet equilibrium temperature and radius. To construct a sample survey, we searched the NASA Exoplanet Archive for all transiting exoplanets with mass measurements, and calculated the change in transit depth of one atmospheric scale height, assuming zero albedo and a heat re-circulation factor of 0.36. We calculated the number of transit observations with *UVEX* required to reach a precision of one atmospheric scale height for each planet. This was motivated by the typical size of atmospheric features in the NUV, which are around 3-5 atmospheric scale heights—thus allowing transit depth measurements with a typical precision of $\sim 3\sigma$. To do this, we estimated the stellar flux in the *UVEX* passbands by first searching for the exoplanet hosts stars in the GALEX database (in the GALEX NUV band). For systems without GALEX data we estimated the NUV flux by scaling the closest stellar model from the PHOENIX grid, and summing the flux in the GALEX NUV passband using *Pyphot*. We then designed the sample survey of the planets most amenable to atmospheric characterization with *UVEX* (those requiring few transit observations to reach the required precision in transit depth). To achieve a sufficient spread in equilibrium temperature, we selected the 15 planets with the highest signal-to-noise in 5 temperature bins: 0–800 K, 800–1300 K, 1300–1800 K, 1800–2300 K, and >2300 K. To provide a sufficient spread in planetary radii, we additionally selected the 15 planets with the highest SNR which were smaller than Neptune (not

counting duplicates from previous step), since larger planets are over-represented when ranking by SNR. This resulted in a total sample of 81 planets ranging from $V=7\text{--}17$ mag, shown in Figures 48 and 49. Of these, 36 can be used to investigate how haze properties of exoplanet atmospheres change with size (from $\sim 1.0\text{--}15 R_{\oplus}$) and temperature (from $\sim 200\text{--}1250$ K), and 45 can be used to investigate metal rain-out in ultra-hot giant planets from $\sim 1300\text{--}3100$ K. In addition to exploration of the two science cases outlined above, all of our targets will have red-optical transit depths measured by the NASA Transiting Exoplanet Survey Satellite (*TESS*) all-sky survey for calculating the $\Delta R_{p,NUV-Red}$ index. By flagging planets that exhibit large offsets, we can effectively identify the most favorable targets for more detailed atmosphere characterization with JWST and ARIEL. For each transit visit of each target we estimate the total observing time as equal to the duration of two full transits (to acquire sufficient out-of-transit baseline) plus one hour of overheads. In total the proposed survey of 81 planets would take 2230 hours to complete—approximately three months.

11.2. Summary

There are many critical exoplanet atmosphere processes that are only understood in the context of ultraviolet observations. The presence and composition of clouds and hazes in cool exoplanets, the rain-out of metal in hot exoplanets, atmospheric escape and mass-

loss processes across highly irradiated planets, and the integrated ultraviolet radiation experienced by a potentially habitable planet, are all only constrained on an individual exoplanet level with targeted ultraviolet observations, and on a population level with a carefully constructed ultraviolet exoplanet atmosphere survey, such as that outlined here. A three-month survey of 81 exoplanets would directly address several of the most important outstanding questions in exoplanet atmospheres, provide a legacy database of spectra for additional study, and, crucially, would enable interpretation of expensive optical and IR spectra obtained by upcoming NASA investments.

12. CONCLUSION

The *UVEX* mission opens a powerful new window to simultaneously explore both the static and dynamic UV sky. With a planned launch date in the late 2020's, *UVEX* fills a critical capability gap – wide-field UV imaging – in the era when Rubin, *Roman*, and *Euclid* will be transforming our understanding of the cosmos. Here we have described just a sampling of the anticipated science yield offered by *UVEX*, which covers the gamut of modern astrophysics, including all three science goals of NASA's Astrophysics division and the Astro2020 decadal survey. As evidenced by the success of projects like the Sloan Digital Sky Survey, by providing timely and high-quality data products to the entire community, the resulting *UVEX* discoveries will be limited only by the creativity of astronomers worldwide.

REFERENCES

- Abbott, B. P., Abbott, R., Abbott, T. D., et al. 2016, ApJL, 818, L22, doi: [10.3847/2041-8205/818/2/L22](https://doi.org/10.3847/2041-8205/818/2/L22)
- . 2017a, ApJL, 848, L12, doi: [10.3847/2041-8213/aa91c9](https://doi.org/10.3847/2041-8213/aa91c9)
- . 2017b, ApJL, 848, L13, doi: [10.3847/2041-8213/aa920c](https://doi.org/10.3847/2041-8213/aa920c)
- . 2020a, Living Reviews in Relativity, 23, 3, doi: [10.1007/s41114-020-00026-9](https://doi.org/10.1007/s41114-020-00026-9)
- Abbott, R., Abbott, T. D., Abraham, S., et al. 2020b, ApJL, 896, L44, doi: [10.3847/2041-8213/ab960f](https://doi.org/10.3847/2041-8213/ab960f)
- . 2020c, PhRvL, 125, 101102, doi: [10.1103/PhysRevLett.125.101102](https://doi.org/10.1103/PhysRevLett.125.101102)
- . 2021, ApJL, 915, L5, doi: [10.3847/2041-8213/ac082e](https://doi.org/10.3847/2041-8213/ac082e)
- Abdo, A. A., Ackermann, M., Ajello, M., et al. 2010, Science, 329, 817, doi: [10.1126/science.1192537](https://doi.org/10.1126/science.1192537)
- Ackley, K., Amati, L., Barbieri, C., et al. 2020, A&A, 643, A113, doi: [10.1051/0004-6361/202037669](https://doi.org/10.1051/0004-6361/202037669)
- Addison, B., Wright, D. J., Wittenmyer, R. A., et al. 2019, PASP, 131, 115003, doi: [10.1088/1538-3873/ab03aa](https://doi.org/10.1088/1538-3873/ab03aa)
- Afshordi, N., & Paczyński, B. 2003, ApJ, 592, 354, doi: [10.1086/375559](https://doi.org/10.1086/375559)
- Alexander, M. J., Hanes, R. J., Povich, M. S., & McSwain, M. V. 2016, AJ, 152, 190, doi: [10.3847/0004-6256/152/6/190](https://doi.org/10.3847/0004-6256/152/6/190)
- Allen, D. A., & Hillier, D. J. 1993, PASA, 10, 338
- Anand, S., Coughlin, M. W., Kasliwal, M. M., et al. 2021, Nature Astronomy, 5, 46, doi: [10.1038/s41550-020-1183-3](https://doi.org/10.1038/s41550-020-1183-3)
- Andreoni, I., Goldstein, D. A., Kasliwal, M. M., et al. 2020, ApJ, 890, 131, doi: [10.3847/1538-4357/ab6a1b](https://doi.org/10.3847/1538-4357/ab6a1b)
- Arcavi, I. 2018, ApJL, 855, L23, doi: [10.3847/2041-8213/aab267](https://doi.org/10.3847/2041-8213/aab267)
- Arcavi, I., Wolf, W. M., Howell, D. A., et al. 2016, ApJ, 819, 35, doi: [10.3847/0004-637X/819/1/35](https://doi.org/10.3847/0004-637X/819/1/35)
- Asif, A., Barschke, M., Bastian-Querner, B., et al. 2021, arXiv e-prints, arXiv:2108.01493, <https://arxiv.org/abs/2108.01493>

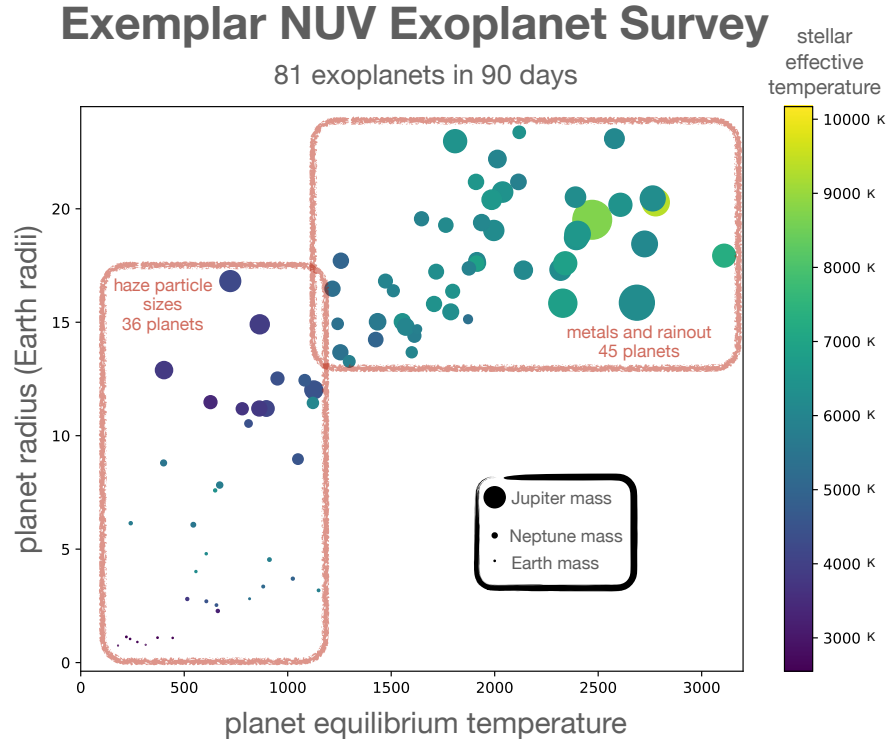


Figure 48. The planet radii and equilibrium temperatures of a sample of 81 planets that would be used to constrain two critical exoplanet atmosphere science cases—how haze properties of cooler exoplanets depend on planet size, equilibrium temperature, and host star properties, and the extent to which metals in ultra-hot atmospheres are raining out. The full sample would take ~3 months to observe, and leave a legacy of FUV/NUV spectra of exoplanets that will be observed by JWST and ARIEL/CASE.

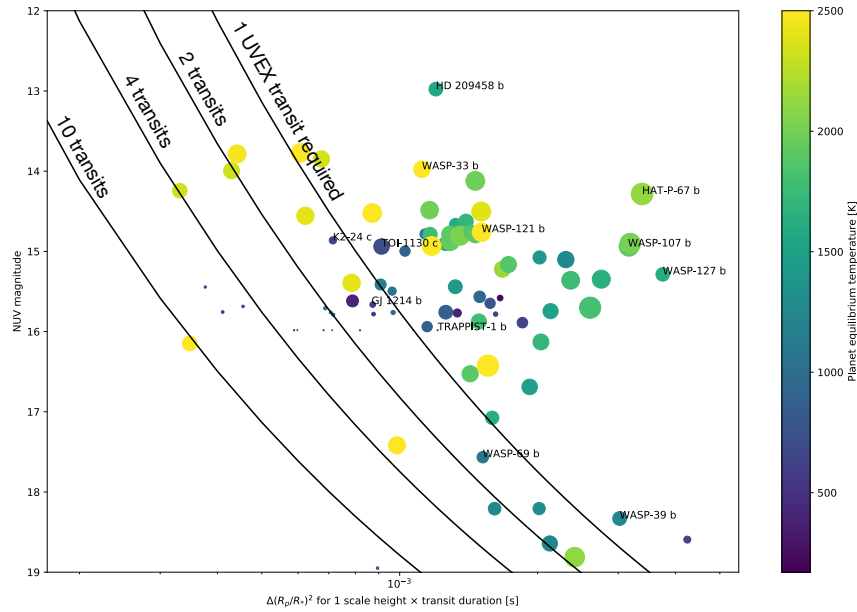


Figure 49. The signal-to-noise (SNR) for each planet in the exemplar survey, defined as the fractional transit depth for one atmospheric scale height multiplied by the transit duration, as a function of the NUV brightness of the host star. Solid lines show the number of *UVEX* transits (1, 2, 4, and 10) required to achieve a given SNR.

- Assef, R. J., Stern, D., Kochanek, C. S., et al. 2013, *ApJ*, 772, 26, doi: [10.1088/0004-637X/772/1/26](https://doi.org/10.1088/0004-637X/772/1/26)
- Aydi, E., Sokolovsky, K. V., Chomiuk, L., et al. 2020, *Nature Astronomy*, 4, 776, doi: [10.1038/s41550-020-1070-y](https://doi.org/10.1038/s41550-020-1070-y)
- Bañados, E., Venemans, B. P., Mazzucchelli, C., et al. 2018, *Nature*, 553, 473, doi: [10.1038/nature25180](https://doi.org/10.1038/nature25180)
- Bade, N., Komossa, S., & Dahlem, M. 1996, *A&A*, 309, L35
- Balbus, S. A., & Hawley, J. F. 1998, *Reviews of Modern Physics*, 70, 1, doi: [10.1103/RevModPhys.70.1](https://doi.org/10.1103/RevModPhys.70.1)
- Barnes, K. L., van Zee, L., & Skillman, E. D. 2011, *ApJ*, 743, 137, doi: [10.1088/0004-637X/743/2/137](https://doi.org/10.1088/0004-637X/743/2/137)
- Baron, E., Branch, D., Hauschildt, P. H., et al. 2000, *ApJ*, 545, 444, doi: [10.1086/317795](https://doi.org/10.1086/317795)
- Barth, A. J., & Stern, D. 2018, *ApJ*, 859, 10, doi: [10.3847/1538-4357/aab3c5](https://doi.org/10.3847/1538-4357/aab3c5)
- Barth, A. J., Bennert, V. N., Canalizo, G., et al. 2015, *ApJS*, 217, 26, doi: [10.1088/0067-0049/217/2/26](https://doi.org/10.1088/0067-0049/217/2/26)
- Begelman, M. C., Armitage, P. J., & Reynolds, C. S. 2015, *ApJ*, 809, 118, doi: [10.1088/0004-637X/809/2/118](https://doi.org/10.1088/0004-637X/809/2/118)
- Begelman, M. C., McKee, C. F., & Shields, G. A. 1983, *ApJ*, 271, 70, doi: [10.1086/161178](https://doi.org/10.1086/161178)
- Belczynski, K., Bulik, T., Fryer, C. L., et al. 2010, *ApJ*, 714, 1217, doi: [10.1088/0004-637X/714/2/1217](https://doi.org/10.1088/0004-637X/714/2/1217)
- Ben-Ami, S., Hachinger, S., Gal-Yam, A., et al. 2015, *ApJ*, 803, 40, doi: [10.1088/0004-637X/803/1/40](https://doi.org/10.1088/0004-637X/803/1/40)
- Berger, E., Kulkarni, S. R., & Chevalier, R. A. 2002, *ApJL*, 577, L5, doi: [10.1086/344045](https://doi.org/10.1086/344045)
- Bersten, M. C., Folatelli, G., García, F., et al. 2018, *Nature*, 554, 497, doi: [10.1038/nature25151](https://doi.org/10.1038/nature25151)
- Bigiel, F., Leroy, A., Walter, F., et al. 2008, *AJ*, 136, 2846, doi: [10.1088/0004-6256/136/6/2846](https://doi.org/10.1088/0004-6256/136/6/2846)
- Björklund, R., Sundqvist, J. O., Puls, J., & Najarro, F. 2021, *Astronomy & Astrophysics*, 648, A36, doi: [10.1051/0004-6361/202038384](https://doi.org/10.1051/0004-6361/202038384)
- Blagorodnova, N., Gezari, S., Hung, T., et al. 2017, *ApJ*, 844, 46, doi: [10.3847/1538-4357/aa7579](https://doi.org/10.3847/1538-4357/aa7579)
- Blagorodnova, N., Cenko, S. B., Kulkarni, S. R., et al. 2019, *ApJ*, 873, 92, doi: [10.3847/1538-4357/ab04b0](https://doi.org/10.3847/1538-4357/ab04b0)
- Bland-Hawthorn, J., & Gerhard, O. 2016, *ARA&A*, 54, 529, doi: [10.1146/annurev-astro-081915-023441](https://doi.org/10.1146/annurev-astro-081915-023441)
- Blandford, R. D., & McKee, C. F. 1982, *ApJ*, 255, 419, doi: [10.1086/159843](https://doi.org/10.1086/159843)
- Blum, R. D., Damiani, A., & Conti, P. S. 1999, *AJ*, 117, 1392, doi: [10.1086/300791](https://doi.org/10.1086/300791)
- Bode, M. F., & Evans, A. 2008, *Classical Novae*, Vol. 43 (Cambridge University Press)
- Boian, I., & Groh, J. H. 2020, *MNRAS*, 496, 1325, doi: [10.1093/mnras/staa1540](https://doi.org/10.1093/mnras/staa1540)
- Boksenberg, A., Evans, R. G., Fowler, R. G., et al. 1973, *MNRAS*, 163, 291, doi: [10.1093/mnras/163.3.291](https://doi.org/10.1093/mnras/163.3.291)
- Bonito, R., Hartigan, P., Venuti, L., et al. 2018, arXiv e-prints, arXiv:1812.03135, <https://arxiv.org/abs/1812.03135>
- Bouret, J. C., Lanz, T., Hillier, D. J., et al. 2015, *MNRAS*, 449, 1545, doi: [10.1093/mnras/stv379](https://doi.org/10.1093/mnras/stv379)
- Branch, D., & Wheeler, J. C. 2017, *Supernova Explosions* (Springer-Verlag), doi: [10.1007/978-3-662-55054-0](https://doi.org/10.1007/978-3-662-55054-0)
- Bright, J. S., Margutti, R., Matthews, D., et al. 2021, arXiv e-prints, arXiv:2110.05514, <https://arxiv.org/abs/2110.05514>
- Brosch, N. 1999, *Experimental Astronomy*, 9, 119
- Brown, J. S., Kochanek, C. S., Holoiien, T. W. S., et al. 2018, *MNRAS*, 473, 1130, doi: [10.1093/mnras/stx2372](https://doi.org/10.1093/mnras/stx2372)
- Brown, P. J., Dawson, K. S., de Pasquale, M., et al. 2012, *ApJ*, 753, 22, doi: [10.1088/0004-637X/753/1/22](https://doi.org/10.1088/0004-637X/753/1/22)
- Bruch, R. J., Gal-Yam, A., Schulze, S., et al. 2021a, *ApJ*, 912, 46, doi: [10.3847/1538-4357/abef05](https://doi.org/10.3847/1538-4357/abef05)
- . 2021b, *ApJ*, 912, 46, doi: [10.3847/1538-4357/abef05](https://doi.org/10.3847/1538-4357/abef05)
- Bufano, F., Immler, S., Turatto, M., et al. 2009, *ApJ*, 700, 1456, doi: [10.1088/0004-637X/700/2/1456](https://doi.org/10.1088/0004-637X/700/2/1456)
- Cackett, E. M., Bentz, M. C., & Kara, E. 2021, *iScience*, 24, 102557, doi: [10.1016/j.isci.2021.102557](https://doi.org/10.1016/j.isci.2021.102557)
- Calvet, N., & Gullbring, E. 1998, *ApJ*, 509, 802, doi: [10.1086/306527](https://doi.org/10.1086/306527)
- Calzetti, D., Armus, L., Bohlin, R. C., et al. 2000, *ApJ*, 533, 682, doi: [10.1086/308692](https://doi.org/10.1086/308692)
- Camacho, I., Garcia, M., Herrero, A., & Simón-Díaz, S. 2016, *A&A*, 585, A82, doi: [10.1051/0004-6361/201425533](https://doi.org/10.1051/0004-6361/201425533)
- Campana, S., Mangano, V., Blustin, A. J., et al. 2006, *Nature*, 442, 1008, doi: [10.1038/nature04892](https://doi.org/10.1038/nature04892)
- Cano, Z., Wang, S.-Q., Dai, Z.-G., & Wu, X.-F. 2017, *Advances in Astronomy*, 2017, 8929054, doi: [10.1155/2017/8929054](https://doi.org/10.1155/2017/8929054)
- Cardelli, J. A., Clayton, G. C., & Mathis, J. S. 1989, *ApJ*, 345, 245, doi: [10.1086/167900](https://doi.org/10.1086/167900)
- Carney, B. W. 1979, *ApJ*, 233, 211, doi: [10.1086/157383](https://doi.org/10.1086/157383)
- Cartledge, S. I. B., Clayton, G. C., Gordon, K. D., et al. 2005, *ApJ*, 630, 355, doi: [10.1086/431922](https://doi.org/10.1086/431922)
- Castor, J. I., & Lamers, H. J. G. L. M. 1979, *ApJS*, 39, 481, doi: [10.1086/190583](https://doi.org/10.1086/190583)
- Cenko, S. B., Kulkarni, S. R., Horesh, A., et al. 2013, *ApJ*, 769, 130, doi: [10.1088/0004-637X/769/2/130](https://doi.org/10.1088/0004-637X/769/2/130)
- Cenko, S. B., Cucchiara, A., Roth, N., et al. 2016, *ApJL*, 818, L32, doi: [10.3847/2041-8205/818/2/L32](https://doi.org/10.3847/2041-8205/818/2/L32)
- Charisi, M., Bartos, I., Haiman, Z., et al. 2016, *MNRAS*, 463, 2145, doi: [10.1093/mnras/stw1838](https://doi.org/10.1093/mnras/stw1838)
- Chen, H.-Y., Fishbach, M., & Holz, D. E. 2018, *Nature*, 562, 545, doi: [10.1038/s41586-018-0606-0](https://doi.org/10.1038/s41586-018-0606-0)

- Chevalier, R. A., & Fransson, C. 2006, *ApJ*, 651, 381, doi: [10.1086/507606](https://doi.org/10.1086/507606)
- . 2017, *Thermal and Non-thermal Emission from Circumstellar Interaction*, ed. A. W. Alsabti & P. Murdin (Springer), 875, doi: [10.1007/978-3-319-21846-5_34](https://doi.org/10.1007/978-3-319-21846-5_34)
- Chevalier, R. A., & Irwin, C. M. 2011, *ApJL*, 729, L6, doi: [10.1088/2041-8205/729/1/L6](https://doi.org/10.1088/2041-8205/729/1/L6)
- Chiang, Y.-K., & Ménard, B. 2019, *ApJ*, 870, 120, doi: [10.3847/1538-4357/aaf4f6](https://doi.org/10.3847/1538-4357/aaf4f6)
- Chomiuk, L., Metzger, B. D., & Shen, K. J. 2020, arXiv e-prints, arXiv:2011.08751. <https://arxiv.org/abs/2011.08751>
- Chomiuk, L., Soderberg, A. M., Moe, M., et al. 2012, *ApJ*, 750, 164, doi: [10.1088/0004-637X/750/2/164](https://doi.org/10.1088/0004-637X/750/2/164)
- Cioni, M. R. L., Storm, J., Bell, C. P. M., et al. 2019, *The Messenger*, 175, 54, doi: [10.18727/0722-6691/5128](https://doi.org/10.18727/0722-6691/5128)
- Cioni, M. R. L., Clementini, G., Girardi, L., et al. 2011, *A&A*, 527, A116, doi: [10.1051/0004-6361/201016137](https://doi.org/10.1051/0004-6361/201016137)
- Cohn, J. H., Walsh, J. L., Boizelle, B. D., et al. 2021, *ApJ*, 919, 77, doi: [10.3847/1538-4357/ac0f78](https://doi.org/10.3847/1538-4357/ac0f78)
- Cole, A. A., Skillman, E. D., Tolstoy, E., et al. 2007, *ApJL*, 659, L17, doi: [10.1086/516711](https://doi.org/10.1086/516711)
- Coppejans, D. L., & Knigge, C. 2020, *NewAR*, 89, 101540, doi: [10.1016/j.newar.2020.101540](https://doi.org/10.1016/j.newar.2020.101540)
- Coppejans, D. L., Margutti, R., Terreran, G., et al. 2020, *ApJL*, 895, L23, doi: [10.3847/2041-8213/ab8cc7](https://doi.org/10.3847/2041-8213/ab8cc7)
- Corsi, A., Gal-Yam, A., Kulkarni, S. R., et al. 2016, *ApJ*, 830, 42, doi: [10.3847/0004-637X/830/1/42](https://doi.org/10.3847/0004-637X/830/1/42)
- Crossfield, I. J. M., & Kreidberg, L. 2017, *AJ*, 154, 261, doi: [10.3847/1538-3881/aa9279](https://doi.org/10.3847/1538-3881/aa9279)
- Crowther, P. A., Caballero-Nieves, S. M., Bostroem, K. A., et al. 2016, *MNRAS*, 458, 624, doi: [10.1093/mnras/stw273](https://doi.org/10.1093/mnras/stw273)
- Dalcanton, J. J., Williams, B. F., Lang, D., et al. 2012, *ApJS*, 200, 18, doi: [10.1088/0067-0049/200/2/18](https://doi.org/10.1088/0067-0049/200/2/18)
- Darvish, B., Martin, C., Gonçalves, T. S., et al. 2018, *ApJ*, 853, 155, doi: [10.3847/1538-4357/aaa5a4](https://doi.org/10.3847/1538-4357/aaa5a4)
- De, K., Kasliwal, M. M., Hankins, M. J., et al. 2021, *ApJ*, 912, 19, doi: [10.3847/1538-4357/abeb75](https://doi.org/10.3847/1538-4357/abeb75)
- De Cicco, D., Paolillo, M., Falocco, S., et al. 2019, *A&A*, 627, A33, doi: [10.1051/0004-6361/201935659](https://doi.org/10.1051/0004-6361/201935659)
- de Jager, C., Hoekstra, R., van der Hucht, K. A., et al. 1974, *Ap&SS*, 26, 207, doi: [10.1007/BF00642637](https://doi.org/10.1007/BF00642637)
- de Jager, C., Lamers, H. J. G. L. M., & van der Hucht, K. A. 1975, *Ap&SS*, 38, 313, doi: [10.1007/BF00647130](https://doi.org/10.1007/BF00647130)
- de Sá-Freitas, C., Gonçalves, T. S., de Carvalho, R. R., et al. 2021, *MNRAS*, doi: [10.1093/mnras/stab3230](https://doi.org/10.1093/mnras/stab3230)
- De Silva, G. M., Freeman, K. C., Bland-Hawthorn, J., et al. 2015, *MNRAS*, 449, 2604, doi: [10.1093/mnras/stv327](https://doi.org/10.1093/mnras/stv327)
- della Valle, M., Bianchini, A., Livio, M., & Origo, M. 1992, *A&A*, 266, 232
- Della Valle, M., & Izzo, L. 2020, *A&A Rv*, 28, 3, doi: [10.1007/s00159-020-0124-6](https://doi.org/10.1007/s00159-020-0124-6)
- Deng, L.-C., Newberg, H. J., Liu, C., et al. 2012, *Research in Astronomy and Astrophysics*, 12, 735, doi: [10.1088/1674-4527/12/7/003](https://doi.org/10.1088/1674-4527/12/7/003)
- Derdzinski, A. M., Metzger, B. D., & Lazzati, D. 2017, *MNRAS*, 469, 1314, doi: [10.1093/mnras/stx829](https://doi.org/10.1093/mnras/stx829)
- Dessart, L., John Hillier, D., & Audit, E. 2017a, *A&A*, 605, A83, doi: [10.1051/0004-6361/201730942](https://doi.org/10.1051/0004-6361/201730942)
- . 2017b, *A&A*, 605, A83, doi: [10.1051/0004-6361/201730942](https://doi.org/10.1051/0004-6361/201730942)
- Dixon, D., Tayar, J., & Stassun, K. G. 2020, *AJ*, 160, 12, doi: [10.3847/1538-3881/ab9080](https://doi.org/10.3847/1538-3881/ab9080)
- D’Orazio, D. J., & Di Stefano, R. 2018, *MNRAS*, 474, 2975, doi: [10.1093/mnras/stx2936](https://doi.org/10.1093/mnras/stx2936)
- D’Orazio, D. J., Haiman, Z., & Schiminovich, D. 2015, *Nature*, 525, 351, doi: [10.1038/nature15262](https://doi.org/10.1038/nature15262)
- Draine, B. T. 2003, *ARA&A*, 41, 241, doi: [10.1146/annurev.astro.41.011802.094840](https://doi.org/10.1146/annurev.astro.41.011802.094840)
- . 2011, *Physics of the Interstellar and Intergalactic Medium* (Princeton University Press)
- Drout, M. R., Chornock, R., Soderberg, A. M., et al. 2014, *ApJ*, 794, 23, doi: [10.1088/0004-637X/794/1/23](https://doi.org/10.1088/0004-637X/794/1/23)
- Drout, M. R., Piro, A. L., Shappee, B. J., et al. 2017, *Science*, 358, 1570, doi: [10.1126/science.aag0049](https://doi.org/10.1126/science.aag0049)
- Edelstein, J., Korpel, E. J., Adolfo, J., et al. 2006, *ApJL*, 644, L159, doi: [10.1086/505205](https://doi.org/10.1086/505205)
- Ehrenreich, D., Lovis, C., Allart, R., et al. 2020, *Nature*, 580, 597–601, doi: [10.1038/s41586-020-2107-1](https://doi.org/10.1038/s41586-020-2107-1)
- Elahi, P. J., Welker, C., Power, C., et al. 2018, *MNRAS*, 475, 5338, doi: [10.1093/mnras/sty061](https://doi.org/10.1093/mnras/sty061)
- Eldridge, J. J., Izzard, R. G., & Tout, C. A. 2008, *MNRAS*, 384, 1109, doi: [10.1111/j.1365-2966.2007.12738.x](https://doi.org/10.1111/j.1365-2966.2007.12738.x)
- Eldridge, J. J., & Stanway, E. R. 2009, *MNRAS*, 400, 1019, doi: [10.1111/j.1365-2966.2009.15514.x](https://doi.org/10.1111/j.1365-2966.2009.15514.x)
- Eldridge, J. J., Stanway, E. R., Xiao, L., et al. 2017, *PASA*, 34, e058, doi: [10.1017/pasa.2017.51](https://doi.org/10.1017/pasa.2017.51)
- Estrela, R., & Valio, A. 2018, *Astrobiology*, 18, 1414, doi: [10.1089/ast.2017.1724](https://doi.org/10.1089/ast.2017.1724)
- Evans, C. J., Howarth, I. D., Irwin, M. J., Burnley, A. W., & Harries, T. J. 2004, *MNRAS*, 353, 601, doi: [10.1111/j.1365-2966.2004.08096.x](https://doi.org/10.1111/j.1365-2966.2004.08096.x)
- Evans, C. J., Lennon, D. J., Smartt, S. J., & Trundle, C. 2006, *A&A*, 456, 623, doi: [10.1051/0004-6361:20064988](https://doi.org/10.1051/0004-6361:20064988)
- Evans, C. J., Taylor, W. D., Hénault-Brunet, V., et al. 2011, *A&A*, 530, A108, doi: [10.1051/0004-6361/201116782](https://doi.org/10.1051/0004-6361/201116782)

- Evans, P. A., Cenko, S. B., Kennea, J. A., et al. 2017, *Science*, 358, 1565, doi: [10.1126/science.aap9580](https://doi.org/10.1126/science.aap9580)
- Evans, T. M., Sing, D. K., Goyal, J. M., et al. 2018, *AJ*, 156, 283, doi: [10.3847/1538-3881/aaebff](https://doi.org/10.3847/1538-3881/aaebff)
- Feeney, S. M., Peiris, H. V., Nissanke, S. M., & Mortlock, D. J. 2021, *PhRvL*, 126, 171102, doi: [10.1103/PhysRevLett.126.171102](https://doi.org/10.1103/PhysRevLett.126.171102)
- Feigelson, E. D., Getman, K. V., Townsley, L. K., et al. 2011, *ApJS*, 194, 9, doi: [10.1088/0067-0049/194/1/9](https://doi.org/10.1088/0067-0049/194/1/9)
- Fender, R., & Belloni, T. 2004, *ARA&A*, 42, 317, doi: [10.1146/annurev.astro.42.053102.134031](https://doi.org/10.1146/annurev.astro.42.053102.134031)
- Fender, R., & Muñoz-Darias, T. 2016, *The Balance of Power: Accretion and Feedback in Stellar Mass Black Holes*, Vol. 905 (Springer Verlag), 65, doi: [10.1007/978-3-319-19416-5_3](https://doi.org/10.1007/978-3-319-19416-5_3)
- Fernández, R., & Metzger, B. D. 2016, *Annual Review of Nuclear and Particle Science*, 66, 23, doi: [10.1146/annurev-nucl-102115-044819](https://doi.org/10.1146/annurev-nucl-102115-044819)
- Ferrarese, L., & Merritt, D. 2000, *ApJL*, 539, L9, doi: [10.1086/312838](https://doi.org/10.1086/312838)
- Ferreira, J., & Pelletier, G. 1995, *A&A*, 295, 807
- Findeisen, K., & Hillenbrand, L. 2010, *AJ*, 139, 1338, doi: [10.1088/0004-6256/139/4/1338](https://doi.org/10.1088/0004-6256/139/4/1338)
- Fisher, D. B., Bolatto, A. D., Herrera-Camus, R., et al. 2014, *Nature*, 505, 186, doi: [10.1038/nature12765](https://doi.org/10.1038/nature12765)
- Fitzpatrick, E. L., & Massa, D. 2007, *ApJ*, 663, 320, doi: [10.1086/518158](https://doi.org/10.1086/518158)
- Fitzpatrick, E. L., Massa, D., Gordon, K. D., Bohlin, R., & Clayton, G. C. 2019, *ApJ*, 886, 108, doi: [10.3847/1538-4357/ab4c3a](https://doi.org/10.3847/1538-4357/ab4c3a)
- Fossati, L., Haswell, C. A., Froning, C. S., et al. 2010, *The Astrophysical Journal*, 714, L222–L227, doi: [10.1088/2041-8205/714/2/l222](https://doi.org/10.1088/2041-8205/714/2/l222)
- Foucart, F. 2012, *PhRvD*, 86, 124007, doi: [10.1103/PhysRevD.86.124007](https://doi.org/10.1103/PhysRevD.86.124007)
- France, K., Duvvuri, G., Egan, H., et al. 2020, *AJ*, 160, 237, doi: [10.3847/1538-3881/abb465](https://doi.org/10.3847/1538-3881/abb465)
- Frankowiak, A., Jean, P., Wood, M., Cheung, C. C., & Buson, S. 2018, *A&A*, 609, A120, doi: [10.1051/0004-6361/201731516](https://doi.org/10.1051/0004-6361/201731516)
- Fransson, C., Challis, P. M., Chevalier, R. A., et al. 2005, *ApJ*, 622, 991, doi: [10.1086/426495](https://doi.org/10.1086/426495)
- Fransson, C., Ergon, M., Challis, P. J., et al. 2014, *ApJ*, 797, 118, doi: [10.1088/0004-637X/797/2/118](https://doi.org/10.1088/0004-637X/797/2/118)
- Fraser, M., Stritzinger, M. D., Brennan, S. J., et al. 2021, *arXiv e-prints*, arXiv:2108.07278, <https://arxiv.org/abs/2108.07278>
- Frederick, S., Gezari, S., Graham, M. J., et al. 2021, *ApJ*, 920, 56, doi: [10.3847/1538-4357/ac110f](https://doi.org/10.3847/1538-4357/ac110f)
- Fremling, C., Miller, A. A., Sharma, Y., et al. 2020, *ApJ*, 895, 32, doi: [10.3847/1538-4357/ab8943](https://doi.org/10.3847/1538-4357/ab8943)
- Fu, G., Deming, D., Knutson, H., et al. 2017, *ApJL*, 847, L22, doi: [10.3847/2041-8213/aa8e40](https://doi.org/10.3847/2041-8213/aa8e40)
- Fu, G., Deming, D., Lothringer, J., et al. 2021, *The Astronomical Journal*, 162, 108, doi: [10.3847/1538-3881/ac1200](https://doi.org/10.3847/1538-3881/ac1200)
- Fuller, J., & Ro, S. 2018, *MNRAS*, 476, 1853, doi: [10.1093/mnras/sty369](https://doi.org/10.1093/mnras/sty369)
- Gal-Yam, A., Bufano, F., Barlow, T. A., et al. 2008, *ApJL*, 685, L117, doi: [10.1086/592744](https://doi.org/10.1086/592744)
- Gal-Yam, A., Arcavi, I., Ofek, E. O., et al. 2014, *Nature*, 509, 471, doi: [10.1038/nature13304](https://doi.org/10.1038/nature13304)
- Gal-Yam, A., Bruch, R., Schulze, S., et al. 2021, *arXiv e-prints*, arXiv:2111.12435, <https://arxiv.org/abs/2111.12435>
- Galama, T. J., Vreeswijk, P. M., van Paradijs, J., et al. 1998, *Nature*, 395, 670, doi: [10.1038/27150](https://doi.org/10.1038/27150)
- Gao, P., Marley, M. S., Zahnle, K., Robinson, T. D., & Lewis, N. K. 2017, *AJ*, 153, 139, doi: [10.3847/1538-3881/aa5fab](https://doi.org/10.3847/1538-3881/aa5fab)
- Garcia, M. 2018, *MNRAS*, 474, L66, doi: [10.1093/mnrasl/slx194](https://doi.org/10.1093/mnrasl/slx194)
- Garcia, M., Herrero, A., Najarro, F., Camacho, I., & Lorenzo, M. 2019a, *MNRAS*, 484, 422, doi: [10.1093/mnras/sty3503](https://doi.org/10.1093/mnras/sty3503)
- Garcia, M., Evans, C. J., Bestenlehner, J. M., et al. 2019b, *arXiv e-prints*, arXiv:1908.04687, <https://arxiv.org/abs/1908.04687>
- Gebhardt, K., Bender, R., Bower, G., et al. 2000, *ApJL*, 539, L13, doi: [10.1086/312840](https://doi.org/10.1086/312840)
- Geha, M., Blanton, M. R., Yan, R., & Tinker, J. L. 2012, *ApJ*, 757, 85, doi: [10.1088/0004-637X/757/1/85](https://doi.org/10.1088/0004-637X/757/1/85)
- Gezari, S. 2021, *arXiv e-prints*, arXiv:2104.14580, <https://arxiv.org/abs/2104.14580>
- Gezari, S., Dessart, L., Basa, S., et al. 2008a, *ApJL*, 683, L131, doi: [10.1086/591647](https://doi.org/10.1086/591647)
- Gezari, S., Basa, S., Martin, D. C., et al. 2008b, *ApJ*, 676, 944, doi: [10.1086/529008](https://doi.org/10.1086/529008)
- Gezari, S., Heckman, T., Cenko, S. B., et al. 2009, *ApJ*, 698, 1367, doi: [10.1088/0004-637X/698/2/1367](https://doi.org/10.1088/0004-637X/698/2/1367)
- Gezari, S., Chornock, R., Rest, A., et al. 2012, *Nature*, 485, 217, doi: [10.1038/nature10990](https://doi.org/10.1038/nature10990)
- Gezari, S., Martin, D. C., Forster, K., et al. 2013, *ApJ*, 766, 60, doi: [10.1088/0004-637X/766/1/60](https://doi.org/10.1088/0004-637X/766/1/60)
- Ghez, A. M., Salim, S., Weinberg, N. N., et al. 2008, *ApJ*, 689, 1044, doi: [10.1086/592738](https://doi.org/10.1086/592738)
- Gibson, N. P., Merritt, S., Nugroho, S. K., et al. 2020, *Monthly Notices of the Royal Astronomical Society*, 493, 2215–2228, doi: [10.1093/mnras/staa228](https://doi.org/10.1093/mnras/staa228)

- Goldstein, D. A., Andreoni, I., Nugent, P. E., et al. 2019, *ApJL*, 881, L7, doi: [10.3847/2041-8213/ab3046](https://doi.org/10.3847/2041-8213/ab3046)
- Gomez, S., Hosseinzadeh, G., Cowperthwaite, P. S., et al. 2019, *ApJL*, 884, L55, doi: [10.3847/2041-8213/ab4ad5](https://doi.org/10.3847/2041-8213/ab4ad5)
- Gong, Y., Liu, X., Cao, Y., et al. 2019, *ApJ*, 883, 203, doi: [10.3847/1538-4357/ab391e](https://doi.org/10.3847/1538-4357/ab391e)
- Gordon, K. D., Clayton, G. C., Misselt, K. A., Landolt, A. U., & Wolff, M. J. 2003, *ApJ*, 594, 279, doi: [10.1086/376774](https://doi.org/10.1086/376774)
- Götberg, Y., de Mink, S. E., & Groh, J. H. 2017, *A&A*, 608, A11, doi: [10.1051/0004-6361/201730472](https://doi.org/10.1051/0004-6361/201730472)
- Götberg, Y., de Mink, S. E., Groh, J. H., et al. 2018, *A&A*, 615, A78, doi: [10.1051/0004-6361/201732274](https://doi.org/10.1051/0004-6361/201732274)
- Götberg, Y., de Mink, S. E., Groh, J. H., Leitherer, C., & Norman, C. 2019, *A&A*, 629, A134, doi: [10.1051/0004-6361/201834525](https://doi.org/10.1051/0004-6361/201834525)
- Götberg, Y., de Mink, S. E., McQuinn, M., et al. 2020a, *A&A*, 634, A134, doi: [10.1051/0004-6361/201936669](https://doi.org/10.1051/0004-6361/201936669)
- Götberg, Y., Korol, V., Lamberts, A., et al. 2020b, *ApJ*, 904, 56, doi: [10.3847/1538-4357/abbd5](https://doi.org/10.3847/1538-4357/abbd5)
- Gottlieb, O., Lalakos, A., Bromberg, O., Liska, M., & Tchekhovskoy, A. 2021, arXiv e-prints, arXiv:2109.14619. <https://arxiv.org/abs/2109.14619>
- Gottlieb, O., Nakar, E., Piran, T., & Hotokezaka, K. 2018, *MNRAS*, 479, 588, doi: [10.1093/mnras/sty1462](https://doi.org/10.1093/mnras/sty1462)
- Graham, A. W., Trujillo, I., & Caon, N. 2001, *AJ*, 122, 1707, doi: [10.1086/323090](https://doi.org/10.1086/323090)
- Graham, M. J., Djorgovski, S. G., Drake, A. J., et al. 2014, *MNRAS*, 439, 703, doi: [10.1093/mnras/stt2499](https://doi.org/10.1093/mnras/stt2499)
- . 2017, *MNRAS*, 470, 4112, doi: [10.1093/mnras/stx1456](https://doi.org/10.1093/mnras/stx1456)
- Graham, M. J., Djorgovski, S. G., Stern, D., et al. 2015a, *Nature*, 518, 74, doi: [10.1038/nature14143](https://doi.org/10.1038/nature14143)
- . 2015b, *MNRAS*, 453, 1562, doi: [10.1093/mnras/stv1726](https://doi.org/10.1093/mnras/stv1726)
- Graham, M. J., Ford, K. E. S., McKernan, B., et al. 2020a, *PhRvL*, 124, 251102, doi: [10.1103/PhysRevLett.124.251102](https://doi.org/10.1103/PhysRevLett.124.251102)
- Graham, M. J., Ross, N. P., Stern, D., et al. 2020b, *MNRAS*, 491, 4925, doi: [10.1093/mnras/stz3244](https://doi.org/10.1093/mnras/stz3244)
- Green, G. M., Schlafly, E. F., Finkbeiner, D. P., et al. 2015, *ApJ*, 810, 25, doi: [10.1088/0004-637X/810/1/25](https://doi.org/10.1088/0004-637X/810/1/25)
- Greene, J. E., Strader, J., & Ho, L. C. 2020, *ARA&A*, 58, 257, doi: [10.1146/annurev-astro-032620-021835](https://doi.org/10.1146/annurev-astro-032620-021835)
- Gressel, O., Turner, N. J., Nelson, R. P., & McNally, C. P. 2015, *ApJ*, 801, 84, doi: [10.1088/0004-637X/801/2/84](https://doi.org/10.1088/0004-637X/801/2/84)
- Groenewegen, M. A. T., Lamers, H. J. G. L. M., & Pauldrach, A. W. A. 1989, *A&A*, 221, 78
- Groh, J. H. 2014, *A&A*, 572, L11, doi: [10.1051/0004-6361/201424852](https://doi.org/10.1051/0004-6361/201424852)
- Groh, J. H., Oliveira, A. S., & Steiner, J. E. 2008, *A&A*, 485, 245, doi: [10.1051/0004-6361:200809511](https://doi.org/10.1051/0004-6361:200809511)
- Gullbring, E., Hartmann, L., Briceño, C., & Calvet, N. 1998, *ApJ*, 492, 323, doi: [10.1086/305032](https://doi.org/10.1086/305032)
- Guo, H., Malkan, M. A., Gu, M., et al. 2016, *ApJ*, 826, 186, doi: [10.3847/0004-637X/826/2/186](https://doi.org/10.3847/0004-637X/826/2/186)
- Hagen, L. M. Z., Siegel, M. H., Hoversten, E. A., et al. 2017, *MNRAS*, 466, 4540, doi: [10.1093/mnras/stw2954](https://doi.org/10.1093/mnras/stw2954)
- Hameury, J. M. 2020, *Advances in Space Research*, 66, 1004, doi: [10.1016/j.asr.2019.10.022](https://doi.org/10.1016/j.asr.2019.10.022)
- Han, Z., Podsiadlowski, P., & Lynas-Gray, A. E. 2007, *MNRAS*, 380, 1098, doi: [10.1111/j.1365-2966.2007.12151.x](https://doi.org/10.1111/j.1365-2966.2007.12151.x)
- Han, Z., Podsiadlowski, P., Maxted, P. F. L., Marsh, T. R., & Ivanova, N. 2002, *MNRAS*, 336, 449, doi: [10.1046/j.1365-8711.2002.05752.x](https://doi.org/10.1046/j.1365-8711.2002.05752.x)
- Harris, J., & Zaritsky, D. 2004, *AJ*, 127, 1531, doi: [10.1086/381953](https://doi.org/10.1086/381953)
- . 2009, *AJ*, 138, 1243, doi: [10.1088/0004-6256/138/5/1243](https://doi.org/10.1088/0004-6256/138/5/1243)
- Hartmann, L., Herczeg, G., & Calvet, N. 2016, *ARA&A*, 54, 135, doi: [10.1146/annurev-astro-081915-023347](https://doi.org/10.1146/annurev-astro-081915-023347)
- He, C., Horst, S. M., Lewis, N. K., et al. 2020, *Haze Formation in Warm H2-rich Exoplanet Atmospheres*. <https://arxiv.org/abs/2008.09700>
- Helmi, A. 2008, *A&A Rv*, 15, 145, doi: [10.1007/s00159-008-0009-6](https://doi.org/10.1007/s00159-008-0009-6)
- Helmi, A., White, S. D. M., de Zeeuw, P. T., & Zhao, H. 1999, *Nature*, 402, 53, doi: [10.1038/46980](https://doi.org/10.1038/46980)
- Hensley, B. S., & Draine, B. T. 2021, *ApJ*, 906, 73, doi: [10.3847/1538-4357/abc8f1](https://doi.org/10.3847/1538-4357/abc8f1)
- Hillier, D. J. 2020, *Galaxies*, 8, 60, doi: [10.3390/galaxies8030060](https://doi.org/10.3390/galaxies8030060)
- Hillier, D. J., Lanz, T., Heap, S. R., et al. 2003, *ApJ*, 588, 1039, doi: [10.1086/374329](https://doi.org/10.1086/374329)
- Hjorth, J., & Bloom, J. S. 2012, *The Gamma-Ray Burst - Supernova Connection* (Cambridge University Press), 169–190
- Ho, A. Y. Q., Phinney, E. S., Ravi, V., et al. 2019a, *ApJ*, 871, 73, doi: [10.3847/1538-4357/aaf473](https://doi.org/10.3847/1538-4357/aaf473)
- Ho, A. Y. Q., Goldstein, D. A., Schulze, S., et al. 2019b, arXiv e-prints, arXiv:1904.11009. <https://arxiv.org/abs/1904.11009>
- . 2019c, *ApJ*, 887, 169, doi: [10.3847/1538-4357/ab55ec](https://doi.org/10.3847/1538-4357/ab55ec)
- Ho, A. Y. Q., Perley, D. A., Kulkarni, S. R., et al. 2020a, arXiv e-prints, arXiv:2003.01222. <https://arxiv.org/abs/2003.01222>
- Ho, A. Y. Q., Perley, D. A., Beniamini, P., et al. 2020b, *ApJ*, 905, 98, doi: [10.3847/1538-4357/abc34d](https://doi.org/10.3847/1538-4357/abc34d)
- Ho, A. Y. Q., Perley, D. A., Gal-Yam, A., et al. 2021a, arXiv e-prints, arXiv:2105.08811. <https://arxiv.org/abs/2105.08811>

- Ho, A. Y. Q., Margalit, B., Bremer, M., et al. 2021b, arXiv e-prints, arXiv:2110.05490.
<https://arxiv.org/abs/2110.05490>
- Ho, L. C. 2008, *ARA&A*, 46, 475,
 doi: [10.1146/annurev.astro.45.051806.110546](https://doi.org/10.1146/annurev.astro.45.051806.110546)
- Hosek, Matthew W., J., Lu, J. R., Lam, C. Y., et al. 2020, *AJ*, 160, 143, doi: [10.3847/1538-3881/aba533](https://doi.org/10.3847/1538-3881/aba533)
- Hosseinzadeh, G., Cowperthwaite, P. S., Gomez, S., et al. 2019, *ApJL*, 880, L4, doi: [10.3847/2041-8213/ab271c](https://doi.org/10.3847/2041-8213/ab271c)
- Hotokezaka, K., Beniamini, P., & Piran, T. 2018, *International Journal of Modern Physics D*, 27, 1842005, doi: [10.1142/S0218271818420051](https://doi.org/10.1142/S0218271818420051)
- Hotokezaka, K., & Nakar, E. 2020, *The Astrophysical Journal*, 891, 152
- Humphries, C. M., Jamar, C., Malaise, D., & Wroe, H. 1976, *A&A*, 49, 389
- Hung, T., Cenko, S. B., Roth, N., et al. 2019, *ApJ*, 879, 119, doi: [10.3847/1538-4357/ab24de](https://doi.org/10.3847/1538-4357/ab24de)
- Hung, T., Foley, R. J., Veilleux, S., et al. 2021, *ApJ*, 917, 9, doi: [10.3847/1538-4357/abf4c3](https://doi.org/10.3847/1538-4357/abf4c3)
- Hurley, J. R., Pols, O. R., & Tout, C. A. 2000, *MNRAS*, 315, 543, doi: [10.1046/j.1365-8711.2000.03426.x](https://doi.org/10.1046/j.1365-8711.2000.03426.x)
- Hurley, J. R., Tout, C. A., & Pols, O. R. 2002, *MNRAS*, 329, 897, doi: [10.1046/j.1365-8711.2002.05038.x](https://doi.org/10.1046/j.1365-8711.2002.05038.x)
- Hörst, S. M., He, C., Lewis, N. K., et al. 2018, *Nature Astronomy*, 2, 303–306, doi: [10.1038/s41550-018-0397-0](https://doi.org/10.1038/s41550-018-0397-0)
- IceCube Collaboration, Aartsen, M. G., Ackermann, M., et al. 2018, *Science*, 361, eaat1378, doi: [10.1126/science.aat1378](https://doi.org/10.1126/science.aat1378)
- Ilbert, O., McCracken, H. J., Le Fèvre, O., et al. 2013, *A&A*, 556, A55, doi: [10.1051/0004-6361/201321100](https://doi.org/10.1051/0004-6361/201321100)
- Ingleby, L., Calvet, N., Herczeg, G., et al. 2013, *ApJ*, 767, 112, doi: [10.1088/0004-637X/767/2/112](https://doi.org/10.1088/0004-637X/767/2/112)
- Ivezić, Ž., Kahn, S. M., Tyson, J. A., et al. 2019, *ApJ*, 873, 111, doi: [10.3847/1538-4357/ab042c](https://doi.org/10.3847/1538-4357/ab042c)
- Ivezić, Ž., Sesar, B., Jurić, M., et al. 2008, *ApJ*, 684, 287, doi: [10.1086/589678](https://doi.org/10.1086/589678)
- Iyer, A. R., Swain, M. R., Zellem, R. T., et al. 2016, *ApJ*, 823, 109, doi: [10.3847/0004-637X/823/2/109](https://doi.org/10.3847/0004-637X/823/2/109)
- Jacobson-Galán, W., Dessart, L., Jones, D., et al. 2021, arXiv e-prints, arXiv:2109.12136.
<https://arxiv.org/abs/2109.12136>
- Janka, H.-T. 2017, *Neutrino-Driven Explosions*, ed. A. W. Alsabti & P. Murdin (Springer), 1095, doi: [10.1007/978-3-319-21846-5_109](https://doi.org/10.1007/978-3-319-21846-5_109)
- Jiang, Y.-F., Guillochon, J., & Loeb, A. 2016, *ApJ*, 830, 125, doi: [10.3847/0004-637X/830/2/125](https://doi.org/10.3847/0004-637X/830/2/125)
- Jo, Y.-S., Seon, K.-I., Min, K.-W., et al. 2017, *ApJS*, 231, 21, doi: [10.3847/1538-4365/aa8091](https://doi.org/10.3847/1538-4365/aa8091)
- Jo, Y.-S., Seon, K.-I., Min, K.-W., et al. 2019, *ApJS*, 243, 9, doi: [10.3847/1538-4365/ab22ae](https://doi.org/10.3847/1538-4365/ab22ae)
- Johns-Krull, C. M. 2007, *ApJ*, 664, 975, doi: [10.1086/519017](https://doi.org/10.1086/519017)
- Johnson, B. D., Schiminovich, D., Seibert, M., et al. 2007a, *ApJS*, 173, 392, doi: [10.1086/522960](https://doi.org/10.1086/522960)
- . 2007b, *ApJS*, 173, 377, doi: [10.1086/522932](https://doi.org/10.1086/522932)
- Juvela, M., & Montillaud, J. 2016, *A&A*, 585, A38, doi: [10.1051/0004-6361/201425112](https://doi.org/10.1051/0004-6361/201425112)
- Karachentsev, I. D., & Kaisina, E. I. 2019, *Astrophysical Bulletin*, 74, 111, doi: [10.1134/S1990341319020019](https://doi.org/10.1134/S1990341319020019)
- Kasen, D. 2010, *ApJ*, 708, 1025, doi: [10.1088/0004-637X/708/2/1025](https://doi.org/10.1088/0004-637X/708/2/1025)
- Kasen, D., Fernández, R., & Metzger, B. D. 2015, *MNRAS*, 450, 1777, doi: [10.1093/mnras/stv721](https://doi.org/10.1093/mnras/stv721)
- Kasen, D., Metzger, B., Barnes, J., Quataert, E., & Ramirez-Ruiz, E. 2017, *Nature*, 551, 80, doi: [10.1038/nature24453](https://doi.org/10.1038/nature24453)
- Kasliwal, M. M., Nakar, E., Singer, L. P., et al. 2017, *Science*, 358, 1559, doi: [10.1126/science.aap9455](https://doi.org/10.1126/science.aap9455)
- Kasliwal, M. M., Anand, S., Ahumada, T., et al. 2020, *ApJ*, 905, 145, doi: [10.3847/1538-4357/abc335](https://doi.org/10.3847/1538-4357/abc335)
- Kawaguchi, K., Kyutoku, K., Shibata, M., & Tanaka, M. 2016, *ApJ*, 825, 52, doi: [10.3847/0004-637X/825/1/52](https://doi.org/10.3847/0004-637X/825/1/52)
- Kawaguchi, K., Shibata, M., & Tanaka, M. 2020, *ApJ*, 889, 171, doi: [10.3847/1538-4357/ab61ff](https://doi.org/10.3847/1538-4357/ab61ff)
- Kennicutt, Jr., R. C. 1998, *ApJ*, 498, 541, doi: [10.1086/305588](https://doi.org/10.1086/305588)
- Kesden, M. 2012, *PhRvD*, 85, 024037, doi: [10.1103/PhysRevD.85.024037](https://doi.org/10.1103/PhysRevD.85.024037)
- Kippenhahn, R., & Weigert, A. 1967, *ZA*, 65, 251
- Koenigl, A. 1991, *ApJL*, 370, L39, doi: [10.1086/185972](https://doi.org/10.1086/185972)
- Komossa, S., & Bade, N. 1999, *A&A*, 343, 775.
<https://arxiv.org/abs/astro-ph/9901141>
- Kormendy, J., & Richstone, D. 1995, *ARA&A*, 33, 581, doi: [10.1146/annurev.aa.33.090195.003053](https://doi.org/10.1146/annurev.aa.33.090195.003053)
- Kounkel, M., Covey, K., & Stassun, K. G. 2020, *AJ*, 160, 279, doi: [10.3847/1538-3881/abc0e6](https://doi.org/10.3847/1538-3881/abc0e6)
- Kozłowski, S., Onken, C. A., Kochanek, C. S., et al. 2013, *ApJ*, 775, 92, doi: [10.1088/0004-637X/775/2/92](https://doi.org/10.1088/0004-637X/775/2/92)
- Kraft, R. P. 1967, *ApJ*, 150, 551, doi: [10.1086/149359](https://doi.org/10.1086/149359)
- Krüger, C. J., & Foucart, F. 2020, *PhRvD*, 101, 103002, doi: [10.1103/PhysRevD.101.103002](https://doi.org/10.1103/PhysRevD.101.103002)
- Krumholz, M. R. 2013, *MNRAS*, 436, 2747, doi: [10.1093/mnras/stt1780](https://doi.org/10.1093/mnras/stt1780)
- . 2014, *PhR*, 539, 49, doi: [10.1016/j.physrep.2014.02.001](https://doi.org/10.1016/j.physrep.2014.02.001)
- Kuin, N. P. M., Wu, K., Oates, S., et al. 2019, *MNRAS*, 487, 2505, doi: [10.1093/mnras/stz053](https://doi.org/10.1093/mnras/stz053)
- Kulkarni, S. R. 2005, arXiv e-prints, astro.
<https://arxiv.org/abs/astro-ph/0510256>

- . 2021, arXiv e-prints, arXiv:2107.09585.
<https://arxiv.org/abs/2107.09585>
- Kulkarni, S. R., Frail, D. A., Wieringa, M. H., et al. 1998, *Nature*, 395, 663, doi: [10.1038/27139](https://doi.org/10.1038/27139)
- Lada, C. J., & Lada, E. A. 2003, *ARA&A*, 41, 57, doi: [10.1146/annurev.astro.41.011802.094844](https://doi.org/10.1146/annurev.astro.41.011802.094844)
- LaMassa, S. M., Cales, S., Moran, E. C., et al. 2015, *ApJ*, 800, 144, doi: [10.1088/0004-637X/800/2/144](https://doi.org/10.1088/0004-637X/800/2/144)
- Latimer, C. J., Reines, A. E., Plotkin, R. M., Russell, T. D., & Condon, J. J. 2019, *ApJ*, 884, 78, doi: [10.3847/1538-4357/ab3289](https://doi.org/10.3847/1538-4357/ab3289)
- Lawrence, A., Bruce, A. G., MacLeod, C., et al. 2016, *MNRAS*, 463, 296, doi: [10.1093/mnras/stw1963](https://doi.org/10.1093/mnras/stw1963)
- Lazzati, D., Morsony, B. J., Blackwell, C. H., & Begelman, M. C. 2012, *ApJ*, 750, 68, doi: [10.1088/0004-637X/750/1/68](https://doi.org/10.1088/0004-637X/750/1/68)
- Lee, J. C., Gil de Paz, A., Tremonti, C., et al. 2009a, *ApJ*, 706, 599, doi: [10.1088/0004-637X/706/1/599](https://doi.org/10.1088/0004-637X/706/1/599)
- . 2009b, *ApJ*, 706, 599, doi: [10.1088/0004-637X/706/1/599](https://doi.org/10.1088/0004-637X/706/1/599)
- Lemonias, J. J., Schiminovich, D., Thilker, D., et al. 2011, *ApJ*, 733, 74, doi: [10.1088/0004-637X/733/2/74](https://doi.org/10.1088/0004-637X/733/2/74)
- Leung, S.-C., & Fuller, J. 2020, *ApJ*, 900, 99, doi: [10.3847/1538-4357/abac5d](https://doi.org/10.3847/1538-4357/abac5d)
- Li, A. 2020, *Nature Astronomy*, 4, 339, doi: [10.1038/s41550-020-1051-1](https://doi.org/10.1038/s41550-020-1051-1)
- Li, A., Misselt, K. A., & Wang, Y. J. 2006, *ApJL*, 640, L151, doi: [10.1086/503798](https://doi.org/10.1086/503798)
- Li, K.-L., Hamsch, F.-J., Munari, U., et al. 2020, *ApJ*, 905, 114, doi: [10.3847/1538-4357/abc3be](https://doi.org/10.3847/1538-4357/abc3be)
- Li, K.-L., Metzger, B. D., Chomiuk, L., et al. 2017, *Nature Astronomy*, 1, 697, doi: [10.1038/s41550-017-0222-1](https://doi.org/10.1038/s41550-017-0222-1)
- Li, L.-X., & Paczyński, B. 1998, *ApJL*, 507, L59, doi: [10.1086/311680](https://doi.org/10.1086/311680)
- Li, L.-X., & Paczyński, B. 1998, *The Astrophysical Journal Letters*, 507, L59
- Li, W., Chornock, R., Leaman, J., et al. 2011, *MNRAS*, 412, 1473, doi: [10.1111/j.1365-2966.2011.18162.x](https://doi.org/10.1111/j.1365-2966.2011.18162.x)
- Liang, E., Zhang, B., Virgili, F., & Dai, Z. G. 2007, *ApJ*, 662, 1111, doi: [10.1086/517959](https://doi.org/10.1086/517959)
- Liu, Y. 2021, in 43rd COSPAR Scientific Assembly. Held 28 January - 4 February, Vol. 43, 1642
- Liu, Z.-W., Moriya, T. J., & Stancliffe, R. J. 2015, *MNRAS*, 454, 1192, doi: [10.1093/mnras/stv2076](https://doi.org/10.1093/mnras/stv2076)
- Long, M., Romanova, M. M., & Lovelace, R. V. E. 2005, *ApJ*, 634, 1214, doi: [10.1086/497000](https://doi.org/10.1086/497000)
- Lothringer, J. D., Fu, G., Sing, D. K., & Barman, T. S. 2020, *ApJL*, 898, L14, doi: [10.3847/2041-8213/aba265](https://doi.org/10.3847/2041-8213/aba265)
- Lu, W., & Bonnerot, C. 2020, *MNRAS*, 492, 686, doi: [10.1093/mnras/stz3405](https://doi.org/10.1093/mnras/stz3405)
- Lu, W., & Kumar, P. 2018, *ApJ*, 865, 128, doi: [10.3847/1538-4357/aad54a](https://doi.org/10.3847/1538-4357/aad54a)
- Lundquist, M. J., Paterson, K., Fong, W., et al. 2019, *The Astrophysical Journal*, 881, L26, doi: [10.3847/2041-8213/ab32f2](https://doi.org/10.3847/2041-8213/ab32f2)
- MacLeod, C. L., Brooks, K., Ivezić, Ž., et al. 2011, *ApJ*, 728, 26, doi: [10.1088/0004-637X/728/1/26](https://doi.org/10.1088/0004-637X/728/1/26)
- Madau, P., & Dickinson, M. 2014, *ARA&A*, 52, 415, doi: [10.1146/annurev-astro-081811-125615](https://doi.org/10.1146/annurev-astro-081811-125615)
- Madhusudhan, N., & Redfield, S. 2015, *International Journal of Astrobiology*, 14, 177, doi: [10.1017/S1473550414000421](https://doi.org/10.1017/S1473550414000421)
- Magorrian, J., Tremaine, S., Richstone, D., et al. 1998, *AJ*, 115, 2285, doi: [10.1086/300353](https://doi.org/10.1086/300353)
- Majewski, S. R., Schiavon, R. P., Frinchaboy, P. M., et al. 2017, *AJ*, 154, 94, doi: [10.3847/1538-3881/aa784d](https://doi.org/10.3847/1538-3881/aa784d)
- Manara, C. F., Robberto, M., Da Rio, N., et al. 2012, *ApJ*, 755, 154, doi: [10.1088/0004-637X/755/2/154](https://doi.org/10.1088/0004-637X/755/2/154)
- Maoz, D., Mannucci, F., & Nelemans, G. 2014, *ARA&A*, 52, 107, doi: [10.1146/annurev-astro-082812-141031](https://doi.org/10.1146/annurev-astro-082812-141031)
- Marconi, A., & Hunt, L. K. 2003, *ApJL*, 589, L21, doi: [10.1086/375804](https://doi.org/10.1086/375804)
- Marconi, A., Risaliti, G., Gilli, R., et al. 2004, *MNRAS*, 351, 169, doi: [10.1111/j.1365-2966.2004.07765.x](https://doi.org/10.1111/j.1365-2966.2004.07765.x)
- Margutti, R., & Chornock, R. 2020, arXiv e-prints, arXiv:2012.04810. <https://arxiv.org/abs/2012.04810>
- Margutti, R., Milisavljevic, D., Soderberg, A. M., et al. 2014, *ApJ*, 780, 21, doi: [10.1088/0004-637X/780/1/21](https://doi.org/10.1088/0004-637X/780/1/21)
- Margutti, R., Kamble, A., Milisavljevic, D., et al. 2017, *ApJ*, 835, 140, doi: [10.3847/1538-4357/835/2/140](https://doi.org/10.3847/1538-4357/835/2/140)
- Margutti, R., Metzger, B. D., Chornock, R., et al. 2019, *ApJ*, 872, 18, doi: [10.3847/1538-4357/aafa01](https://doi.org/10.3847/1538-4357/aafa01)
- Marion, G. H., Vinko, J., Kirshner, R. P., et al. 2014, *ApJ*, 781, 69, doi: [10.1088/0004-637X/781/2/69](https://doi.org/10.1088/0004-637X/781/2/69)
- Marshall, D. J., Robin, A. C., Reylé, C., Schultheis, M., & Picaud, S. 2006, *A&A*, 453, 635, doi: [10.1051/0004-6361:20053842](https://doi.org/10.1051/0004-6361:20053842)
- Martin, C., Hurwitz, M., & Bowyer, S. 1990, *ApJ*, 354, 220, doi: [10.1086/168681](https://doi.org/10.1086/168681)
- Martin, D. C., Gonçalves, T. S., Darvish, B., Seibert, M., & Schiminovich, D. 2017, *ApJ*, 842, 20, doi: [10.3847/1538-4357/aa71a9](https://doi.org/10.3847/1538-4357/aa71a9)
- Martin, D. C., Wyder, T. K., Schiminovich, D., et al. 2007a, *ApJS*, 173, 342, doi: [10.1086/516639](https://doi.org/10.1086/516639)
- Martin, D. C., Small, T., Schiminovich, D., et al. 2007b, *ApJS*, 173, 415, doi: [10.1086/522088](https://doi.org/10.1086/522088)
- Massa, D., Fitzpatrick, E. L., & Gordon, K. D. 2020, *ApJ*, 891, 67, doi: [10.3847/1538-4357/ab6f01](https://doi.org/10.3847/1538-4357/ab6f01)
- Massey, P., & Hunter, D. A. 1998, *ApJ*, 493, 180, doi: [10.1086/305126](https://doi.org/10.1086/305126)

- Massey, P., Neugent, K. F., & Morrell, N. 2015, *ApJ*, 807, 81, doi: [10.1088/0004-637X/807/1/81](https://doi.org/10.1088/0004-637X/807/1/81)
- . 2017, *ApJ*, 837, 122, doi: [10.3847/1538-4357/aa5d17](https://doi.org/10.3847/1538-4357/aa5d17)
- Massey, P., Neugent, K. F., Morrell, N., & Hillier, D. J. 2014, *ApJ*, 788, 83, doi: [10.1088/0004-637X/788/1/83](https://doi.org/10.1088/0004-637X/788/1/83)
- Masuda, K., & Hotokezaka, K. 2019, *ApJ*, 883, 169, doi: [10.3847/1538-4357/ab3a4f](https://doi.org/10.3847/1538-4357/ab3a4f)
- Matthews, T. A., & Sandage, A. R. 1963, *ApJ*, 138, 30, doi: [10.1086/147615](https://doi.org/10.1086/147615)
- McConnachie, A. W. 2012, *AJ*, 144, 4, doi: [10.1088/0004-6256/144/1/4](https://doi.org/10.1088/0004-6256/144/1/4)
- McKernan, B., Ford, K. E. S., Cantiello, M., et al. 2021, arXiv e-prints, arXiv:2110.03741. <https://arxiv.org/abs/2110.03741>
- McKernan, B., Ford, K. E. S., O'Shaughnessy, R., & Wysocki, D. 2020, *MNRAS*, 494, 1203, doi: [10.1093/mnras/staa740](https://doi.org/10.1093/mnras/staa740)
- McKernan, B., Ford, K. E. S., Bartos, I., et al. 2019, *ApJL*, 884, L50, doi: [10.3847/2041-8213/ab4886](https://doi.org/10.3847/2041-8213/ab4886)
- Medina, A. A., Winters, J. G., Irwin, J. M., & Charbonneau, D. 2020, *ApJ*, 905, 107, doi: [10.3847/1538-4357/abc686](https://doi.org/10.3847/1538-4357/abc686)
- Meixner, M., Gordon, K. D., Indebetouw, R., et al. 2006, *AJ*, 132, 2268, doi: [10.1086/508185](https://doi.org/10.1086/508185)
- Meixner, M., Panuzzo, P., Roman-Duval, J., et al. 2013, *AJ*, 146, 62, doi: [10.1088/0004-6256/146/3/62](https://doi.org/10.1088/0004-6256/146/3/62)
- Merloni, A., & Heinz, S. 2008, *MNRAS*, 388, 1011, doi: [10.1111/j.1365-2966.2008.13472.x](https://doi.org/10.1111/j.1365-2966.2008.13472.x)
- Merritt, J., Night, C., & Sion, E. M. 2007, *PASP*, 119, 251, doi: [10.1086/513611](https://doi.org/10.1086/513611)
- Metzger, B. D., Bauswein, A., Goriely, S., & Kasen, D. 2015, *MNRAS*, 446, 1115, doi: [10.1093/mnras/stu2225](https://doi.org/10.1093/mnras/stu2225)
- Metzger, B. D., & Stone, N. C. 2016, *MNRAS*, 461, 948, doi: [10.1093/mnras/stw1394](https://doi.org/10.1093/mnras/stw1394)
- Metzger, B. D., Martínez-Pinedo, G., Darbha, S., et al. 2010, *MNRAS*, 406, 2650, doi: [10.1111/j.1365-2966.2010.16864.x](https://doi.org/10.1111/j.1365-2966.2010.16864.x)
- Meurer, G. R., Wong, O. I., Kim, J. H., et al. 2009a, in American Astronomical Society Meeting Abstracts, Vol. 213, American Astronomical Society Meeting Abstracts #213, 443.06
- Meurer, G. R., Wong, O. I., Kim, J. H., et al. 2009b, *ApJ*, 695, 765, doi: [10.1088/0004-637X/695/1/765](https://doi.org/10.1088/0004-637X/695/1/765)
- Milisavljevic, D., Margutti, R., Kamble, A., et al. 2015, *ApJ*, 815, 120, doi: [10.1088/0004-637X/815/2/120](https://doi.org/10.1088/0004-637X/815/2/120)
- Mishra, A., & Li, A. 2015, *ApJ*, 809, 120, doi: [10.1088/0004-637X/809/2/120](https://doi.org/10.1088/0004-637X/809/2/120)
- Moe, M., & Di Stefano, R. 2013, *ApJ*, 778, 95, doi: [10.1088/0004-637X/778/2/95](https://doi.org/10.1088/0004-637X/778/2/95)
- . 2015, *ApJ*, 810, 61, doi: [10.1088/0004-637X/810/1/61](https://doi.org/10.1088/0004-637X/810/1/61)
- Montalto, M., Piotto, G., Marrese, P. M., et al. 2021, arXiv e-prints, arXiv:2108.13712. <https://arxiv.org/abs/2108.13712>
- Morley, C. V., Fortney, J. J., Marley, M. S., et al. 2015, *ApJ*, 815, 110, doi: [10.1088/0004-637X/815/2/110](https://doi.org/10.1088/0004-637X/815/2/110)
- Morozova, V., Piro, A. L., Fuller, J., & Van Dyk, S. D. 2020, *ApJL*, 891, L32, doi: [10.3847/2041-8213/ab77c8](https://doi.org/10.3847/2041-8213/ab77c8)
- Morrissey, P., Conrow, T., Barlow, T. A., et al. 2007, *ApJS*, 173, 682, doi: [10.1086/520512](https://doi.org/10.1086/520512)
- Moster, B. P., Naab, T., & White, S. D. M. 2013, *MNRAS*, 428, 3121, doi: [10.1093/mnras/sts261](https://doi.org/10.1093/mnras/sts261)
- Mróz, P., Udalski, A., Poleski, R., et al. 2016, *ApJS*, 222, 9, doi: [10.3847/0067-0049/222/1/9](https://doi.org/10.3847/0067-0049/222/1/9)
- Muñoz-Darias, T., Casares, J., Mata Sánchez, D., et al. 2016, *Nature*, 534, 75, doi: [10.1038/nature17446](https://doi.org/10.1038/nature17446)
- Nakar, E. 2015, *ApJ*, 807, 172, doi: [10.1088/0004-637X/807/2/172](https://doi.org/10.1088/0004-637X/807/2/172)
- Nedora, V., Schianchi, F., Bernuzzi, S., et al. 2020, arXiv e-prints, arXiv:2011.11110. <https://arxiv.org/abs/2011.11110>
- Nelemans, G., Yungelson, L. R., & Portegies Zwart, S. F. 2004, *MNRAS*, 349, 181, doi: [10.1111/j.1365-2966.2004.07479.x](https://doi.org/10.1111/j.1365-2966.2004.07479.x)
- Nelson, T., Mukai, K., Li, K.-L., et al. 2019, *ApJ*, 872, 86, doi: [10.3847/1538-4357/aafb6d](https://doi.org/10.3847/1538-4357/aafb6d)
- Nidever, D. L., Olsen, K., Walker, A. R., et al. 2017, *AJ*, 154, 199, doi: [10.3847/1538-3881/aa8d1c](https://doi.org/10.3847/1538-3881/aa8d1c)
- Noeske, K. G., Weiner, B. J., Faber, S. M., et al. 2007, *ApJL*, 660, L43, doi: [10.1086/517926](https://doi.org/10.1086/517926)
- Nuza, S. E., Kitaura, F.-S., Heß, S., Libeskind, N. I., & Müller, V. 2014, *MNRAS*, 445, 988, doi: [10.1093/mnras/stu1746](https://doi.org/10.1093/mnras/stu1746)
- Oates, S. R., Marshall, F. E., Breeveld, A. A., et al. 2021, *MNRAS*, 507, 1296, doi: [10.1093/mnras/stab2189](https://doi.org/10.1093/mnras/stab2189)
- O'Connell, R. W. 1987, *AJ*, 94, 876, doi: [10.1086/114522](https://doi.org/10.1086/114522)
- Ofek, E. O., Rabinak, I., Neill, J. D., et al. 2010, *ApJ*, 724, 1396, doi: [10.1088/0004-637X/724/2/1396](https://doi.org/10.1088/0004-637X/724/2/1396)
- Ofek, E. O., Sullivan, M., Shaviv, N. J., et al. 2014, *ApJ*, 789, 104, doi: [10.1088/0004-637X/789/2/104](https://doi.org/10.1088/0004-637X/789/2/104)
- Okumura, S.-i., Mori, A., Nishihara, E., Watanabe, E., & Yamashita, T. 2000, *ApJ*, 543, 799, doi: [10.1086/317116](https://doi.org/10.1086/317116)
- Pancoast, A., Brewer, B. J., Treu, T., et al. 2014, *MNRAS*, 445, 3073, doi: [10.1093/mnras/stu1419](https://doi.org/10.1093/mnras/stu1419)
- Panda, S., Martínez-Aldama, M. L., & Zajaček, M. 2019, *Frontiers in Astronomy and Space Sciences*, 6, 75, doi: [10.3389/fspas.2019.00075](https://doi.org/10.3389/fspas.2019.00075)
- Parsons, S. G., Rebassa-Mansergas, A., Schreiber, M. R., et al. 2016, *MNRAS*, 463, 2125, doi: [10.1093/mnras/stw2143](https://doi.org/10.1093/mnras/stw2143)

- Parsons, S. G., Schreiber, M. R., Gänsicke, B. T., et al. 2015, *MNRAS*, 452, 1754, doi: [10.1093/mnras/stv1395](https://doi.org/10.1093/mnras/stv1395)
- Pastorello, A., Cappellaro, E., Inzerra, C., et al. 2013, *ApJ*, 767, 1, doi: [10.1088/0004-637X/767/1/1](https://doi.org/10.1088/0004-637X/767/1/1)
- Paxton, B., Marchant, P., Schwab, J., et al. 2015, *ApJS*, 220, 15, doi: [10.1088/0067-0049/220/1/15](https://doi.org/10.1088/0067-0049/220/1/15)
- Peek, J. E. G., & Schiminovich, D. 2013, *ApJ*, 771, 68, doi: [10.1088/0004-637X/771/1/68](https://doi.org/10.1088/0004-637X/771/1/68)
- Perley, D. A., Mazzali, P. A., Yan, L., et al. 2019, *MNRAS*, 484, 1031, doi: [10.1093/mnras/sty3420](https://doi.org/10.1093/mnras/sty3420)
- Perley, D. A., Ho, A. Y. Q., Yao, Y., et al. 2021a, arXiv e-prints, arXiv:2103.01968. <https://arxiv.org/abs/2103.01968>
- Perley, D. A., Sollerman, J., Schulze, S., et al. 2021b, arXiv e-prints, arXiv:2111.12110. <https://arxiv.org/abs/2111.12110>
- Petrov, P., Singer, L. P., Coughlin, M. W., et al. 2021, arXiv e-prints, arXiv:2108.07277. <https://arxiv.org/abs/2108.07277>
- Petrucci, P.-O., Ferreira, J., Henri, G., & Pelletier, G. 2008, *MNRAS*, 385, L88, doi: [10.1111/j.1745-3933.2008.00439.x](https://doi.org/10.1111/j.1745-3933.2008.00439.x)
- Pian, E., D'Avanzo, P., Benetti, S., et al. 2017, *Nature*, 551, 67, doi: [10.1038/nature24298](https://doi.org/10.1038/nature24298)
- Pichara, K., Protopapas, P., Kim, D. W., Marquette, J. B., & Tisserand, P. 2012, *MNRAS*, 427, 1284, doi: [10.1111/j.1365-2966.2012.22061.x](https://doi.org/10.1111/j.1365-2966.2012.22061.x)
- Piran, T. 2004, *Reviews of Modern Physics*, 76, 1143, doi: [10.1103/RevModPhys.76.1143](https://doi.org/10.1103/RevModPhys.76.1143)
- Piran, T., Svirski, G., Krolik, J., Cheng, R. M., & Shiokawa, H. 2015, *ApJ*, 806, 164, doi: [10.1088/0004-637X/806/2/164](https://doi.org/10.1088/0004-637X/806/2/164)
- Piro, A. L., & Kollmeier, J. A. 2018, *The Astrophysical Journal*, 855, 103
- Planck Collaboration, Abergel, A., Ade, P. A. R., et al. 2014, *A&A*, 571, A11, doi: [10.1051/0004-6361/201323195](https://doi.org/10.1051/0004-6361/201323195)
- Ponti, G., Fender, R. P., Begelman, M. C., et al. 2012, *MNRAS*, 422, L11, doi: [10.1111/j.1745-3933.2012.01224.x](https://doi.org/10.1111/j.1745-3933.2012.01224.x)
- Portegies Zwart, S. F., McMillan, S. L. W., & Gieles, M. 2010, *ARA&A*, 48, 431, doi: [10.1146/annurev-astro-081309-130834](https://doi.org/10.1146/annurev-astro-081309-130834)
- Pouliasis, E., Georgantopoulos, I., Bonanos, A. Z., et al. 2019, *MNRAS*, 487, 4285, doi: [10.1093/mnras/stz1483](https://doi.org/10.1093/mnras/stz1483)
- Povich, M. S., Smith, N., Majewski, S. R., et al. 2011, *ApJS*, 194, 14, doi: [10.1088/0067-0049/194/1/14](https://doi.org/10.1088/0067-0049/194/1/14)
- Prentice, S. J., Maguire, K., Smartt, S. J., et al. 2018, *ApJ*, 865, L3, doi: [10.3847/2041-8213/aadd90](https://doi.org/10.3847/2041-8213/aadd90)
- Prinja, R. K., Barlow, M. J., & Howarth, I. D. 1990, *ApJ*, 361, 607, doi: [10.1086/169224](https://doi.org/10.1086/169224)
- Proga, D., & Kallman, T. R. 2002, *ApJ*, 565, 455, doi: [10.1086/324534](https://doi.org/10.1086/324534)
- Pun, C. S. J., Kirshner, R. P., Sonneborn, G., et al. 1995, *ApJS*, 99, 223, doi: [10.1086/192185](https://doi.org/10.1086/192185)
- Pursiainen, M., Childress, M., Smith, M., et al. 2018, *MNRAS*, 481, 894, doi: [10.1093/mnras/sty2309](https://doi.org/10.1093/mnras/sty2309)
- Quataert, E., Fernández, R., Kasen, D., Klion, H., & Paxton, B. 2016, *MNRAS*, 458, 1214, doi: [10.1093/mnras/stw365](https://doi.org/10.1093/mnras/stw365)
- Quataert, E., & Shiode, J. 2012, *MNRAS*, 423, L92, doi: [10.1111/j.1745-3933.2012.01264.x](https://doi.org/10.1111/j.1745-3933.2012.01264.x)
- Quimby, R. M., Yuan, F., Akerlof, C., & Wheeler, J. C. 2013, *MNRAS*, 431, 912, doi: [10.1093/mnras/stt213](https://doi.org/10.1093/mnras/stt213)
- Ramírez-Agudelo, O. H., Simón-Díaz, S., Sana, H., et al. 2013, *A&A*, 560, A29, doi: [10.1051/0004-6361/201321986](https://doi.org/10.1051/0004-6361/201321986)
- Ramírez-Agudelo, O. H., Sana, H., de Mink, S. E., et al. 2015, *A&A*, 580, A92, doi: [10.1051/0004-6361/201425424](https://doi.org/10.1051/0004-6361/201425424)
- Reines, A. E., & Comastri, A. 2016, *PASA*, 33, e054, doi: [10.1017/pasa.2016.46](https://doi.org/10.1017/pasa.2016.46)
- Reines, A. E., Greene, J. E., & Geha, M. 2013, *ApJ*, 775, 116, doi: [10.1088/0004-637X/775/2/116](https://doi.org/10.1088/0004-637X/775/2/116)
- Reines, A. E., & Volonteri, M. 2015, *ApJ*, 813, 82, doi: [10.1088/0004-637X/813/2/82](https://doi.org/10.1088/0004-637X/813/2/82)
- Reusch, S., Stein, R., Kowalski, M., et al. 2021, arXiv e-prints, arXiv:2111.09390. <https://arxiv.org/abs/2111.09390>
- Ricci, C., Loewenstein, M., Kara, E., et al. 2021, *ApJS*, 255, 7, doi: [10.3847/1538-4365/abe94b](https://doi.org/10.3847/1538-4365/abe94b)
- Ricker, G. R., Winn, J. N., Vanderspek, R., et al. 2015, *Journal of Astronomical Telescopes, Instruments, and Systems*, 1, 014003, doi: [10.1117/1.JATIS.1.1.014003](https://doi.org/10.1117/1.JATIS.1.1.014003)
- Riess, A. G., Filippenko, A. V., Challis, P., et al. 1998, *AJ*, 116, 1009, doi: [10.1086/300499](https://doi.org/10.1086/300499)
- Robertson, B. E., Ellis, R. S., Furlanetto, S. R., & Dunlop, J. S. 2015a, *ApJL*, 802, L19, doi: [10.1088/2041-8205/802/2/L19](https://doi.org/10.1088/2041-8205/802/2/L19)
- . 2015b, *ApJL*, 802, L19, doi: [10.1088/2041-8205/802/2/L19](https://doi.org/10.1088/2041-8205/802/2/L19)
- Rogerson, J. B., Spitzer, L., Drake, J. F., et al. 1973, *ApJL*, 181, L97, doi: [10.1086/181194](https://doi.org/10.1086/181194)
- Roman-Duval, J., Proffitt, C., Monroe, T., Carlberg, J., & Taylor, J. 2020. https://www.stsci.edu/files/live/sites/www/files/home/hst/about/space-telescope-users-committee/presentations-and-documentation/_documents/2020_apr_ullyses.pdf
- Romanova, M. M., Blinova, A. A., Ustyugova, G. V., Koldoba, A. V., & Lovelace, R. V. E. 2018, *NewA*, 62, 94, doi: [10.1016/j.newast.2018.01.011](https://doi.org/10.1016/j.newast.2018.01.011)
- Roming, P. W. A., Kennedy, T. E., Mason, K. O., et al. 2005, *SSRv*, 120, 95, doi: [10.1007/s11214-005-5095-4](https://doi.org/10.1007/s11214-005-5095-4)

- Rosen, A. L., & Krumholz, M. R. 2020, *AJ*, 160, 78, doi: [10.3847/1538-3881/ab9abf](https://doi.org/10.3847/1538-3881/ab9abf)
- Ross, N. P., Ford, K. E. S., Graham, M., et al. 2018, *MNRAS*, 480, 4468, doi: [10.1093/mnras/sty2002](https://doi.org/10.1093/mnras/sty2002)
- Roth, N., Kasen, D., Guillochon, J., & Ramirez-Ruiz, E. 2016, *ApJ*, 827, 3, doi: [10.3847/0004-637X/827/1/3](https://doi.org/10.3847/0004-637X/827/1/3)
- Sabbi, E., Anderson, J., Lennon, D. J., et al. 2013, *AJ*, 146, 53, doi: [10.1088/0004-6256/146/3/53](https://doi.org/10.1088/0004-6256/146/3/53)
- Sagiv, I., Gal-Yam, A., Ofek, E. O., et al. 2014, *AJ*, 147, 79, doi: [10.1088/0004-6256/147/4/79](https://doi.org/10.1088/0004-6256/147/4/79)
- Sahnow, D. J., Moos, H. W., Ake, T. B., et al. 2000, *ApJL*, 538, L7, doi: [10.1086/312794](https://doi.org/10.1086/312794)
- Salim, S., & Narayanan, D. 2020, *ARA&A*, 58, 529, doi: [10.1146/annurev-astro-032620-021933](https://doi.org/10.1146/annurev-astro-032620-021933)
- Salim, S., Rich, R. M., Charlot, S., et al. 2007, *ApJS*, 173, 267, doi: [10.1086/519218](https://doi.org/10.1086/519218)
- Sana, H., & Shenar, T. 2019. <https://www.eso.org/sci/meetings/2020/4MOST2/MultiplicityMCs4most.pdf>
- Sana, H., de Mink, S. E., de Koter, A., et al. 2012a, *Science*, 337, 444, doi: [10.1126/science.1223344](https://doi.org/10.1126/science.1223344)
- . 2012b, *Science*, 337, 444, doi: [10.1126/science.1223344](https://doi.org/10.1126/science.1223344)
- Sanders, D. B., Phinney, E. S., Neugebauer, G., Soifer, B. T., & Matthews, K. 1989, *ApJ*, 347, 29, doi: [10.1086/168094](https://doi.org/10.1086/168094)
- Saxton, R., Komossa, S., Auchettl, K., & Jonker, P. G. 2020, *SSRv*, 216, 85, doi: [10.1007/s11214-020-00708-4](https://doi.org/10.1007/s11214-020-00708-4)
- Sazonov, S., Gilfanov, M., Medvedev, P., et al. 2021, *MNRAS*, 508, 3820, doi: [10.1093/mnras/stab2843](https://doi.org/10.1093/mnras/stab2843)
- Schiminovich, D., Wyder, T. K., Martin, D. C., et al. 2007, *ApJS*, 173, 315, doi: [10.1086/524659](https://doi.org/10.1086/524659)
- Schlegel, D. J., Finkbeiner, D. P., & Davis, M. 1998, *ApJ*, 500, 525, doi: [10.1086/305772](https://doi.org/10.1086/305772)
- Schmidt, M. 1963, *Nature*, 197, 1040, doi: [10.1038/1971040a0](https://doi.org/10.1038/1971040a0)
- Schootemeijer, A., Götzberg, Y., de Mink, S. E., Gies, D., & Zapartas, E. 2018, *A&A*, 615, A30, doi: [10.1051/0004-6361/201731194](https://doi.org/10.1051/0004-6361/201731194)
- Secunda, A., Cen, R., Kimm, T., Götzberg, Y., & de Mink, S. E. 2020, *ApJ*, 901, 72, doi: [10.3847/1538-4357/abaefa](https://doi.org/10.3847/1538-4357/abaefa)
- Seibert, M., Martin, D. C., Heckman, T. M., et al. 2005, *ApJL*, 619, L55, doi: [10.1086/427843](https://doi.org/10.1086/427843)
- Senchyna, P., & Stark, D. P. 2019, *MNRAS*, 484, 1270, doi: [10.1093/mnras/stz058](https://doi.org/10.1093/mnras/stz058)
- Seon, K.-I., Edelstein, J., Korpela, E., et al. 2011, *ApJS*, 196, 15, doi: [10.1088/0067-0049/196/2/15](https://doi.org/10.1088/0067-0049/196/2/15)
- Shankar, F., Weinberg, D. H., & Miralda-Escudé, J. 2009, *ApJ*, 690, 20, doi: [10.1088/0004-637X/690/1/20](https://doi.org/10.1088/0004-637X/690/1/20)
- Shara, M. M., Crawford, S. M., Vanbeveren, D., et al. 2017, *MNRAS*, 464, 2066, doi: [10.1093/mnras/stw2450](https://doi.org/10.1093/mnras/stw2450)
- . 2020, *MNRAS*, 492, 4430, doi: [10.1093/mnras/staa038](https://doi.org/10.1093/mnras/staa038)
- Shore, S. N. 2012, *Bulletin of the Astronomical Society of India*, 40, 185. <https://arxiv.org/abs/1211.3176>
- Shore, S. N., De Gennaro Aquino, I., Schwarz, G. J., et al. 2013, *A&A*, 553, A123, doi: [10.1051/0004-6361/201321095](https://doi.org/10.1051/0004-6361/201321095)
- Shu, F., Najita, J., Ostriker, E., et al. 1994, *ApJ*, 429, 781, doi: [10.1086/174363](https://doi.org/10.1086/174363)
- Shustov, B., Gómez de Castro, A. I., Sachkov, M., et al. 2018, *Ap&SS*, 363, 62, doi: [10.1007/s10509-018-3280-7](https://doi.org/10.1007/s10509-018-3280-7)
- Simons, R., Thilker, D., Bianchi, L., & Wyder, T. 2014, *Advances in Space Research*, 53, 939, doi: [10.1016/j.asr.2013.07.016](https://doi.org/10.1016/j.asr.2013.07.016)
- Sing, D. K., Lecavelier des Etangs, A., Fortney, J. J., et al. 2013, *MNRAS*, 436, 2956, doi: [10.1093/mnras/stt1782](https://doi.org/10.1093/mnras/stt1782)
- Sing, D. K., Fortney, J. J., Nikolov, N., et al. 2016, *Nature*, 529, 59, doi: [10.1038/nature16068](https://doi.org/10.1038/nature16068)
- Sion, E. M., Cheng, F. H., Gänsicke, B. T., & Szkody, P. 2004, *ApJL*, 614, L61, doi: [10.1086/425497](https://doi.org/10.1086/425497)
- Smartt, S. J., Chen, T. W., Jerkstrand, A., et al. 2017, *Nature*, 551, 75, doi: [10.1038/nature24303](https://doi.org/10.1038/nature24303)
- Smith, N. 2006, *ApJ*, 644, 1151, doi: [10.1086/503766](https://doi.org/10.1086/503766)
- . 2014a, *ARA&A*, 52, 487, doi: [10.1146/annurev-astro-081913-040025](https://doi.org/10.1146/annurev-astro-081913-040025)
- . 2014b, *ARA&A*, 52, 487, doi: [10.1146/annurev-astro-081913-040025](https://doi.org/10.1146/annurev-astro-081913-040025)
- Smith, N., Götzberg, Y., & de Mink, S. E. 2018, *MNRAS*, 475, 772, doi: [10.1093/mnras/stx3181](https://doi.org/10.1093/mnras/stx3181)
- Soderberg, A. M., Nakar, E., Berger, E., & Kulkarni, S. R. 2006a, *ApJ*, 638, 930, doi: [10.1086/499121](https://doi.org/10.1086/499121)
- Soderberg, A. M., Berger, E., Kasliwal, M., et al. 2006b, *ApJ*, 650, 261, doi: [10.1086/506429](https://doi.org/10.1086/506429)
- Soderberg, A. M., Chakraborti, S., Pignata, G., et al. 2010, *Nature*, 463, 513, doi: [10.1038/nature08714](https://doi.org/10.1038/nature08714)
- Sokolovsky, K. V., Mukai, K., Chomiuk, L., et al. 2020, *MNRAS*, 497, 2569, doi: [10.1093/mnras/staa2104](https://doi.org/10.1093/mnras/staa2104)
- Southworth, J., Mancini, L., Madhusudhan, N., et al. 2017, *AJ*, 153, 191, doi: [10.3847/1538-3881/aa6477](https://doi.org/10.3847/1538-3881/aa6477)
- Spera, M., Mapelli, M., & Bressan, A. 2015, *MNRAS*, 451, 4086, doi: [10.1093/mnras/stv1161](https://doi.org/10.1093/mnras/stv1161)
- Stanway, E. R., Eldridge, J. J., & Becker, G. D. 2016, *MNRAS*, 456, 485, doi: [10.1093/mnras/stv2661](https://doi.org/10.1093/mnras/stv2661)
- Stein, R., Velzen, S. v., Kowalski, M., et al. 2021, *Nature Astronomy*, 5, 510, doi: [10.1038/s41550-020-01295-8](https://doi.org/10.1038/s41550-020-01295-8)
- Steiner, J. E., & Oliveira, A. S. 2005, *A&A*, 444, 895, doi: [10.1051/0004-6361:20052782](https://doi.org/10.1051/0004-6361:20052782)
- Stelzer, B., Damasso, M., Scholz, A., & Matt, S. P. 2016, *MNRAS*, 463, 1844, doi: [10.1093/mnras/stw1936](https://doi.org/10.1093/mnras/stw1936)
- Stern, D., Eisenhardt, P., Gorjian, V., et al. 2005, *ApJ*, 631, 163, doi: [10.1086/432523](https://doi.org/10.1086/432523)

- Stern, D., Assef, R. J., Benford, D. J., et al. 2012, *ApJ*, 753, 30, doi: [10.1088/0004-637X/753/1/30](https://doi.org/10.1088/0004-637X/753/1/30)
- Stern, D., McKernan, B., Graham, M. J., et al. 2018, *ApJ*, 864, 27, doi: [10.3847/1538-4357/aac726](https://doi.org/10.3847/1538-4357/aac726)
- Stone, N. C., & Metzger, B. D. 2016, *MNRAS*, 455, 859, doi: [10.1093/mnras/stv2281](https://doi.org/10.1093/mnras/stv2281)
- Strotjohann, N. L., Ofek, E. O., Gal-Yam, A., et al. 2021, *ApJ*, 907, 99, doi: [10.3847/1538-4357/abd032](https://doi.org/10.3847/1538-4357/abd032)
- Sun, M., Jiang, B., Yuan, H., & Li, J. 2021, *ApJS*, 254, 38, doi: [10.3847/1538-4365/abf929](https://doi.org/10.3847/1538-4365/abf929)
- Sunyaev, R., Arefiev, V., Babushkin, V., et al. 2021, arXiv e-prints, arXiv:2104.13267. <https://arxiv.org/abs/2104.13267>
- Sutherland, R. S., & Dopita, M. A. 1993, *ApJS*, 88, 253, doi: [10.1086/191823](https://doi.org/10.1086/191823)
- Tartaglia, L., Sollerman, J., Barbarino, C., et al. 2021, *A&A*, 650, A174, doi: [10.1051/0004-6361/202039068](https://doi.org/10.1051/0004-6361/202039068)
- Tauris, T. M., Kramer, M., Freire, P. C. C., et al. 2017, *ApJ*, 846, 170, doi: [10.3847/1538-4357/aa7e89](https://doi.org/10.3847/1538-4357/aa7e89)
- The LIGO Scientific Collaboration, The Virgo Collaboration, & The KAGRA Scientific Collaboration. 2021a, arXiv e-prints, arXiv:2111.03634. <https://arxiv.org/abs/2111.03634>
- The LIGO Scientific Collaboration, the Virgo Collaboration, Abbott, R., et al. 2021b, *ApJL*, 913, L7, doi: [10.3847/2041-8213/abe949](https://doi.org/10.3847/2041-8213/abe949)
- Thilker, D. A., Bianchi, L., Boissier, S., et al. 2005, *ApJL*, 619, L79, doi: [10.1086/425251](https://doi.org/10.1086/425251)
- Thilker, D. A., Bianchi, L., Meurer, G., et al. 2007, *ApJS*, 173, 538, doi: [10.1086/523853](https://doi.org/10.1086/523853)
- Thompson, G. I., Nandy, K., Jamar, C., et al. 1978, Catalogue of stellar ultraviolet fluxes : a compilation of absolute stellar fluxes measured by the Sky Survey Telescope (S2/68) aboard the ESRO satellite TD-1 / (The Science Research Council, UK)
- Tinyantont, S., Ridden-Harper, R., Foley, R. J., et al. 2021, *MNRAS*, doi: [10.1093/mnras/stab2887](https://doi.org/10.1093/mnras/stab2887)
- Townsley, L. K., Broos, P. S., Corcoran, M. F., et al. 2011, *ApJS*, 194, 1, doi: [10.1088/0067-0049/194/1/1](https://doi.org/10.1088/0067-0049/194/1/1)
- Tremonti, C. A., Heckman, T. M., Kauffmann, G., et al. 2004, *ApJ*, 613, 898, doi: [10.1086/423264](https://doi.org/10.1086/423264)
- Tripp, T. 2019, *BAAS*, 51, 309
- Tully, R. B., Courtois, H. M., Hoffman, Y., & Pomarède, D. 2016, in *The Zeldovich Universe: Genesis and Growth of the Cosmic Web*, ed. R. van de Weygaert, S. Shandarin, E. Saar, & J. Einasto, Vol. 308, 305–309, doi: [10.1017/S174392131601005X](https://doi.org/10.1017/S174392131601005X)
- Tully, R. B., Karachentsev, I. D., Rizzi, L., & Shaya, E. J. 2019, Every Known Nearby Galaxy, HST Proposal
- Tumlinson, J., Peebles, M. S., & Werk, J. K. 2017, *ARA&A*, 55, 389, doi: [10.1146/annurev-astro-091916-055240](https://doi.org/10.1146/annurev-astro-091916-055240)
- Udalski, A., Szymanski, M., Kubiak, M., et al. 2000, *AcA*, 50, 307. <https://arxiv.org/abs/astro-ph/0010150>
- Valenti, J. A., Basri, G., & Johns, C. M. 1993, *AJ*, 106, 2024, doi: [10.1086/116783](https://doi.org/10.1086/116783)
- Vallée, J. P. 2014, *ApJS*, 215, 1, doi: [10.1088/0067-0049/215/1/1](https://doi.org/10.1088/0067-0049/215/1/1)
- van den Bergh, S., Herbst, E., & Pritchett, C. 1973, *AJ*, 78, 375, doi: [10.1086/111426](https://doi.org/10.1086/111426)
- van den Heuvel, E. P. J., & De Loore, C. 1973, *A&A*, 25, 387
- van der Hucht, K. A., Lamers, H. J. G. L. M., Faraggiana, R., Hack, M., & Stalio, R. 1976, *A&AS*, 25, 65
- van Kerkwijk, M. H., Charles, P. A., Geballe, T. R., et al. 1992, *Nature*, 355, 703, doi: [10.1038/355703a0](https://doi.org/10.1038/355703a0)
- van Velzen, S. 2018, *ApJ*, 852, 72, doi: [10.3847/1538-4357/aa998e](https://doi.org/10.3847/1538-4357/aa998e)
- van Velzen, S., Holoien, T. W. S., Onori, F., Hung, T., & Arcavi, I. 2020, *SSRv*, 216, 124, doi: [10.1007/s11214-020-00753-z](https://doi.org/10.1007/s11214-020-00753-z)
- van Velzen, S., Stone, N. C., Metzger, B. D., et al. 2019, *ApJ*, 878, 82, doi: [10.3847/1538-4357/ab1844](https://doi.org/10.3847/1538-4357/ab1844)
- van Velzen, S., Stein, R., Gilfanov, M., et al. 2021a, arXiv e-prints, arXiv:2111.09391. <https://arxiv.org/abs/2111.09391>
- van Velzen, S., Gezari, S., Hammerstein, E., et al. 2021b, *ApJ*, 908, 4, doi: [10.3847/1538-4357/abc258](https://doi.org/10.3847/1538-4357/abc258)
- Vaughan, S., Uttley, P., Markowitz, A. G., et al. 2016, *MNRAS*, 461, 3145, doi: [10.1093/mnras/stw1412](https://doi.org/10.1093/mnras/stw1412)
- Vieira, N., Ruan, J. J., Haggard, D., et al. 2020, *ApJ*, 895, 96, doi: [10.3847/1538-4357/ab917d](https://doi.org/10.3847/1538-4357/ab917d)
- Vigna-Gómez, A., MacLeod, M., Neijssel, C. J., et al. 2020, *PASA*, 37, e038, doi: [10.1017/pasa.2020.31](https://doi.org/10.1017/pasa.2020.31)
- Villar, V. A., Guillochon, J., Berger, E., et al. 2017, *ApJL*, 851, L21, doi: [10.3847/2041-8213/aa9c84](https://doi.org/10.3847/2041-8213/aa9c84)
- Vink, J. S. 2021, arXiv e-prints, arXiv:2109.08164. <https://arxiv.org/abs/2109.08164>
- Vink, J. S., & Sander, A. A. C. 2021, arXiv:2103.12736 [astro-ph]. <https://arxiv.org/abs/2103.12736>
- Volonteri, M., & Natarajan, P. 2009, *MNRAS*, 400, 1911, doi: [10.1111/j.1365-2966.2009.15577.x](https://doi.org/10.1111/j.1365-2966.2009.15577.x)
- von Essen, C., Mallonn, M., Welbanks, L., et al. 2019, *A&A*, 622, A71, doi: [10.1051/0004-6361/201833837](https://doi.org/10.1051/0004-6361/201833837)
- Wakeford, H. R., Wilson, T. J., Stevenson, K. B., & Lewis, N. K. 2019, *Research Notes of the American Astronomical Society*, 3, 7, doi: [10.3847/2515-5172/aafc63](https://doi.org/10.3847/2515-5172/aafc63)

- Walborn, N. R., Lennon, D. J., Heap, S. R., et al. 2000, *PASP*, 112, 1243, doi: [10.1086/316617](https://doi.org/10.1086/316617)
- Wang, L., Gies, D. R., Peters, G. J., et al. 2021, *AJ*, 161, 248, doi: [10.3847/1538-3881/abf144](https://doi.org/10.3847/1538-3881/abf144)
- Waxman, E., & Katz, B. 2017, *Shock Breakout Theory*, ed. A. W. Alsabti & P. Murdin (Springer), 967, doi: [10.1007/978-3-319-21846-5_33](https://doi.org/10.1007/978-3-319-21846-5_33)
- Weber, E. J., & Davis, Leverett, J. 1967, *ApJ*, 148, 217, doi: [10.1086/149138](https://doi.org/10.1086/149138)
- Weisz, D. R., Dolphin, A. E., Skillman, E. D., et al. 2014a, *ApJ*, 789, 147, doi: [10.1088/0004-637X/789/2/147](https://doi.org/10.1088/0004-637X/789/2/147)
- . 2014b, *ApJ*, 789, 148, doi: [10.1088/0004-637X/789/2/148](https://doi.org/10.1088/0004-637X/789/2/148)
- . 2015, *ApJ*, 804, 136, doi: [10.1088/0004-637X/804/2/136](https://doi.org/10.1088/0004-637X/804/2/136)
- Weisz, D. R., Johnson, B. D., & Conroy, C. 2014c, *ApJL*, 794, L3, doi: [10.1088/2041-8205/794/1/L3](https://doi.org/10.1088/2041-8205/794/1/L3)
- Weisz, D. R., Johnson, B. D., Johnson, L. C., et al. 2012a, *ApJ*, 744, 44, doi: [10.1088/0004-637X/744/1/44](https://doi.org/10.1088/0004-637X/744/1/44)
- . 2012b, *ApJ*, 744, 44, doi: [10.1088/0004-637X/744/1/44](https://doi.org/10.1088/0004-637X/744/1/44)
- Weston, J. H. S., Sokoloski, J. L., Chomiuk, L., et al. 2016a, *MNRAS*, 460, 2687, doi: [10.1093/mnras/stw1161](https://doi.org/10.1093/mnras/stw1161)
- Weston, J. H. S., Sokoloski, J. L., Metzger, B. D., et al. 2016b, *MNRAS*, 457, 887, doi: [10.1093/mnras/stv3019](https://doi.org/10.1093/mnras/stv3019)
- Woosley, S. E. 2017, *ApJ*, 836, 244, doi: [10.3847/1538-4357/836/2/244](https://doi.org/10.3847/1538-4357/836/2/244)
- Woosley, S. E., & Bloom, J. S. 2006, *ARA&A*, 44, 507, doi: [10.1146/annurev.astro.43.072103.150558](https://doi.org/10.1146/annurev.astro.43.072103.150558)
- Wu, S., & Fuller, J. 2021, *ApJ*, 906, 3, doi: [10.3847/1538-4357/abc87c](https://doi.org/10.3847/1538-4357/abc87c)
- Wu, Y., Chen, X., Chen, H., Li, Z., & Han, Z. 2020, *A&A*, 634, A126, doi: [10.1051/0004-6361/201935792](https://doi.org/10.1051/0004-6361/201935792)
- Wyatt, M. C. 2008, *ARA&A*, 46, 339, doi: [10.1146/annurev.astro.45.051806.110525](https://doi.org/10.1146/annurev.astro.45.051806.110525)
- Wyder, T. K., Martin, D. C., Schiminovich, D., et al. 2007, *ApJS*, 173, 293, doi: [10.1086/521402](https://doi.org/10.1086/521402)
- Wyder, T. K., Martin, D. C., Barlow, T. A., et al. 2009, *ApJ*, 696, 1834, doi: [10.1088/0004-637X/696/2/1834](https://doi.org/10.1088/0004-637X/696/2/1834)
- Xin, C., Charisi, M., Haiman, Z., et al. 2020, *MNRAS*, 496, 1683, doi: [10.1093/mnras/staa1643](https://doi.org/10.1093/mnras/staa1643)
- Yaron, O., Prialnik, D., Shara, M. M., & Kovetz, A. 2005, *ApJ*, 623, 398, doi: [10.1086/428435](https://doi.org/10.1086/428435)
- Ye, C. S., Fong, W.-f., Kremer, K., et al. 2020, *ApJL*, 888, L10, doi: [10.3847/2041-8213/ab5dc5](https://doi.org/10.3847/2041-8213/ab5dc5)
- Zanni, C., & Ferreira, J. 2013, *A&A*, 550, A99, doi: [10.1051/0004-6361/201220168](https://doi.org/10.1051/0004-6361/201220168)
- Zaritsky, D., Harris, J., Thompson, I. B., & Grebel, E. K. 2004, *AJ*, 128, 1606, doi: [10.1086/423910](https://doi.org/10.1086/423910)
- Zaritsky, D., Harris, J., Thompson, I. B., Grebel, E. K., & Massey, P. 2002, *AJ*, 123, 855, doi: [10.1086/338437](https://doi.org/10.1086/338437)
- Zhan, H. 2018, in 42nd COSPAR Scientific Assembly, Vol. 42, E1.16–4–18
- Zhang, M., Knutson, H. A., Wang, L., et al. 2021, arXiv e-prints, arXiv:2106.05273. <https://arxiv.org/abs/2106.05273>

APPENDIX

 A. *UVEX* TDE DISCOVERY RATE

Here we calculate the *UVEX* TDE discovery rate. At a typical temperature of 3×10^4 K, we have $L_{\text{UV}}/L_g = 6.0$ in the FUV band which we focus on in the following. Based on the *g*-band luminosity function measured by van Velzen (2018), we infer the volumetric rate of TDE as a function of UV luminosity L :

$$\frac{d\dot{N}}{dL} = \frac{\dot{N}_0}{L_0} \left(\frac{L}{L_0} \right)^\alpha \quad (\text{A1})$$

where $L_0 = 10^{43} \text{ erg s}^{-1}$, $\alpha \approx -2.5$, and $\dot{N}_0 = \frac{\dot{N}_{0,g}}{\ln(10)} \times 6.0^{-(\alpha+1)} \approx 1.2 \times 10^{-6} \text{ Mpc}^{-3} \text{ yr}^{-1}$. The number of detected events per year will be

$$\mathcal{R} = \int_0^{D_{\text{max}}} \Omega D^2 dD \int_{L_{\text{min}}}^{L_{\text{max}}} \frac{dN}{dL_{\text{UV}}} dL_{\text{UV}} \quad (\text{A2a})$$

$$= \frac{\Omega \dot{N}_0}{3 L_0} \int_{L_{\text{min}}}^{L_{\text{max}}} D_{\text{max}}^3 \left(\frac{L}{L_0} \right)^\alpha dL \quad (\text{A2b})$$

where Ω is the solid angle of the surveyed area.

We note that the sample of luminous TDE is currently poorly characterized – among the 13 TDEs used by van Velzen (2018), only ASASSN-15lh peaked at $> 10^{44} \text{ erg s}^{-1}$, and it has distinct spectral properties compared with other events. The shape of the luminosity function at the high end is poorly explored. Therefore, to be conservative, hereafter we only consider the rate of TDEs peaking below $10^{44} \text{ erg s}^{-1}$.

For each L , there is a maximum distance out to which the UV rise of a TDE can be **characterized**. We have $4\pi D_{\text{max}}^2 f_{\text{thre}} = L$. Note that the threshold flux, f_{thre} , **doesn't** correspond to $f_0 \equiv 0.56 \times 10^{-14} \text{ erg s}^{-1} \text{ cm}^{-2}$ at 25 mag (limit magnitude with a 900 s dwell). Instead, we require $f_{\text{thre}} = 10f_0$ to ensure that the TDEs peak at least 2.5 mag above the survey threshold, such that the light curve UV rise and decay can be well measured! Hence, we have

$$\mathcal{R} = \frac{\Omega \dot{N}_0}{3 L_0} \int_{L_{\text{min}}}^{10^{44} \text{ erg s}^{-1}} \left(\frac{L}{4\pi f_0 \times 10} \right)^{3/2} \left(\frac{L}{L_0} \right)^{-2.5} dL \quad (\text{A3})$$

We define a new parameter $x \equiv L/L_0$.

$$\mathcal{R} = \frac{\Omega \dot{N}_0}{3} \int_{x_{\text{min}}}^{10} \left(\frac{L_0}{4\pi f_0 \times 10} \right)^{3/2} x^{-1} dx \quad (\text{A4a})$$

$$= \frac{\Omega \dot{N}_0 (1216 \text{ Mpc})^3 \times \ln \left(\frac{10}{x_{\text{min}}} \right)}{3} \quad (\text{A4b})$$

$$= 2531\Omega \quad (\text{A4c})$$

where we have assumed $x_{\text{min}} = 10^{42.5} \text{ erg s}^{-1}$ (iPTF16fnl is the faintest and fastest TDE ever discovered, see Blagorodnova et al. 2017). Note that \mathcal{R} does not strongly depends on x_{min} .

We assume a mission lifetime of 2 years and require that TDEs peak after the first 2 months and before the last 2 months (such that both the rise and decay can be characterized). Therefore, the effective survey period is 1.67 yr. In order to characterize 1000 TDEs (see requirement justified in §9.5), using Eq. (A4), we have

$$2531 \times \Omega \text{ yr}^{-1} \times (1.67) \text{ yr} = 1000 \quad (\text{A5})$$

$$\Omega = 0.24 \quad (\text{A6})$$

The observed fields should be selected to avoid low Galactic latitude, low declination, and regions of high Galactic extinction. The total number of visits per band per field will be $365 \times 2 \times 0.7/25 = 20.5$. The proposed exposure time per dwell is 900 s (simultaneously in FUV and NUV with a dichroic). We assume that a given field is visible to *UVEX* for 70% of the survey time (due to Sun constraint, etc). Thus, the surveyed solid angle should be $0.24/0.7 = 0.34$, corresponding to 1200 deg^2 (≈ 110 fields). Taken together, such an imaging survey will cost 3–4% of the total *UVEX* time.